Jianhua Tong

Biomechanics of Abdominal Aortic Aneurysms

Monographic Series TU Graz

Computation in Engineering and Science

Series Editors

Monographic Series TU Graz

Computation in Engineering and Science **Volume 18**

Jianhua Tong

Biomechanics of Abdominal Aortic Aneurysms

An Experimental Approach towards a Better Understanding of Pathological Progression

---

This work is based on the dissertation *"Biomechanics of Abdominal Aortic Aneurysms: An Experimental Approach towards a Better Understanding of Pathological Progression Cardiovascular Mechanics"*, presented by Jianhua Tong at Graz University of Technology, Institute of Biomechanics in March 2013.
Supervisor: G. A. Holzapfel (Graz University of Technology)
Reviewer: T. Cohnert (Medical University of Graz)

Bibliographic information published by Die Deutsche Bibliothek.
Die Deutsche Bibliothek lists this publication in the Deutsche Nationalbibliografie; detailed bibliographic data are available at http://dnb.ddb.de.

Cover photo	Vier-Spezies-Rechenmaschine by courtesy of the Gottfried Wilhelm Leibniz Bibliothek – Niedersächsische Landesbibliothek Hannover
Layout	Wolfgang Karl, TU Graz / Universitätsbibliothek Christina Fraueneder, TU Graz / Büro des Rektorates
Printed	by TU Graz / Büroservice

Verlag der Technischen Universität Graz

www.ub.tugraz.at/Verlag

ISBN: 978-3-85125-279-8 (print)
ISBN: 978-3-85125-280-4 (e-book)

DOI: 10.3217/978-3-85125-279-8

JIANHUA TONG

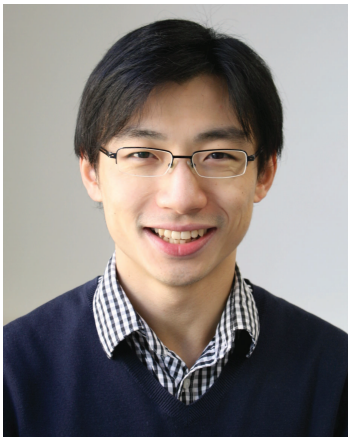

Jianhua Tong was awarded Bachelor's degree in Engineering Mechanics at Tongji University, Shanghai, P. R. China. Then he moved to the Royal Institute of Technology (KTH), Stockholm, Sweden, to pursue his Master's degree. During two years of his master program he switched his research direction to biomechanics and worked on several projects that focused on arterial wall biomechanics. After completing his Master Thesis, he immediately started his PhD in Biomedical Engineering at the Institute of Biomechanics, Graz University of Technology, Austria, supervised by Professor Gerhard A. Holzapfel. His PhD research mainly focused on experimental investigation of the mechanical properties of arteries in health and disease, specifically in human abdominal aortic aneurysms. His effort was also towards an investigation of the pathological progression of cardiovascular diseases by correlating biomechanics with tissue morphology and associated microstructural characteristics. He co-authored four peer-reviewed journal papers and two book chapters, and has presented on several international conferences.

Abstract

An abdominal aortic aneurysm (AAA) is a complex vascular pathology which leads to a localized and asymmetric dilation of the abdominal aorta. Ruptures of untreated AAAs are common and catastrophic events which may account for high mortality rates, particularly in elder males. It is well known that biomechanical factors play fundamental roles in AAA lesion growth, remodeling and rupture. Compared to tremendous advances during the past decade in our understanding of the biomechanics of diseased aneurysmal tissue and healthy aorta, it is more important to explore changes in the biomechanical properties of aneurysmal tissue in the AAA pathological progression. This provides us a basis to better understand AAA degeneration and the associated rupture mechanism, from a mechanical point of view.

This PhD thesis mainly focuses on experimental investigations of the biomechanical properties of two major types of tissues within the AAA, i.e. intraluminal thrombus (ILT) and thrombus-covered wall. By performing biaxial extension and peeling tests, we systematically explore biaxial mechanical responses and quantitatively determine dissection properties of ILTs and the thrombus-covered walls, and further develop a more appropriate 3D material model to characterize the biaxial mechanical behaviors of both tissue types. Another key contribution of this thesis is to determine the relative thrombus age within the AAA by characterizing the microstructure of ILT samples using histology and by investigating changes in the biomechanical properties of thrombotic tissues. As a novel factor in the AAA research, the relative thrombus age is critically important to show the initiation and progression of the ILT and its potential effects on AAA wall mechanics. Further, we find that ILT aging relates to wall weakening in the AAAs. Mass fraction analysis is aiming to quantify dry weight percentages of two protein components elastin and collagen within the AAA wall, which, in turn, determine mechanical properties at the tissue level. Moreover, gender differences in biomechanical properties of AAA are also discussed.

Zusammenfassung

Ein abdominales Aortenaneurysma (AAA) ist eine komplexe Gefäßerkrankung, bei der es zu einer lokalen und asymmetrischen Ausweitung der abdominalen Aorta kommt. Rupturierungen unbehandelter AAAs sind häufige und katastrophale Ereignisse, die besonders bei älteren Männern eine hohe Sterblichkeitsrate bedingen. Es ist wohlbekannt, dass biomechanische Faktoren eine fundamentale Rolle für das Wachstum, die Remodellierung und den Bruch eines AAAs spielen. Verglichen mit den enormen Fortschritten des letzten Jahrzehnts bezüglich des Verständnisses der Biomechanik des erkrankten aneurysmatischen Gewebes und der gesunden Aorta, ist es nun wichtig, die Veränderungen der biomechanischen Eigenschaften von aneurysmatischem Gewebe während der pathologischen Entwicklung des AAAs zu erforschen. Dies liefert uns ein grundlegendes und besseres Verständnis der AAA-Degeneration und den damit verbundenen Bruchmechanismen vom mechanischen Gesichtspunkt aus.

Diese Doktorarbeit konzentriert sich hauptsächlich auf die experimentelle Bestimmung der biomechanischen Eigenschaften von zwei Gewebehaupttypen innerhalb des AAAs - dem intraluminalen Thrombus (ILT) und der mit dem Thrombus bedeckten AAA-Wand. Mittels biaxialen Zug- und sogenannten Peeling-Versuchen konnten wir die biaxialen mechanischen Eigenschaften und die Dissektionseigenschaften der ILTs und der thrombusbedeckten AAA-Wände systematisch erforschen. Ferner konnten wir damit ein geeigneteres 3D Materialmodell für die Charakterisierung des biaxialen mechanischen Verhaltens beider Gewebstypen entwickeln. Ein weiterer wichtiger Beitrag dieser Arbeit ist, dass wir als erste das relative Thrombusalter innerhalb des AAAs durch Korrelation der Änderung der mechanischen Eigenschaften von thrombotischem Gewebe mit dessen mikrostrukturellen Charakteristiken in der Histologie bestimmten. Als einen neuartigen Faktor in der AAA-Forschung kann das vorgeschlagene relative Thromusalter von entscheidender Bedeutung für die Entstehung und Progression des ILT und ihre mögliche Auswirkung auf die Mechanik der AAA-Wand gesehen werden. Darüber hinaus fanden wir eine Beziehung zwischen Alter des ILT und der Wandschwächung des AAA. Eine Massenanteil-Analyse wurde durchgeführt, um das relative Trockengewicht der zwei mechanisch relevantesten Proteine Kollagen und Elastin im AAA bestimmen zu können. Des Weiteren wurden geschlechtsspezifische Unterschiede der biomechanischen Eigenschaften der AAAs diskutiert.

CONTENTS

1 INTRODUCTION AND MOTIVATION

1.1 Arterial Structure

It is well known that the normal arterial wall consists of three distinct layers: the intima (*tunica intima*), media (*tunica media*) and adventitia (*tunica externa*) [77, 79, 85, 86], see Fig. 1.1 for a schematic illustration. As the innermost layer, the intima consists of a monolayer of endothelial cells attached to a basement membrane composed of collagen (type IV) and laminin [79, 88]. The intima plays a key role in regulating agents from blood flow to reach the media. During aging process, the thickening and stiffening of the intima may contribute significantly to the mechanical responses of the arterial walls. The pathological changes of the intima may result in severe cardiovascular diseases such as atherosclerosis, which involves atherosclerotic plaque consisting of fatty substances, calcium, collagen fibers, cellular waste products and fibrin [79, 82]. The pathological changes of the intima leads to alterations in the mechanical properties of arterial wall tissue.

The middle layer media is separated from the intima and the adventitia by two thin layers (interfaces) called internal elastic lamina and external elastic lamina [79, 86]. From a histological point of view, the media is a complex three-dimensional network which consists of smooth muscle cells (SMCs) embedded in an extracellular matrix with elastin and multiple types of collagen (types I and III). It has been long suggested that the fibrils in the media (both SMCs and collagen) are almost circumferentially oriented. A recent paper by Schriefl et al. [163] quantitatively determined the layer-specific distributed collagen fiber orientations of human non-atherosclerotic thoracic and abdominal aortas and common iliac arteries. Specifically in all human aortas, two fiber families were present for the media and were almost symmetrically arranged with respect to the cylinder axis closer to the circumferential direction in the media. This structural alignment of fibrils also brings the media anisotropic mechanical properties when subjected to multi-axial loadings. From the mechanical point of view, the media is the most significant layer in a healthy artery.

The adventitia is the outermost layer of the arterial wall and consists of fibroblasts embedded in a network of collagen (mainly in type I) mixed with elastin and nerves. Surrounded by loose connective tissue, the adventitia is much less stiff at low pressures as compared to the media. In the high pressure domain, however, the collagen fibers within the adventitia straighten to resist loads and to prevent the arteries from overstretch and acute rupture [79, 82]. For example, in human coronary arteries, Holzapfel and his colleagues [82] reported that ultimate tensile stresses of the adventitia could be in average three times higher than those of the intima and media.

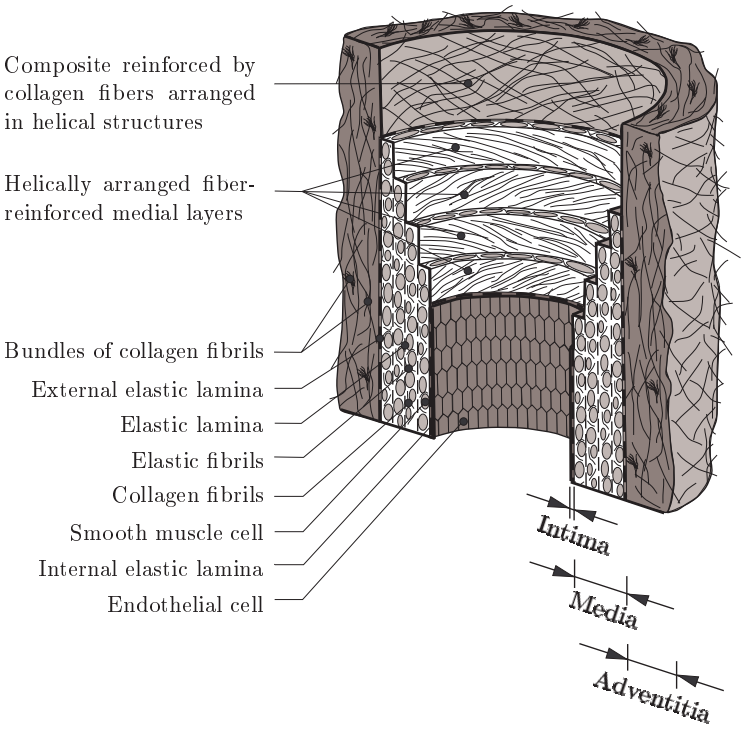

Figure 1.1: Schematic illustration of an elastic arterial structure consisting of three layers: intima, media and adventitia. Adapted from Holzapfel et al. [79].

1.2 Abdominal Aortic Aneurysm

An aneurysm is classically defined as a focal dilation of the arterial wall. According to Humphrey and Taylor [88], the most common types of aneurysms are intracranial saccular aneurysms (ISAs) and abdominal aortic aneurysms (AAAs). ISAs are focal outpouchings of the wall of a proximal intracranial artery, typically at a site of bifurcation, and mainly pointing in the direction of blood flow in the absence of the bifurcation [8]. AAAs mainly occur in the human infrarenal aorta, i.e. the aortic portion between renal arteries and aorto-illac bifurcation, approximately 12 cm long, 2 cm in diameter and 0.2 cm thick [87, 88].

The AAA, characterized by localized, asymmetric balloon-like bulge of the infrarenal aortas, represents a significant disease in the western population especially for elder men over 65 years [52,142,196,197]. The lesion may lead to dilations of aortas which exceed the normal diameter by more than 50% (a 1.5 or more fold increase). Previous studies [16, 25, 87] estimated AAA expansion rates, i.e. between 0.1 to 0.8 cm/year, which is independent of the AAA size. For example, both Solberg et al. [172] and Mofidi et al. [128] proposed that female AAA with a relatively smaller size may have a much faster expansion or growth

rate than that of males with a larger size.

1.2.1 Morphology

The shape of an aneurysm is frequently described as being fusiform, saccular (see, e.g., Fig. 1.2) or hourglass. It should be noted that most AAAs are fusiform and they are shaped like a spindle with widening all around the circumference of the human abdominal aorta. The more common fusiform shaped aneurysm bulges or balloons out on all sides of the aorta, while saccular shaped aneurysm bulges or balloons out only on one side. The aneurysm shape significantly influences the biomechanical conditions especially the stress distribution within the AAA, as discussed and emphasized by an early study [42].

The mean wall thickness of AAAs was measured and averaged to be 0.15 cm [145], which was, in general, lower than that of the normal human aorta, i.e. 0.2 cm. Note, however, that wall thicknesses of AAAs varied regionally and between AAA from as low as 0.23 mm at a rupture site to 4.26 mm at a calcified site [145]. Also, the wall thickness was found to be slightly lower in the posterior and right regions.

1.2.2 Risk factors

Primary risk factors in developing AAAs include male gender, aging, smoking, hypertension, inflammation and atherosclerosis [87]. Grootenboer et al. [66] reported that older men were 6 times more likely than older women to have an AAA and a similar conclusion was derived by Singh et al. [171], suggesting a prevalence of 4 : 1 male to female ratio susceptible to developing the AAAs. However, reasons for gender differences remain unclear. Cigarette smoking is summarized as the leading self-inflicted risk factor for cardiovascular diseases [35] and it causes arterial stiffening with serious sequelae such as atherosclerosis and AAAs [43]. As further suggested by Brady et al. [16], smoking increases AAA growth and thus the rupture risk. Another factor, i.e. hypertension, leads to stiffening of the human aorta and local hemodynamic environmental change [99, 136], which is regarded as one of the causes to initiate aneurysmal formation. Besides the hypertension, atherosclerosis also correlates directly with arterial wall stiffening, which alters the hemodynamics of blood flow and further develops aortic aneurysms [86, 88]. Moreover, focus has also been on the investigation of genetic factors that play a key role in explaining AAA formation and rupture mechanism, see, e.g., Choke et al. [25] and Sakalihasan et al. [159].

1.2.3 Intraluminal thrombus

AAAs have complex structural and morphological characteristics. An intraluminal thrombus (ILT) presents in most AAAs (approximately 75% of AAAs) with a clinically relevant

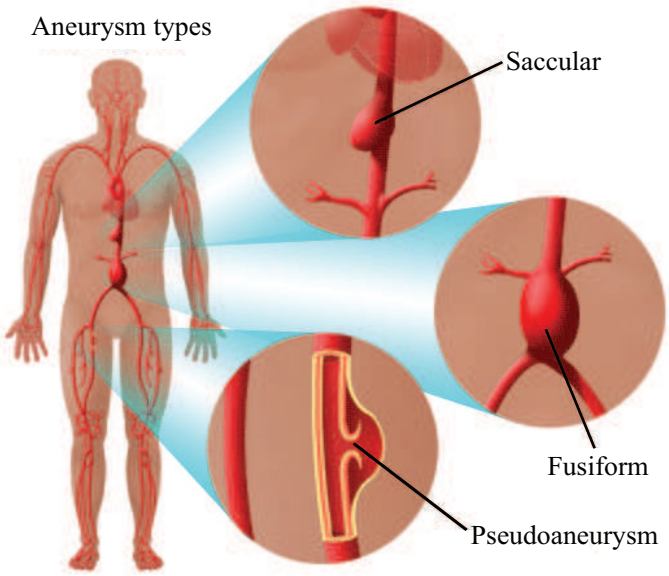

Figure 1.2: Representative sketch of saccular and fusiform shaped aneurysms in contrast to pseudoaneurysm. Image taken from www.jeffersonhospital.org.

size [25, 71, 181], see, e.g., Fig. 1.3. The ILT is a three-dimensional fibrin structure with blood proteins, blood cells, platelets and cellular debris [72]. The heterogeneity of the ILT structure can be distinguished by its three individual layers from the lumen to the ablumen side: luminal (red), medial (a bit white) and abluminal (dark yellow) layers, see Fig. 1.4. According to Kazi et al. [93], the presence of the ILT influences the proteolytic degradation of the underlying aneurysmal wall segment. Prior to that, the Vorp group [199] indicated that the ILT also served as a barrier to attenuate the oxygen supply from the lumen, leading to hypoxia of the aortic wall. The role of the ILT within an AAA structural stability, specifically in relation to the risk of rupture, has not been clarified yet. For example, computed tomography (CT), as documented in [209], suggested that an increased AAA thrombus load was associated with a higher likelihood of rapid expansion. Satta et al. [160] suggested that thrombus thickness was associated with the rupture risk, since the ruptured AAAs had thicker ILT when compared to the non-ruptured ones. These findings exist in the clinical observations, however, whether they can be applied to other AAA cases is still a debate.

1.2.4 Rupture assessment

Most AAAs are typically asymptomatic until the catastrophic event of rupture. However, a rapidly expanding AAA can cause a sudden onset of severe and steady mid-abdominal pain and back pain. Rupture of AAA is defined as the end-stage mechanical failure of the

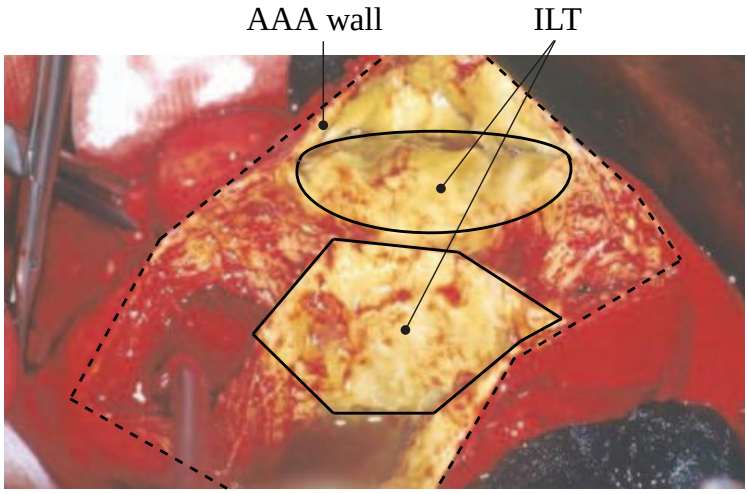

Figure 1.3: Representative image of a AAA including the ILT and the thrombus-covered wall after open surgical cut.

diseased aneurysmal aortic wall and may cause an overall mortality rate of between 75% and 90% [52]. According to Powell and Brady [141], rupture of AAAs rank as the 13th leading cause of death in the US. From a biomechanical point of view, AAA rupture occurs when the local strength of the degenerated aortic wall is insufficient to withstand the pressure-induced peak wall stress (PWS) [199]. The rupture risk of AAAs is thought to be associated with increased levels of wall stress [193]. Since there is no reliable technique to quantify the risk of rupture for individual AAA, clinical assessment of rupture risk and decision to electively repair an AAA is still commonly based on the unreliable 'maximum diameter criterion', i.e. 5 to 5.5 cm. According to this criterion, the AAAs with the diameters reaching or exceeding this value range should be considered for elective surgical repair [40, 103]. However, several previous studies indicated that aneurysms with a diameter less than 5.5 cm can also rupture [26, 135], in particular for female patients [19, 20, 74] and some of large AAAs do not [30]. The 'maximum diameter criterion' is established based on the Law of Laplace [197], stating that the stress in the AAA wall is proportional to its diameter. However, it should be emphasized that the AAA wall has a complex 3D geometry including major and minor wall curvatures [42, 158], rather than a simple cylindrical tube. Therefore, mechanical stress in the aneurysm wall is non-homogeneous and the highest stress within the entire AAA wall, defined as the PWS, can be distributed into several points on the wall surface. Moreover, simply considering wall stress is insufficient to predict material failure. The local wall strength is also a key factor which can determine the likelihood of rupture. Hence, the stress to strength ratio, rather than the AAA maximum diameter, is a more rational criterion in the current assessment of biomechanical rupture risk.

Over the last decade, an effort has been made to find other factors which are more appropri-

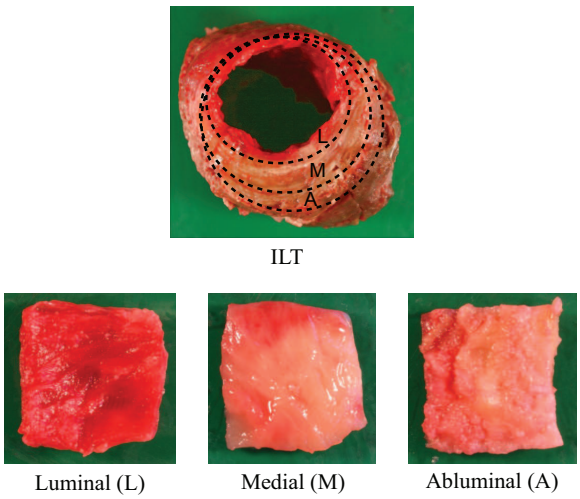

Figure 1.4: Representative images of three individual ILT layers: luminal (L), medial (M) and abluminal (A).

ate to assess the AAA rupture risk. For example, aneurysm expansion rate was estimated so as to be linked to lesion development and rupture [16, 137, 177]. In particular, Stenbaek et al. [177] showed that aneurysm expansion rate was associated with the ILT growth and Parr et al. [137] further observed that the median or larger ILT volume ($\geq 25.0\,\mathrm{cm}^2$) was associated with rapid AAA volumetric growth ($\geq 25.0\,\mathrm{cm}^3/\mathrm{yr}$) independent of the initial AAA diameter. If these conclusions are available for most AAA samples, quantitative measurements of the thrombus volume in a patient-specific geometry could be an effective tool to evaluate AAA dilation and associated rupture potential. Based on two-dimensional CT scans, Fillinger and colleagues [47] found relations between aortic tortuosity, diameter asymmetry and rupture risk. By analyzing anatomic characteristics of 259 patients, ruptured AAAs tend to be less tortuous, yet have greater cross-sectional diameter asymmetry when matched for age, gender and diameter. More recently, Doyle et al. [37] introduced vessel asymmetry as an additional diagnostic tool to assess AAA lesion. Based on realistic geometries, posterior wall stress was found to be proportional increased with AAA asymmetry, i.e. excessive bulging on the anterior surface. This work is the very first to link the AAA morphology on the one surface with wall stress on the opposite surface. Since stress level on the anterior surface increased faster than that of the posterior surface, consideration of morphological characteristics alone is not essentially helpful to provide an overall prediction of rupture risk.

1.2.5 Pathogenesis

Investigators also made an effort to interpret pathogenesis of the AAA. Blood flow pattern, i.e. the reversal flow in early diastole in the human infrarenal aorta, was thought to

be the main cause to initiate AAA dilations from a hemodynamic point of view [124]. However, such a reversal flow was not observed in the mouse-model [5]. Increased dynamic strain of the anterior wall due to increased elastin fatigue, may also help explain why human AAAs' dilations initially develop anteriorly [63]. In addition, the AAAs were suggested as a consequence of a ruptured atherosclerotic plaque and formation of the ILT [4, 25, 159, 183]. Therefore, the process of the AAA formation can be interpreted sequentially as first atherosclerosis within the abdominal aortic walls due to pathological changes, then formation of the ILT, and finally aneurysmal dilations. This hypothesis needs further investigations from a biochemical point of view. Elastin and smooth muscle loss [73, 86, 93, 111] within the aortic media is commonly thought to be the main reason to trigger instability of the aortic wall and thus, leads to realignment of collagen fibers accompanied by an increase of old collagen cross-links and a stoppage of new collagen biosynthesis [25, 86, 88, 93, 111, 159]. Such an imbalance between degradation and biosynthesis of the collagen is, in part, responsible for AAA development and rupture.

1.3 AAA Biomechanics

The stresses and strains exerted on blood vessels have been shown as important factors in the initialization and development of cardiovascular diseases [191]. Accordingly, there is a need for investigators to study how these mechanical factors influence the progression of certain vascular pathologies. Over the past few decades, AAA biomechanics has been widely used to characterize the mechanical properties of aneurysmal tissues and to quantitatively assess AAA rupture risk based on finite element analysis (FEA). Compared to clinical and biochemical data, patient-specific biomechanical factors may be more reliable in predicting AAA rupture [115, 123, 200].

1.3.1 Experimental characterization and constitutive modeling

Experimental biomechanics and related constitutive modeling of AAA is an effective methodology to characterize mechanical responses of the aneurysmal tissues. An analysis of these data does allow a better understanding of changes in the mechanical properties of aneurysmal aortic tissue when compared with healthy human abdominal aortas. For example, early studies [111, 179] investigated non-invasively the pressure-strain elastic modulus or aortic stiffness, suggesting the notable stiffness or inelasticity of dilated or aneurysmal vessels. Other mechanical measurements [73] showed that AAAs were less distensible and much stiffer than non-aneurysmal aortas. Moreover, an increase of the volume fractions of collagen and ground substance and a decrease of the volume fractions of elastin and muscle were noted. A later study by Vorp et al. [201] reported their measures of AAA wall stiffness by using uniaxial tensile test. By developing a microstructure-based constitutive

model, Raghavan and colleagues [148] characterized *ex vivo* biomechanical behaviors of AAA wall. Note, too, that parameters of this constitutive model represent the separate contribution of elastin and collagen to total aortic tissue stiffness as well as a collagen recruitment. To estimate wall stresses in intact, three-dimensional vessels, a two-parameter hyperelastic continuum-based constitutive model [146] in the form of

$$W = \alpha(I_B - 3) + \beta(I_B - 3)^2 \tag{1.1}$$

was further utilized to quantify experimental data obtained from one-dimentional uniaxial tensile tests on human AAA specimens. In Eq. (1.1), I_B is the first invariant of $\mathbf{B}$ and it can be further determined by $I_B = \mathrm{tr}\mathbf{B} = \mathrm{tr}(\mathbf{F}\mathbf{F}^{\mathrm{T}})$, where $\mathbf{F}$ is the deformation gradient. Despite limitations such as inaccurate prediction of multiaxial constitutive relations of aneurysmal tissue, the model associated with the quantified two mechanical parameters α and β has been widely used in later studies on computational stress analysis of AAAs [46, 48, 122, 147, 204].

Since both non-aneurysmal and aneurysmal aortic tissues are under multiaxial loading conditions *in vivo*, the uniaxial tensile test is insufficient/inappropriate for the characterization of mechanical responses. Hence, experimental protocols were developed to perform biaxial tensile tests [156, 157]. In order to compare the mechanical behaviors of the aneurysmal aorta to the native aorta, Vande Geest and his colleagues [191] first performed biaxial tensile tests on human infrarenal aortic tissue and correlated test data with age, showing that aging may lead to a significant shift in peak wall stretch and stiffening of normal aortic tissue. Subsequently, they performed the same protocol on aneurysmal aortic tissue, suggesting that aneurysmal degeneration of the abdominal aorta is associated with an increase in mechanical anisotropy with preferential stiffening in the circumferential direction [192]. Due to the exhibited mechanical anisotropy, they also established constitutive relations of AAA tissues by utilizing an anisotropic exponential strain-energy function developed for canine pericardium [24], i.e.

$$W = b_0 \left\{ \exp[(1/2)b_1 E_{\theta\theta}^2] + \exp[(1/2)b_2 E_{zz}^2] + \exp[b_3 E_{\theta\theta} E_{zz}] - 3 \right\}, \tag{1.2}$$

where E_{ij} and b_i are components of Green-Lagrange strain tensor and material parameters, respectively. Compare to the Fung elastic model for the skin [188], the constitutive parameters derived from the model (1.2) are physically reasonable. The biaxial experimental data and constitutive relations in [192] have been extensively used in related material modeling of aneurysmal aortic wall and computational stress analysis [10, 45, 152, 153, 194]. Other comprehensive biaxial data for the AAA wall were recently derived by our lab [184] and all chosen specimens were aneurysmal aortic walls covered by the ILT. A three-dimensional strain-energy function based on an arterial wall model [76, 82] was used to characterize the mechanical behaviors of aneurysmal tissues. As an important extension to previous biaxial data [192], our work can better understand the potential weakening effect of the ILT on its underlying wall segment.

The ILT plays a key role in AAA pathogenesis and rupture. In recent biomechanical investigations, more attention has been paid to the mechanical properties of the ILT since the mechanical role of the ILT on wall stress distribution and underlying local wall strength is unclear yet. Mechanical cushioning effect of the ILT has been emphasized by both Inzoli et al. [89] and Wang et al. [204]. Using non-invasive ultrasonographic measurements, Vorp and colleagues [198] reported that the ILT underwent nonlinear strains *in vivo* and was virtually incompressible. The first complete mechanical data regarding the ILT was documented by DiMartino et al. [121], who suggested a linear stress-strain relation of the ILT. Later, Wang et al. [203] reported the most comprehensive study on the biomechanical properties of the ILT by using uniaxial tensile tests. It revealed that the ILT was slightly nonlinear over large strains and nearly isotropic, but highly nonhomogeneous indicating that tissue from the luminal region was stiffer and stronger than that from the middle region, i.e. medial plus abluminal layers. The constitutive relation was derived based on a one-dimensional material model

$$W = c_1(II_B - 3) + c_2(II_B - 3)^2, \tag{1.3}$$

where II_B is the second invariant of $\mathbf{B}$ and it is determined by $II_B = [\mathrm{tr}(\mathbf{B})^2 - \mathrm{tr}(\mathbf{B}^2)]/2$. Two material parameters, i.e. c_1 and c_2, within the luminal and middle regions were found to be statistically equivalent between the circumferential and longitudinal directions, suggesting mechanical isotropy of the ILT. Biaxial mechanical behaviors of the ILT were first measured by Vande Geest et al. [193]. The peak stretch and maximum tangential modulus at the equibiaxial tention-controlled protocol were recorded and statistically compared. Their results were consistent with the conclusions drawn from the previous uniaxial study [203] and, therefore, the ILT was suggested to behave in an isotropic manner during biaxial extension. If the time course of the ILT evolution within the AAA is taken into account, the above-mentioned conclusion needs to be redefined. Our biaxial data [184] showed a clear indication of mechanical anisotropy for several luminal layers of the ILT. Hence, we introduced another key factor, i.e. thrombus age, to provide a more comprehensive assessment of the ILT progression within the AAA. Moreover, our experiments first documented biaxial mechanical responses of fresh thrombi. To model evolving mechanical properties of the ILT, Karsaj and Humphrey [92] proposed a mathematical model based on *in vitro* test data on fibrinogenesis, the stiffness of fibrin gels, and fibrinolysis as well as histological and mechanical data of clots retrieved from patients at surgery or autopsy. This evolving model can better characterize the rapid *in vitro* production of fibrin from fibrinogen and degradation of fibrin. Another mathematical model for studying thrombus formation involved more blood flow induced factors and chemo-mechanical activations of platelets [211].

In addition to multiaxial extension, experiments have been performed to examine other mechanical properties of the aneurysmal tissue such as failure, compressive, and dissection properties. Failure properties are important to estimate ultimate tensile strength of wall tissue, in which uniaxial tensile tests are frequently used. The first *ex vivo* measurements

of AAA wall strength were conducted by the Vorp group [148, 201], who reported that the AAA wall strength was approximately 50% weaker than that of the non-aneurysmal aorta, and suggested wall degeneration within the AAA. Similar results were derived from biomechanical investigations of AAA walls exposed to infection [208]. Differences in failure properties between ruptured and electively repaired AAA walls were also noted, and the tensile strength of the ruptured AAAs was, in general, lower than that of the electively repaired tissue ($54 \pm 6\,\mathrm{N/cm^2}$ vs $82 \pm 9\,\mathrm{N/cm^2}$; P =0.04) [120]. The AAA wall strength was associated with spatial variations and the matrix metalloproteinase (MMP) production within the aneurysmal tissue was regarded as the main cause [189]. Above findings remind us that the AAA wall strength involves complicated cases due to different types of tissue samples, which needs a more careful consideration in the AAA rupture predictions.

The most complete mechanical data regarding failure properties of the ILT are provided by Wang et al. [203]. They suggested that the ultimate tensile strength of the luminal layer was higher when compared to the degraded medial and abluminal layers. Such a continuous decrease of the ILT strength from the luminal to the abluminal layer is probably related to deposition of cellular components during thrombus formation and platelet activation due to shear stress is considered to be the first step in the whole process. However, a more systematic interpretation is needed from a pathophysiological point of view.

The ILT is a poroelastic material and thus, its porous structure may significant influence fluid transport from lumen to aortic tissue. The compressive properties of the ILT was investigated by Ashton et al. [7]. These authors applied compressive strains of 5%, 10%, and 15% to native and engineered ILT samples, and recorded the time-dependent load relaxations. Moreover, the water content of the ILT samples was documented.

Aortic dissection starts with an intimal tear typically occurring when the wall stresses exceed the adhesive strength between individual arterial layers [27]. The intimal tear, which allows for entering of blood to the aortic wall, will progressively split/dissect the media layer to form a ‘false lumen’, which may lead to acute rupture of human aortas due to sudden increase of the wall stresses. Experimental investigation was once performed on the human abdominal aortic media, see, for example, Sommer et al. [173]. Using the same method, i.e. peeling/delamination test, Pasta et al. [138] recently reported a set of dissection data based on ascending thoracic aortic aneurysm (ATAA). However, no study has quantitatively determined dissection properties of the AAA tissue in the literature.

Experimental techniques are also used in predicting AAA rupture sites and characterizing ruptured morphology. Using an *in vitro* setup, Doyle and co-workers [37] inflated experimental AAA model manufactured by silicon rubber and found that ruptures of the idealized silicone models occurred predominantly at the inflection points. Later, the same methodology was executed to identify rupture locations of silicon AAA models with a patient-specific geometry and the result was consistent with the previous one, i.e. the inflection point rather than regions of maximum diameter [39]. Compared to the silicon AAA models, Raghavan et al. [144] characterized rupture sites of the AAA samples, harvested

from fresh cadavers, particularly emphasizing the regional variations in tissue properties. Another representative study [95], with the aim to characterize rupture sites, performed inflation tests on AAA tissues up to failure, and full-field measurements were achieved using stereo digital image correlation (SDIC). This technique can better characterize morphology of local rupture especially the cracks within the aneurysmal tissue. However, the whole experimental measurement is just based on a piece of squared-shaped AAA tissue and relevant results cannot be applied to the real AAA rupture case.

1.3.2 Computational analysis

Computational analysis serves as an important tool in determining AAA wall stress distribution and assessing relevant rupture risk potential. Most early computational studies [42, 89, 132, 178, 202] were based on two-dimensional analysis by assuming, for example, the Law of Laplace, idealized axisymmetric geometry and linear elastic constitutive relations. Note, however, that these inappropriate assumptions may lead to inaccurate or erroneous predictions of wall stress distributions. Therefore, a recent effort has been made to develop more appropriate constitutive models of aneurysmal tissue and to utilize patient-specific AAA geometries. It has also been suggested that the AAA geometry influenced the stress distributions more significantly than variations in material parameters of constitutive tissue models [122, 146]. Using a hyperelastic nonlinear model, three-dimensional geometry reconstructed from CT scans and blood pressure of patients, Fillinger et al. [48] underscored more accuracy of pressure-induced biomechanical stresses in predicting rupture risk of the AAA when compared to other clinical indices. The similar conclusion was drawn by their later study [46], which showed that peak wall stress was better to differentiate patients who later required emergent repair as compared to diameter and peak wall stress higher than $44\,\mathrm{N/cm^2}$ was correlated with rupture potential. To simplify the calculation of peak wall stress in patient-specific AAA models, an automated algorithm was further developed by Raghavan et al. [143]. However, the use of this algorithm on a larger population size still needs to be verified. Despite improvements, above studies [46, 48, 143] involved assumptions of isotropic constitutive relation, homogeneous aortic structure and uniform wall thickness. More importantly, the ILT was never incorporated into computational FEA.

The mechanical role of the ILT on wall stress distribution is basically controversial. Early studies using measurements [32, 164] suggested that the presence of ILT did not reduce the pressure acting on the AAA wall. However, other early computational analysis [89, 121, 132] based on both simplified material models and idealized AAA geometry all suggested that the ILT would reduce the wall stress level. The first study to investigate the effect of ILT on the wall stress distribution in realistic patient-specific AAA models was conducted by Wang et al. [204], who supported the viewpoint that the ILT altered wall stress distribution and reduced peak wall stress. Here, two points should be noted for this paper.

First, a three-dimensional reconstruction based on CT scan images allows for a more realistic AAA geometry and patient-specific ILT thickness. Second, the same constitutive model was applied to both the ILT and the AAA wall and all material parameters were determined by *ex vivo* tissue tests [146, 203]. Despite limitations, the results are more reliable when compared with previous computational FEA. Besides the ILT, another factor, i.e. calcification, is also incorporated into computational FEA for stress analysis. Calcified deposits exist in almost all AAAs and are composed primarily of calcium phosphate with other assorted constituents, showing a complicated microstructure [116]. The mechanical measurements indicate an average elastic modulus in the range of cortical bone and an average hardness similar to nickel and iron. Therefore, the significant difference in stiffness between these hard deposits and the compliant aortic wall may result in local stress concentrations and increase the risk of AAA rupture. Speelman et al. [175] reported that calcification may lead to an increase of local stresses by up to 22%, emphasizing that the location and shape of the calcified regions should be included in rupture risk assessment. Further studies [107, 112] considered both the ILT and the calcification in their patient-specific computational FEA, however, the conclusions were different. Li et al. [107] suggested that the presence of calcification increased the peak wall stress and decreased the biomechanical stability of the AAA. In contrast, Maier and colleagues [112] indicated that the peak wall stress decreased when taking calcification into account probably due to its significant load-bearing effect. However, both agreed that the incorporation of calcification altered stress distributions of the AAA wall.

To capture the anisotropic nature of the AAA tissue [192], Rodríguez et al. [153] first developed a five-parameter exponential strain-energy function to model the anisotropic mechanical behaviors of the AAA tissue. Two families of collagen fibers were assumed to determine the anisotropic contribution in the model. Prior to this work, an evolving mathematical model by Watton et al. [205] described the development of AAA due to microstructural changes, in which collagen remodeled to compensate for loss of elastin. In order to develop a more reliable predictor for AAA rupture risk, Rissland and co-workers [151] subsequently applied an anisotropic wall model to their FSI simulations of patient-specific AAA geometries, indicating that the anisotropic material model led to a broader range of stress values as compared to the isotropic material model. Another computational work [55] examined the influence of model complexity on the assessment of peak wall stress and peak wall rupture risk in FEA. Four different types of FE models, including with and without the ILT as well as uniform and varied wall thickness, were compared between ruptured and non-ruptured AAAs. This study particularly emphasized the importance of including the ILT and patient-specific AAA geometry and thickness into a more sophisticated FEA. As previously mentioned, the ILT is a poroelastic material, in which fissures can be created within the structure. Investigative attention is thus paid to examine impact of the ILT failure mainly due to fissures on the AAA wall stress distributions in terms of FEA. Polzer and co-workers [140] showed that the ILT fissures increased the stress field in the underlying wall but increase of stress magnitude was dependent on

how large part of the ILT is involved by the fissures. For example, the worst case is that the ILT fissures connect the lumen with the wall, causing a twofold increase of the stress for the underlying wall.

Previous computational hemodynamic studies [50, 51, 182, 212] investigated blood flow patterns of the AAAs. In addition, a fluid dynamic approach was used to advance our understanding of the ILT formation and growth [13, 14] due to platelet activation. It should be noted that a few studies focused on fluid solid interactions (FSI) of AAAs in the literature. Representative works in this aspect [151, 165] are limited by simplified assumptions in many key points such as geometry, constitutive models and boundary conditions; see the recent reviews on AAA biomechanical research by Georgakarakos et al. [58] and Humphrey and Holzapfel [87] for more detailed discussions.

1.4 Histology and Pathophysiology

Elastin and collagen (type I and III) are the key structural proteins of the human abdominal aortas. As an extracellular matrix protein, elastin constitutes about 30% of the dry weight of the arteries. Elastic fibers consist of elastin molecules and are organized in long cross-linked filaments: their crosslinks are desmosine (DES) and isodesmosine (isoDES). Organs containing elastin such as aorta, lungs, blood vessels and ligamentum nuchae, can stretch out and recoil. Collagen fibers represent the predominant connective element in arterial vessels as well as the major component of AAA walls. Mature collagen is stabilized mainly by two forms of stable, non-reducible cross-links: pyridinoline (PYR) and deoxypyridinoline (DPD); the former being mostly represented.

Relative content of both fibrous proteins is markedly altered in AAA tissues. Early histological examination of AAAs revealed a thinning of the media, disruption of medial connective tissue structure, and the loss of elastin [22], which is the most striking histological features of AAA tissue. The study conducted by He and Roach [73] quantitatively determined that, within AAAs, the volume fraction of elastin decreased from $22.7\% \pm 5.7\%$ to $2.4\% \pm 2.2\%$, and the volume fraction of smooth muscle cells decreased from $22.6\% \pm 5.5\%$ to $2.2\% \pm 2.0\%$, whereas the volume fraction of collagen and ground substance combined increased from $54.8\% \pm 4.5\%$ to $95.6\% \pm 2.5\%$ when compared with non-aneurysmal aortas. A similar conclusion was drawn by Baxter et al. [11]. Therefore, it is commonly accepted that the loss of elastin and smooth muscle contributes to the initiation of AAA dilation. Thus, the aortic wall thickens as a result of remodeling and involves the deposition of new collagen and perhaps other matrix proteins [4].

The main reason and mechanism of elastin loss within the aortic wall has not been clarified, although atherosclerosis is probably a key factor [4, 86, 159]. It is suspected that persistent hemodynamic, oxidant, or other forms of stress could induce elastin damage and initiate dysfunctional remodeling of the wall through the stretch-induced production of atypical

collagen and elastin by vascular smooth muscle cells [34]. Elastolysis, induced by inflammatory processes, arterial trauma, medial stress and aging, is another factor which plays an active role in aneurysmal dilation. In particular, adventitial elastolysis was suggested as a primary event in the AAA formation, see, for example, the study by White et al. [207]. They observed that the inner portion of adventitia of normal aortic wall was composed of densely compacted alternating lamellae of elastin and collagen, which were grossly disrupted in all aneurysms. Furthermore, Krettek et al. [98] found that the human AAAs have 4 to 6 fold more tropoelastin protein but a 9 fold lower level of desmosin than normal aortas, confirming an ongoing but ineffective elastogenesis by smooth muscle cells and macrophages. The abnormal integration of new collagen and elastic fibers may severely impair the integrity and biomechanical properties of aortic walls, rendering these components more susceptible to further enzymatic degradation [206]. Moreover, elastase and collagenase activity have been found in AAAs, and both have been positively correlated with aneurysm size [21, 214].

Loss of elastin is accompanied by an increase in the collagen content of the aortic wall, resulting in an overall decrease in the elastin to collagen ratio [68]. Another consequence caused by elastin and smooth muscle loss is turnover of collagen, representing a more disorganized microstructure of tissue which correlates with lesion enlargement. Since the orientations of collagen fibers in AAA walls are widely dispersed and vary between different patients, histological data based on a larger patient group are needed in order to provide an overall characterization of collagen distributions when compared to healthy human aortas [163]. Histological data by Carmo et al. [23] showed the notable increase of collagen cross-links and hence, they deduced that biosynthesis of new collagen stopped and old (aged) collagen accumulated cross-links, see comparison of old collagen between normal aorta and AAA by histology in Fig. 1.5. The balance between matrix degradation and new biosynthesis is responsible for local wall weakening, and, thus, affects eventual AAA rupture.

Inflammation is an important feature of AAAs and there is evidence that inflammatory cells mediate connective tissue degradation [168]. An early histological examination of the AAA tissue [154] has shown an obvious inflammation with fibrosis in 72.5% of specimens and a moderate inflammatory reaction in 15.7% of specimens. It involves a prominent infiltration within the adventitia and outer media, consisting of inflammatory cells, cytokines, and immunoglobulins [12, 17, 96, 154]. Another work regarding inflammation and cellular immune responses in the AAAs [170] showed that aortic allografts deficient in interferon-gamma (IFN-gamma) signaling played a key regulatory roles for Th1/Th2 cytokine balance in modulating wall matrix remodeling, and hence was treated as an important implication for the AAA pathophysiology. Note, also, that MMP-2 and MMP-9 are not only responsible for elastolytic activity, but also promote the degradation of other matrix proteins such as laminin, fibronectin, and proteoglycans [134].

The ILT is biologically active rather than being an inert substance [2, 180]. Although the

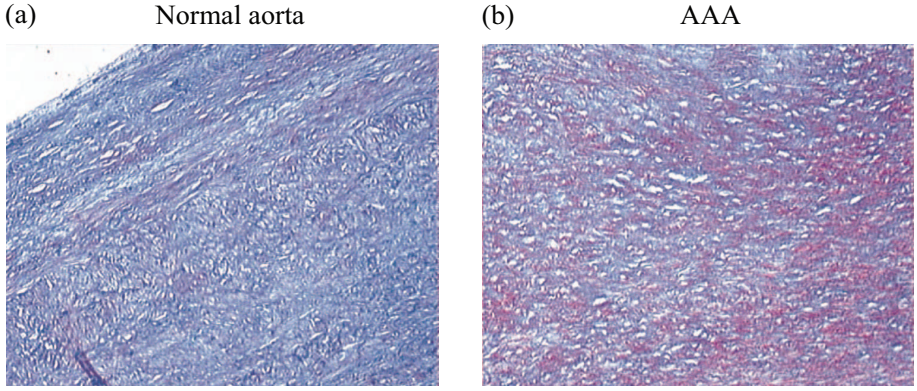

Figure 1.5: Histological images (Novelli's stain): presence of newly biosynthesized collagen (colored in blue) and old collagen (colored in red) within (a) normal aorta and (b) AAA. Original magnification 200×. Adapted from Carmo et al. [23].

structure of ILTs may differ largely among AAA patients, fibrin associated with platelets, erythrocytes, leukocytes, and neutrophils are the main constituents of the ILT within the AAA. It holds a complex structure and is traversed from the luminal to abluminal surface by a continuous network of interconnected canaliculi [2]. This morphological feature allows for cellular passage and most circulating cell types including T-cells, neutrophils, macrophages, platelets, and erythrocytes that are observed during cellular penetration by histology. The ILT is apparently fluid-permeable, as also suggested by Adolph et al. [2], and, therefore, fluid and smaller molecules may pass freely through the thrombus via the canaliculi network. It should be noted that fibrin deposition occurs throughout the ILT thickness, but more active degradation of fibrin is concentrated toward the abluminal regions. This key finding may explain how the layered structure of the ILT forms with different material stiffness. Electron microscopic imaging of the ILT obtained from a female AAA patient showed that the luminal layer was relatively rich in fibrin fibers forming an irregular compact structure with low amounts of erythrocytes and platelets, while the abluminal region was composed of densely packed fibrin with caniculi [117]. The large dense fibrin-rich areas may impair fibrinolysis and stabilize the thrombus size.

The degradation of media by means of proteolytic processes seems to be the basic pathophysiologic mechanism of the AAA development. Henderson et al. [75] reported that many medial SMCs in AAAs held signs of apoptosis or being capable of initiating cell death. Apoptotic death may contribute to the reduction of cellularity and to the impairment of reparative maintenance of the aortic extracellular matrix in AAAs. Investigating potential roles of the ILT in the proteolytic process is of fundamental importance in AAA pathogenesis. The ILT contains large amounts of neutrophils which are involved in the regulation of MMP-9 activity and prevents its inactivation, thus augmenting the proteolytic effect, which has been identified in all layers of the ILT [180]. The presence of MMP-9 complexes throughout the ILT and in the thrombus-covered wall may contribute to the in-

creased proteolytic degradation seen in the wall segment. Kazi et al. [93] compared the histological characteristics between the thrombus-free and the thrombus-covered walls. The latter was found to be thinner and contained fewer cells associated with disrupted structural orientation. Quantitative analysis revealed that total collagen content did not change significantly between two wall types, however, the thrombus-covered wall contained remarkably less elastin, with disorganized elastic lamellae and broken elastin bands. Also, decrease of SMC α-actin was found in the thrombus-covered wall samples. Using electron microscopic imaging techniques, the thrombus-covered walls were discerned as more heterogeneous with a mixture of SMCs and inflammatory cells, larger numbers of dying or dead cells and cell debris (typical signs of cell apoptosis and necrosis). The features at the cellular level implies that the thrombus-covered wall has less structural integrity and more severe tissue destruction than the thrombus-free wall. Hence, these two types of AAA walls are basically different, and in order to advance our understanding of AAA pathological progression, there is a need to distinguish them in future research.

1.5 Organization of the Thesis

The thesis is a compilation of four scientific papers and one book chapter related to the experimental investigations of vascular tissue at the human carotid bifurcation and within the AAA, covering topics of biaxial experiments, tissue dissection, microstructural characterization, mass fraction analysis and gender difference in biomechanical properties.

1. **J. Tong, G. Sommer, P. Regitnig and G.A. Holzapfel**, *Dissection properties and mechanical strength of tissue components in human carotid bifurcations*, Annals of Biomedical Engineering, 39 (2011), 1703–1719.

   The study *'Dissection Properties and Mechanical Strength of Tissue Components in Human Carotid Bifurcations'* investigates the dissection properties and radial mechanical strength of arterial wall tissue at human carotid bifurcation using two experimental methods: direct tension (DT) and peeling tests. Results suggest that the intima-media interface rather than the adventitia-media interface or the media, is more likely to dissect due to its lower radial failure stress in the DT test and lower dissection energy required in the peeling test. The anisotropic dissection properties of the media at the carotid bifurcation are described, and they vary significantly with the location. Histological investigations demonstrate that interfacial ruptures mainly occur in the media in both types of tests but are only 2-5 elastic lamellae away from the external and internal elastic laminae. A remarkably 'rougher' dissection surface is generated during axial peeling tests when compared with tests performed in the circumferential direction.

2. **J. Tong, T. Cohnert, P. Regitnig and G.A. Holzapfel**, *Effects of age on the elastic properties of the intraluminal thrombus and the thrombus-covered wall in abdominal aortic aneurysms: biaxial extension behavior and material modeling*, European Journal of Vascular and Endovascular Surgery, 42 (2011), 207–219.

   The study *'Effects of Age on the Elastic Properties of the Intraluminal Thrombus and the Thrombus-Covered Wall in Abdominal Aortic Aneurysms: Biaxial Extension Behavior and Material Modeling'* characterizes biaxial mechanical responses of the three individual ILT layers and the thrombus-covered walls based on 43 human AAA samples. Histological investigations of all tested thrombi are performed to determine the different age phases and to correlate with the change in the mechanical properties. A 3D material model is fitted to the experimental data. The luminal layers of the ILT exhibit anisotropic stress responses, whereas the medial and the abluminal layers are isotropic materials. Based on histological analysis a four-phase evolution of the thrombi is proposed. The thrombi in the third and fourth phases contribute to wall weakening and to an increase of the mechanical anisotropy of their covered walls. The material models for the thrombi and the thrombus-covered walls are in excellent agreement with the experimental data. This work suggests that thrombus age might be a potential predictor for the strength of the wall underneath the ILT and AAA rupture.

3. **J. Tong, T. Cohnert, P. Regitnig, J. Kohlbacher, R. Birner-Gruenberger, A.J. Schriefl, G. Sommer and G.A. Holzapfel**, *Variations of dissection properties and mass fractions with thrombus age in human abdominal aortic aneurysms*, submitted, (2013).

   The study *'Variations of Dissection Properties and Mass Fractions with Thrombus Age in Human Abdominal Aortic Aneurysms'* shows a correlation between dissection properties of the aneurysmal tissues with the relative thrombus age. Peeling tests are performed to dissect the material (i) through the ILT thickness, (ii) within the individual ILT layers and (iii) within the aneurysm wall underneath the thrombus by using two extension rates. Results indicate that a remarkably lower fracture energy is needed to dissect within the individual layers and through the thicknesses of the old thrombi. With increasing ILT age the dissection energy of the underlying intima-media composite continuously decreases and anisotropic dissection properties for that composite vanish. Moreover, there is a notable decrease in mass fraction of elastin within the thrombus-covered intima-media composite with ILT age, whereas no significant change is found for that of collagen. These findings suggest that an increased ILT age leads to a higher risk of dissection initiation for the ILT and the intima-media composite of the aneurysmal wall, in which a pronounced elastin loss is identified.

4. **J. Tong, A.J. Schriefl, T. Cohnert and G.A. Holzapfel**, *Gender differences in biomechanical properties, thrombus age, mass fraction and clinical factors of abdominal aortic aneurysms*, European Journal of Vascular and Endovascular Surgery, 45 (2013), 364–372.

   The study *'Gender Differences in Biomechanical Properties, Thrombus age, Mass Fraction and Clinical Factors of Abdominal Aortic Aneurysms'* investigates differences in the biomechanical properties, thrombus age, mass fraction and key clinical factors of AAAs between male and female patients. The luminal layers of the female thrombi and the female AAA walls show a significantly lower tissue stiffness (modulus) in the longitudinal direction when compared to males. Gender differences are also shown in the dissection properties of the intima-media composite within the AAA walls, in which a statistically significantly lower energy to propagate a dissection is quantified for females than males. Moreover, 82% of female thrombi are relatively older thrombi (ILT age phases III and IV), twofold that of the male thrombi (43%). A pronounced lower elastin content is identified for the intima-media composites of the male AAA walls, whereas female AAA walls have significantly lower dry weight percentages of collagen. Regarding clinical factors, nicotine pack years, serum creatinine and AAA expansion rate are found to be much higher for male patients. These findings may help to explain higher risks for AAA growth in males and the ruptures of smaller sized AAAs in females.

5. **G.A. Holzapfel, J. Tong, P. Regitnig and T. Cohnert**, Recent Advances in the Biomechanics of Abdominal Aortic Aneurysms. In: N. Chakfé, B. Durand and W. Meichelboeck (eds.), *'ESVB 2011 - New Endovascular Technologies - From Bench Test to Clinical Practice'*, Chapter 3, Europrot, Strasbourg, France (2011), 23–40.

   The book chapter *'Recent Advances in the Biomechanics of Abdominal Aortic Aneurysms'* reviews key advancements of AAA biomechanics over the past decade including both experimental and computational contributions. The chapter begins with an overview of the biomechanical behaviors of the ILT and the aneurysm wall, and then summarizes and compares corresponding material models. The subsequent section focuses on predicting the rupture risk and effort is devoted to the review of a series of representative studies in the literature covering a wide range of important findings and developments based on experimental and computational investigations. Histological section mainly discusses methodology in thrombus age determination. Finally, the current situation of AAA biomechanics is briefly summarized and open questions in future AAA research are mentioned.

In addition, the following 9 conference contributions, in form of abstracts, are also included as a part of the thesis:

J. Tong, T. Cohnert and G.A. Holzapfel, *Gender differences in the biomechanical properties of abdominal aortic aneurysms*, XXVI Annunal Meeting of European Society of Vascular Surgery, Bologna, Italy, September 19–21, 2012.

J. Tong, T. Cohnert, P. Regitnig and G.A. Holzapfel, *Biomechanics of abdominal aortic aneurysms: biaxial experiments and related modeling, tissue dissection and microstructural characterization*, 23rd International Congress of Theoretical and Applied Mechanics, Bejing, China, August 19–24, 2012.

J. Tong, T. Cohnert, P. Regitnig G. Sommer and G.A. Holzapfel, *Relation between the thrombus age and the tissue dissection in abdominal aortic aneurysms*, 8th European Solid Mechanics Conference (ESMC 2012), Graz, Austria, July 9–13, 2012.

G.A. Holzapfel, J. Tong, P. Regitnig and T. Cohnert, *Recent advances in the biomechanics of abdominal aortic aneurysms*, 10th Symposium on 'Endocardiovascular Biomechanics Research' (EBR 2012), Marseille, France, May 3–4, 2012.

T. Cohnert, J. Tong, P. Regitnig and G.A. Holzapfel, *Biomechanics of AAA and treatment consequences–elastic properties of aneurysm wall and intraluminal thrombus*, 12th International Vascular Endovascular Course & 5th European ISVS Congress, Milan, Italy, October 27, 2011.

J. Tong, T. Cohnert, P. Regitnig and G.A. Holzapfel, *Association of thrombus age with the dissection properties of the intraluminal thrombus and the thrombus-covered wall in abdominal aortic aneurysms*, 82nd Annual Meeting of the International Association of Applied Mathematics and Mechanics (GAMM 2011), Graz, Austria, April 18–21, 2011.

J. Tong, T. Cohnert and G.A. Holzapfel, *Experimental investigation and modeling of the intraluminal thrombus and the thrombus-covered wall in abdominal aortic aneurysms*, XXIV Annunal Meeting of European Society of Vascular Surgery, Amsterdam, The Netherlands, September 16–19, 2010.

J. Tong, P. Regitnig and G.A. Holzapfel, *Dissection properties and mechanical strength of tissue components in human carotid bifurcations*, 6th World Congress on Biomechanics, Singapore, August 1–6, 2010.

J. Tong, P. Regitnig and G.A. Holzapfel, *Quantitative determinations of tissue dissection in human carotid bifurcations*, 3rd Viennese Symposium on Biomaterials, Vienna, Austria, November 19–21, 2008.

2 DISSECTION PROPERTIES AND MECHANICAL STRENGTH OF TISSUE COMPONENTS IN HUMAN CAROTID BIFURCATIONS

Abstract Carotid artery dissections can be triggered by several factors. The underlying biomechanical phenomena and properties are unclear. This study investigates the dissection properties of 62 human carotid bifurcations using two experimental methods: direct tension and peeling tests. Direct tension tests study the mechanical strength of the tissue components in radial direction, while peeling tests quantify the fracture energy required to propagate a dissection in a tissue. Results show that the interface between the healthy adventitia and media has the highest radial failure stress (132 ± 20 kPa, mean $\pm$ SD, $n = 25$), whereas the lowest value occurs between the diseased intima and media (104 ± 24 kPa, $n = 18$). The radial tissue strength at the bifurcation is highest compared with locations that are away from the central region of the bifurcation. Force/width values required to separate the individual layers and to dissect the media in the circumferential direction are always lower than related values in the axial direction, suggesting anisotropic dissection properties. Dissection energies per reference area generated during the peeling tests are also lower for strips in the circumferential direction than for axial strips, and they vary significantly with the location, as shown for the media. Histological investigations demonstrate that interfacial ruptures mainly occur in the media in both types of tests and are only 2-5 elastic lamellae away from the external and internal elastic laminae. A remarkably 'rougher' dissection surface is generated during axial peeling tests when compared with tests performed in the circumferential direction.

2.1 Introduction

Carotid artery dissection can be triggered by a variety of risk factors but a dissection is mainly classified as spontaneous or traumatic. The incidence of spontaneous carotid artery dissection is low [104, 130], although case reports and studies have shown that it may go along with some severe vascular diseases such as stroke and chronic systematic hypertension [109]. Some patients with spontaneous internal carotid artery dissection may also have hereditary connective tissue disorders [119]. Compared to spontaneous incidence, carotid artery dissection is more likely to occur when caused by trauma to the head and/or neck, in which a tear forms in the innermost lining of the arterial wall, the tunica intima [104, 129].

An estimated 76% of patients who were found to have blunt carotid injury (including intimal dissections, pseudoaneurysms, thromboses, or fistulas) in hospital after motor vehicle accidents suffered from intimal dissections, pseudoaneurysms, or a combination of the two [44, 131]. Moreover, nowadays multiple forms of catheter-based diagnostic methods or well-established interventional treatments to the human carotid artery have been identified as an alternative way to initiate arterial dissection. This kind of intimal defect leads to an imbalance of distribution of mechanical stresses on the human arterial wall and may propagate the medial dissection [57, 86]. In clinical diagnosis, the dissection may propagate by running to either the lumen side or the adventitia side to form a false lumen or a dissecting aneurysm, which is potentially lethal [31, 97, 129, 161].

In physiology, the human common carotid artery (CCA) serves as an important vessel which bifurcates into an internal carotid artery (ICA) and an external carotid artery (ECA). While both branches travel upward, the ICA takes a deeper (more internal) path, eventually traveling up into the skull to supply the brain [65, 69]. The ECA travels more closely to the surface, and sends off numerous branches that supply the neck and the face [65]. Carotid bifurcation, i.e. the assembly of ICA, ECA and CCA, is a very special site in the cardiovascular tree. The hemodynamic environment in that region, to some extent, affects the atherosclerotic plaque formation [61]. Those plaques, if large and unstable, are a predisposing factor to cause ischemic strokes [109].

In the past few decades, biomechanical properties of the human carotid artery have been explored using several methods, from the solid and fluid mechanics point of view. Specifically, at the carotid bifurcations, hemodynamic analysis and modeling of the interaction between the blood flow and the arterial wall are performed [127, 213]. As for the carotid artery dissection due to spontaneous or accidental trauma, however, related data seem to be not yet existent. A recent experimental study by Sommer et al. [173] provides us with novel and effective experimental methods (direct tension and peeling tests) to quantify radial failure stresses and the fracture energy that is needed to cause arterial dissections, although the study was executed on the human abdominal aortic media. The direct tension and peeling tests are important not only in the quantitative determination of dissection properties of arterial wall tissues, but may also be helpful in studies on therapeutic treatments.

The purpose of the present study is to explore the dissection properties and mechanical strength of tissue components in human carotid bifurcations using the same methodology as proposed by Sommer et al. [173]. The direct tension test (DT test) is designed to obtain data of dissection strength across the lamellae of the arterial tissues in the radial direction, while the peeling test studies the fracture energy that is needed to propagate a dissection. By carrying out DT tests, we also aim to not only measure the dissection strength of the media in the radial direction but also the dissection strength at the interfaces between two arterial layers, i.e. the interface between the intima and the media (I+M), and the interface between the adventitia and the media (A+M). In addition, a region-divided protocol that we designed on the basis of the carotid bifurcation is implemented as a key reference

during the testing procedure, which is helpful to compare and interpret experimental results according to different regions. For the peeling test, we measure and quantify the fracture energy required to propagate a dissection that goes through the interface between the two arterial layers. We also investigate the important issue if more fracture energy is required to cause a rupture in the media or at the interfaces.

2.2 Materials and Methods

2.2.1 Material

In this study, 31 pairs of human carotid bifurcations (age range from 32 to 91, but most patients between 58 to 85) were harvested during autopsy within 24 hours of death. Each pair consists of two human carotid bifurcations (left and right) which were taken from the same patient, including both healthy (without plaque) and diseased (severe atherosclerotic) specimens. However, for the peeling test, we have only chosen healthy specimens selected by a pathologist, while either diseased or non-diseased specimens contributed to the DT tests. All specimens in our experiments were strictly inspected by an experienced pathologist after harvesting. They were then stored in a phosphate buffered saline (PBS) solution at 4°C until use, which was less than 4 hours. Use of autopsy material from human subjects was approved by the Ethics Committee, Medical University Graz, Austria. All tests were finished within 5 to 6 hours after the specimen defrosted from the storage.

2.2.2 Specimen preparation

To begin with the DT test, we cut along the central line on the upper surface of the artery using surgical scissors, until the cut reached the bifurcation. This central line is thought to be parallel to the vessel axes throughout the CCA portion of the bifurcation. Similarly, two axial cuts were then performed in the ICA and the ECA along their central lines, and stopped when they arrived at the previous cutting track in the CCA. The cutting strategy is illustrated by three dashed curves, labeled by the numbers 1, 2 and 3, in Fig. 2.1(a). Therewith, a clear open-cut structure of the human carotid artery bifurcation is achieved. Figures 2.1(b) and (c) illustrate images after the cuts of a healthy carotid bifurcation and of a diseased specimen with severe plaques, respectively. Subsequently, we removed the peripherally attached adipose and loose connective tissues from the adventitia, and the specimens were immersed into a container with phosphate buffered saline solution [81, 82, 173]. Coin-shaped specimens for the DT test were punched out using a cylindrical cutting tool with a diameter of 6.0 mm. Further details on the sequence and location of the specimen extractions are illustrated in the forthcoming protocol part.

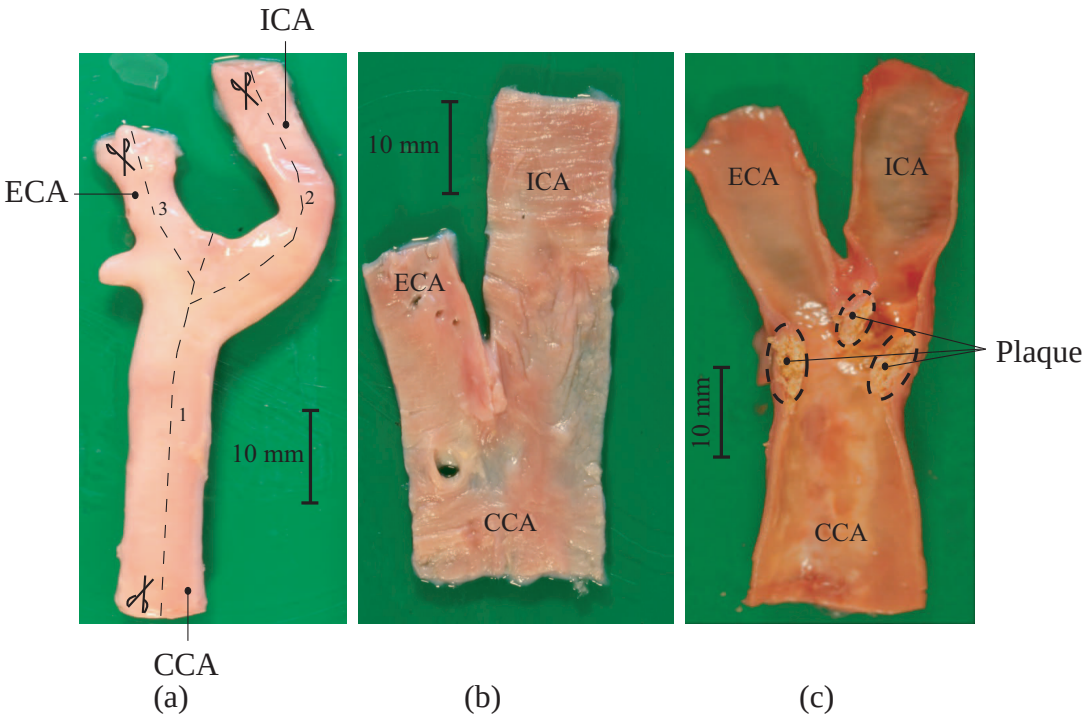

Figure 2.1: Representative images of (a) an intact human carotid bifurcation – donor: female, 75 yrs, (b) a healthy carotid bifurcation after an open cut – donor: male, 63 yrs, and (c) a diseased specimen with severe plaque after an open cut – donor: male, 69 yrs. The cutting strategy and trails for the DT test are denoted by three dashed lines in (a). A typical structure of a human carotid bifurcation with atherosclerosis is shown in (c). Three regions of plaque deposits can be observed. ICA, ECA and CCA represent internal, external and common carotid arteries, respectively.

The performed DT tests can be divided into two parts: (i) healthy tissues involving DT tests of the media, the interface between the intima and media (I+M), and the interface between the adventitia and media (A+M); (ii) diseased tissues with atherosclerotic plaques, where the adventitia was removed and the remaining intima-media composite was used for mechanical failure testing (for the atherosclerotic specimens it was not possible to separate the intima from the media). Particular attention was taken to protect the medial layer during anatomical separation of the three arterial layers since quite a few coin-shaped specimens from the ICA or the ECA adjacent to the bifurcation were quite thin. Therefore, the media could be easily lacerated even though we tried to remove the intima and the adventitia away very carefully. That was also the case for the media strips obtained from the ICA for the peeling tests.

Moreover, in order to better control the initiation of the tissue failure it was required to equip the coin-shaped specimen with an initial cut. In particular, incisions of about 1.0 mm

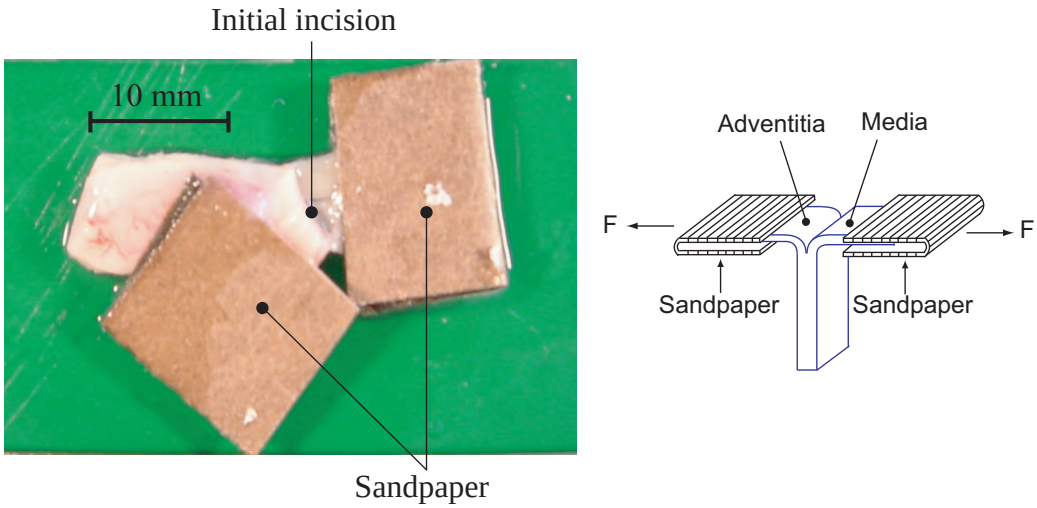

Figure 2.2: Prepared rectangular strip for the peeling test of the interface between the adventitia and media with a 3D sketch for illustration, on the right hand side.

depth were cut around the circumferences of the circular medial specimens using a surgical knife after mounting them in the testing machine. For the DT tests at the interfaces between the two arterial layers, the initial cuts were performed prior to mounting onto the testing machine in order to identify the interface. After a subtle initial cut, the diameter of all specimens reduced from 6.0 (original dimension) to 4.0 mm. All DT tests were performed in open air because these tests could be performed relatively fast. At the beginning of a DT test the specimen was moistened with PBS solution so that any drying could be avoided.

For the peeling tests a dimension of the rectangular strips was about 18.0×6.0 mm (Length $\times$ Width), a dimension established by the geometrical structure of the human carotid bifurcation. In an analogous manner as by Sommer et al. [173], both circumferential and axial rectangular strips were given an initial cut (incision of about 3.0 mm in length) by means of a surgical scalpel so that two 'tongues' were obtained for mounting them into the testing machine. To avoid slippage of the specimens during loading, rectangular pieces of sandpaper were glued with superadhesive gel at both sides of the 'tongues'. A well-prepared specimen for the peeling test of the interface between the adventitia and the media is shown in Fig. 2.2. All peeling tests performed to propagate a dissection in a tissue were executed in PBS solution at 37.0 ± 1.0°C.

In the present study the peeling of diseased specimens was precluded due to the presence of atherosclerotic plaques, which often causes a severe deviation from the propagation route or even leads to an acute rupture at the very beginning of the peeling process. The success rate of DT tests was considerably low. Less than 25% of the tests were successful, whereby DT tests of the interface (between the adventitia and media) turned out to have the highest success rate among all DT tests (about 32%).

2.2.3 Testing machine

A PC-controlled, screw-driven high-precision tensile testing machine, specifically adapted for small biological soft tissues, was used for the mechanical tests. For the DT tests, two plastic rods (15 mm in diameter) with a small cylindrically-shaped recess (deepening) were mounted onto the testing machine by means of the upper and lower fixing clamps. To strengthen the connection between the specimen and the plastic rod, we fixed a sandpaper into the small cylindrically-shaped recess using a superadhesive gel. The specimen was then glued to the sandpaper. During the peeling test both sides of two 'tongues' were fixed tightly by two clamps of the testing machine in order to keep the center part of the specimens in a perspex container filled with 0.9% physiological saline solution maintained at $37.0 \pm 1.0^{\circ}$C by a heater-circulation unit (type Ecoline E 200; LAUDA, LAUDA-Koenigshofen, Germany). Tensile forces were measured with a 10 N class 1 strain gauge-load cell. More details regarding the experimental setup can be found in Sommer et al. [173].

2.2.4 Protocol

Direct tension test. The protocol we designed is based on a region-divided investigation, since we hypothesize that the mechanical properties may change within the geometrical location of the human carotid bifurcation. After an open cut, we marked several regions on the three parts (ICA, ECA, CCA) of the carotid bifurcation by using the dimension of 6 mm, which is the diameter of the cylindrical cutting tool, see Fig. 2.3. The inner circumferences of the ICAs and ECAs of our specimens were measured to be around 13-15 mm, suggesting that at most two coin-shaped specimens can be punched out along the circumferential direction in one region of the ICA or ECA. By referring to Fig. 2.3, the two coin-shaped specimens 1 and 2 belong to ICA of 'region I'.

For the CCA, the inner circumferences were measured between 25 and 27 mm, implying that four specimens can be procured in that region. Four specimens, for example, 3 to 6, as shown in Fig. 2.3, were punched out one by one from the ICA to the ECA side.

Peeling test. For the ICA and the ECA the same cutting method was used as for the DT tests, see the sketch in Fig. 2.4. This gives four axial rectangular strips with a dimension of 18.0 mm $\times$ 6.0 mm (Length $\times$ Width). Note here that three strips out of these four were used to perform the axial peeling tests of the media (called M 1), the interface between the intima and media (I+M), and the interface between the adventitia and media (A+M), but the remaining strip served as a backup just in case of any failure of the other axial peeling tests. For the CCA, however, the cutting track is different as for the DT tests. It starts from the ICA and continues until 18 mm is reached (see the sketch in Fig. 2.4), which is the length for the rectangular strips. From this CCA region we obtained another media (called

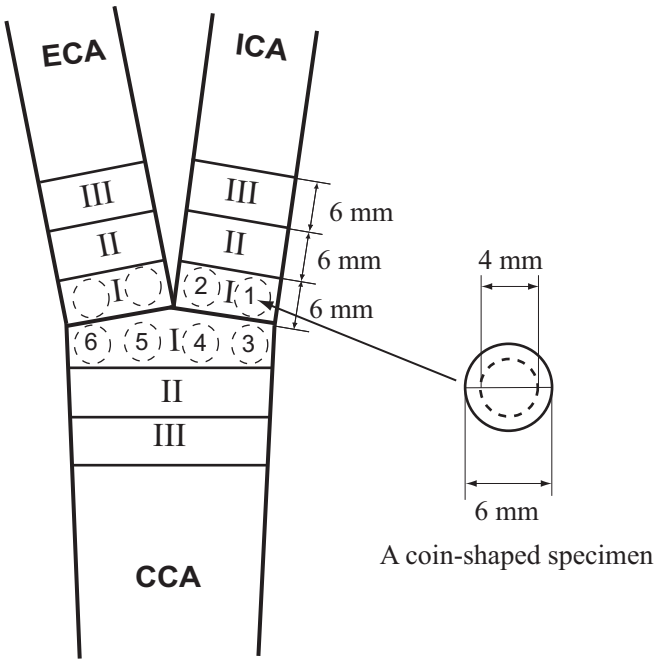

Figure 2.3: Schematic illustration for the specimen cutting regarding the direct tension tests: three regions with 6.0 mm width is displayed and marked by I, II and III. In the ICA and ECA regions two coin-shaped specimens (6.0 mm in diameter) are punched out, while around four such circular specimens are cut from one region across the CCA. An initial cut in the coin-shaped specimen leads to a reduction of the diameter from 6.0 to 4.0 mm.

M 2) for the axial peeling test, and three circumferentially oriented rectangular strips with the dimension 18.0 mm $\times$ 6.0 mm (Length $\times$ Width).

2.2.5 Testing procedure

For the DT tests, a suitable amount of cyanoacrylate glue was placed on the sandpaper into cylindrical recesses of the upper and lower rods of a specially designed specimen holder. The coin-shaped specimen was allocated in the cylindrical recess of the lower rod, which was mounted in the testing machine together with the upper rod first. A compression force of 1.0 N was then applied to the circular specimen for approximately five minutes to strengthen the specimen-rod adhesion. The specimen was moistened with phosphate buffered saline solution until testing. Throughout the test the extension rate of 1.0 mm/min was maintained and the corresponding resisting forces were documented. In most cases failure was prone to occur at the glued connection between the specimen and the holder

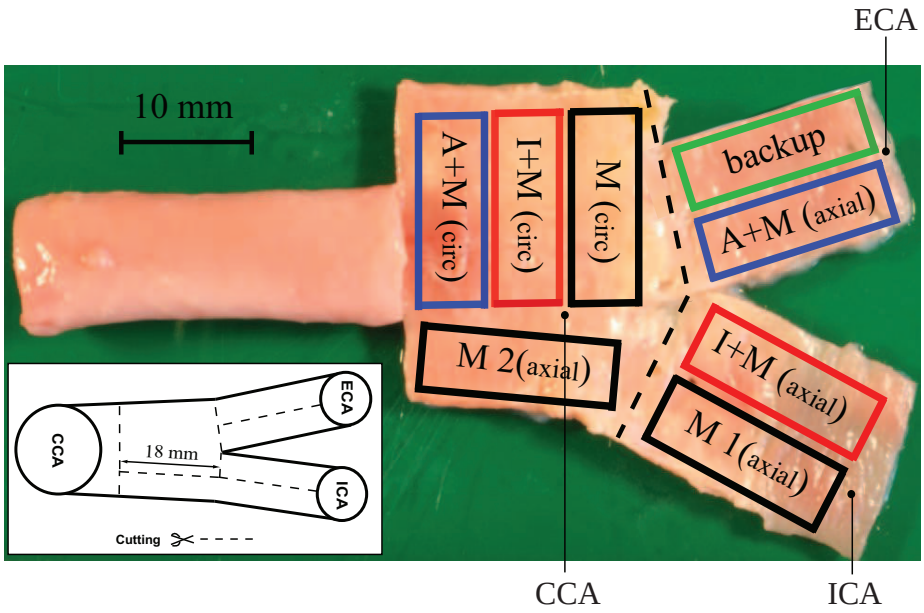

Figure 2.4: Schematic illustration of the experimental protocol of the peeling test with a complementary sketch to show the particular location for cutting the artery.

rather than the place where the initial cut was performed. Any specimen which separated at the glued connection was omitted and not sent for further histological analysis.

For the peeling test, the same extension rate (1.0 mm/min) was used when both 'tongues' of the prepared specimen were clamped in the testing machine. Figs. 2.5(a) and (b) show representative images of a specimen mounted in the machine before the peeling test and during the testing procedure, respectively.

2.2.6 Thickness measurement

Data such as diameter, length and width of the specimen samples are straightforward to measure during tissue preparation. The key point, however, is the measurement of the specimen thickness which was performed for all specimens prior to testing, and for the peeling specimens also after testing. For the coin-shaped specimens (for DT tests) the thickness was recorded by the PC-controlled testing machine. The thicknesses of the rectangular strips used for the peeling tests were measured by a PC-based videoextensometer with a full image CCD camera prior to mounting in the testing machine. The strip was placed on a black object plate with known thickness (1.0 mm) and the upper and lower edges of the strip plus the black object plate below were then detected optically by two perpendicular-orientated boundary sides of the gage region. Of importance is now that both lateral sides of the strip sample and the black object towards the CCD camera are in the same plane. By

subtracting the thickness of the black object (1.0 mm) from the average contour thickness along the gage region, we obtain the resulting thickness values.

2.2.7 Histological investigation

As a vital part of such a study histological investigations of all tested specimens are required to characterize the morphology of the dissected surfaces and the related locations within the arterial wall. Specimens, either DT or peeling tested were fixed in neutral buffered formalin with pH 7.4, and then embedded in paraffin. Paraffin blocks were sectioned at $3\,\mu$m and stained with Elastica van Gieson (EvG), which stains elastic fibres brown to black, collagen red, other tissue elements (mainly smooth muscle cells) yellow, and nuclei brown to black. For the mechanical tests it was significant to verify that the prior layer dissection was correctly performed. Therefore, presence or absence of layers was examined by histology. The intima, media and adventitia were measured and listed in percentages of the whole specimen thickness after test. Subsequently, delamination of layers was investigated microscopically. Thereby, mainly the locations of the dissected surfaces within the arterial wall was investigated.

It needs to be emphasized that all tests that relate to the interface (for both DT and peeling) were given a particular attention during the histological analysis in order to investigate if the dissection occurred at or around the interface, and to quantify the particular location.

2.2.8 Radial failure stress and dissection energy

The (average) radial failure stress that occurs during the DT test is computed by $F_{\max}/(d^2\pi/4)$, where $F_{\max}$ is the maximum force and d is defined to be the effective diameter of 4 mm for the coin-shaped specimens after the initial cut.

The related dissection energy W^{dissect} per reference area generated during the peeling process is obtained by subtracting the elastic energy stored in the rectangular strips from the external work. Based on the measured peeling force/width, denoted as F_{pa} and F_{pc} for an axial and circumferential strip, respectively, the external work W^{ext} during an axial and circumferential peeling test can be estimated as

$$W_{\text{a}}^{\text{ext}} = 2.0 F_{\text{pa}} l_{\text{pa}}, \qquad W_{\text{c}}^{\text{ext}} = 2.0 F_{\text{pc}} l_{\text{pc}}, \tag{2.1}$$

respectively, where l_{pa} and l_{pc} denote the current lengths of the rectangular strips during the axial and circumferential peeling tests just before separation (compare also with Sommer et al. [173]).

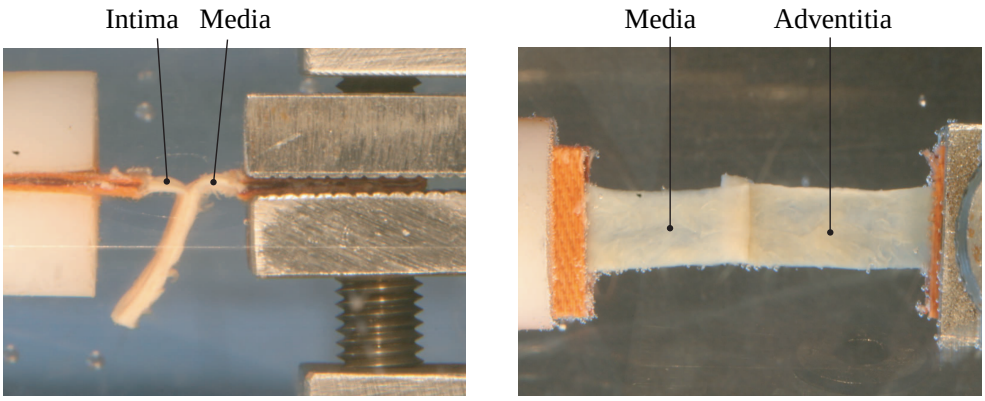

(a) Before the peeling test (b) During the testing procedure

Figure 2.5: Representative photographs of a specimen mounted in the machine (a) before the peeling test (I+M interface, circumferential), shown from the side, and (b) during the testing procedure (A+M interface, axial), shown from the top.

The elastic energy W^{elastic} stored in an axial and circumferential specimen is determined as

$$W_{\text{pa}}^{\text{elastic}} = F_{\text{pa}}(l_{\text{pa}} - L_{\text{pa}}), \qquad W_{\text{pc}}^{\text{elastic}} = F_{\text{pc}}(l_{\text{pc}} - L_{\text{pc}}), \tag{2.2}$$

respectively, where L_{pa} and L_{pc} denote the reference lengths of the rectangular strips in the axial and circumferential directions, which can be assumed to be about 15 mm after an approximately 3 mm incision (for two 'tongues' mounted in the machine) since all rectangular strips for the peeling test were cut in the same dimension. Finally, the dissection energy W^{dissect} per reference area generated during the peeling process is obtained by subtracting (2.2) from (2.1), which gives

$$W_{\text{pa}}^{\text{dissect}} = (W_{\text{a}}^{\text{ext}} - W_{\text{pa}}^{\text{elastic}})/L_{\text{pa}}, \qquad W_{\text{pc}}^{\text{dissect}} = (W_{\text{c}}^{\text{ext}} - W_{\text{pc}}^{\text{elastic}})/L_{\text{pc}}. \tag{2.3}$$

All values in the current study are reported as mean $\pm$ SD.

2.3 Results

2.3.1 Data for the specimen thickness

The average thickness data for the specimens of the DT tests and the peeling tests are provided in the Tables 2.1 and 2.2, respectively.

Table 2.1: Average thickness of coin-shaped specimen before DT test.

	Thickness before DT test
A+M Interface	0.63 ± 0.08 mm
I+M Interface	0.52 ± 0.06 mm
Media	0.35 ± 0.05 mm
I+M with Plaque	1.16 ± 0.17 mm

Table 2.2: Average thickness of rectangular strip before and after peeling tests: A, I and M represent Adventitia, Intima and Media after separation, respectively. The two separated medial strips are denoted by M_u (from the upper fixing clamp) and M_l (from the lower fixing clamp).

	Thickness before peeling test	*Thickness after peeling test*
A+M Interface	0.65 ± 0.09 mm	A: 0.33 ± 0.03 mm M: 0.38 ± 0.05 mm
I+M Interface	0.58 ± 0.09 mm	I: 0.27 ± 0.04 mm M: 0.37 ± 0.03 mm
Media	0.40 ± 0.06 mm	M_u: 0.21 ± 0.03 mm M_l: 0.23 ± 0.06 mm

2.3.2 DT test

For the DT test of the interface between the adventitia and the media (A+M interface) 25 force-displacement curves were collected to demonstrate the (average) evolution of the mechanical forces of the coin-shaped specimens during radial extension, subsequently called u (see the thin grey curves in Fig. 2.6). A mean curve (thick and solid black curve in Fig. 2.6) was calculated by using the data processing software OriginPro 7.5. After complete separation of a specimen the zero load level was reached, and that happens at a certain radial extension u. Note that each individual tissue test has its own ending point on the displacement axes (range from about 6.3 mm to 8.9 mm). The mean curve was computed beyond the first ending point.

The force-displacement behavior of the media of all specimens in the DT tests are shown in Fig. 2.7. Moreover, from Figs. 2.8 and 2.9 the results of the other two types of DT tests can be seen, i.e. the interface between the intima and the media, and the intima and media with plaque, respectively. The related maximum forces $F_{\max}$, the displacements u at $F_{\max}$ and the computed (average) radial failure stresses $F_{\max}/(d^2\pi/4)$ are summarized in Table 2.3.

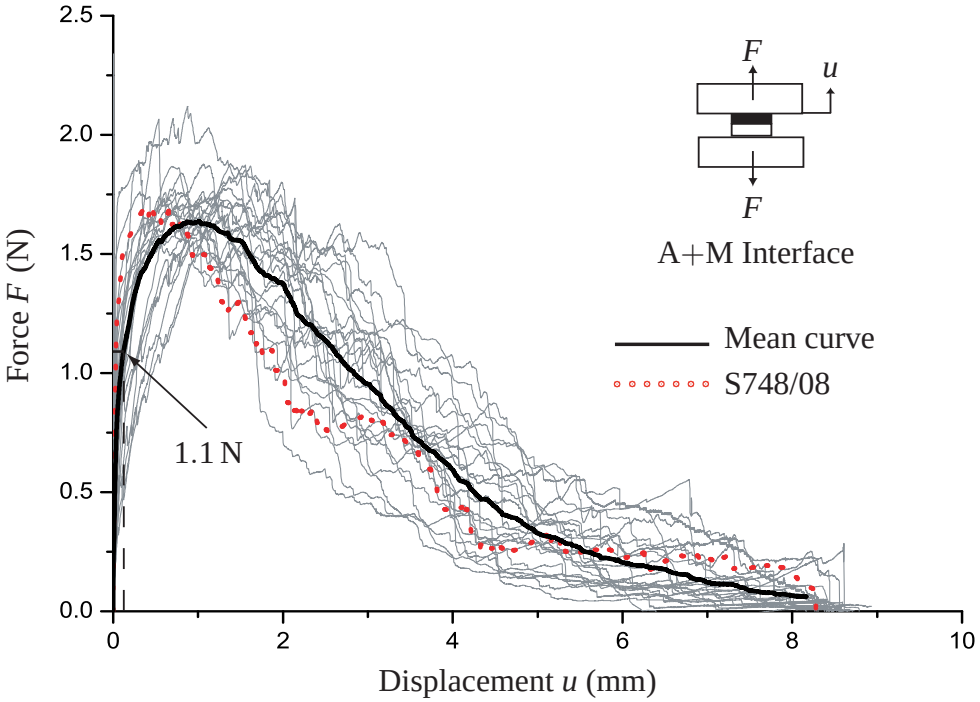

Figure 2.6: Force-displacement responses of all 25 coin-shaped specimens during DT tests of the interface between the adventitia and the media (A+M interface). Below the limit of about 1.1 N an elastic tissue response occurs. The thick and solid black curve represents the mean response of the individual tissue tests. The thick and dotted red curve shows the mechanical behavior of sample S748/08.

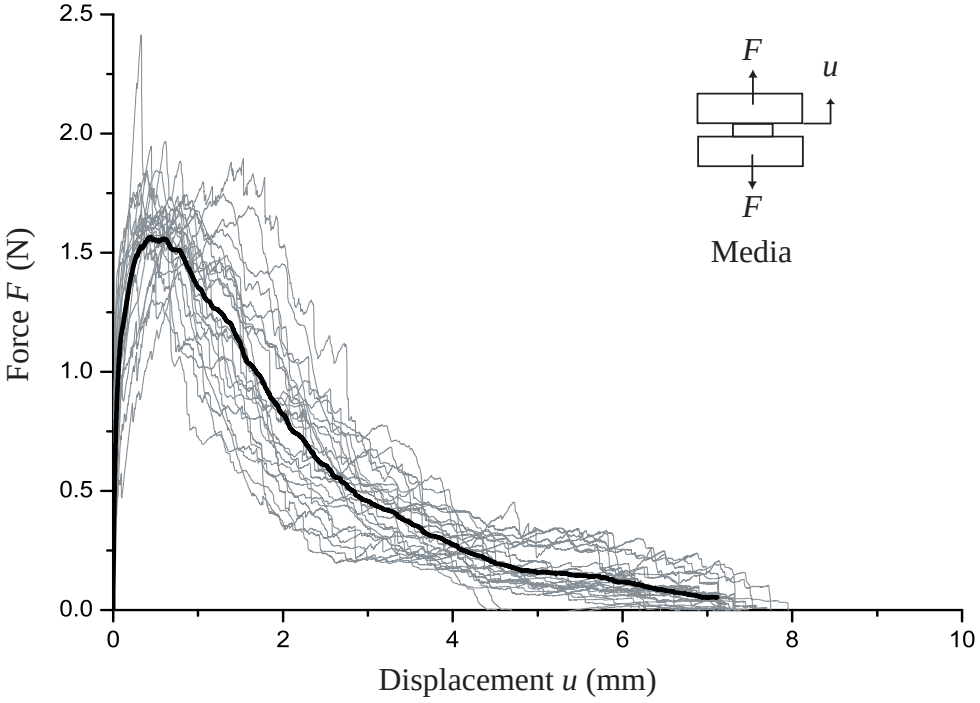

Figure 2.7: Force-displacement responses of all 25 specimens during DT tests of the media. The arithmetic mean response is characterized by the thick black curve.

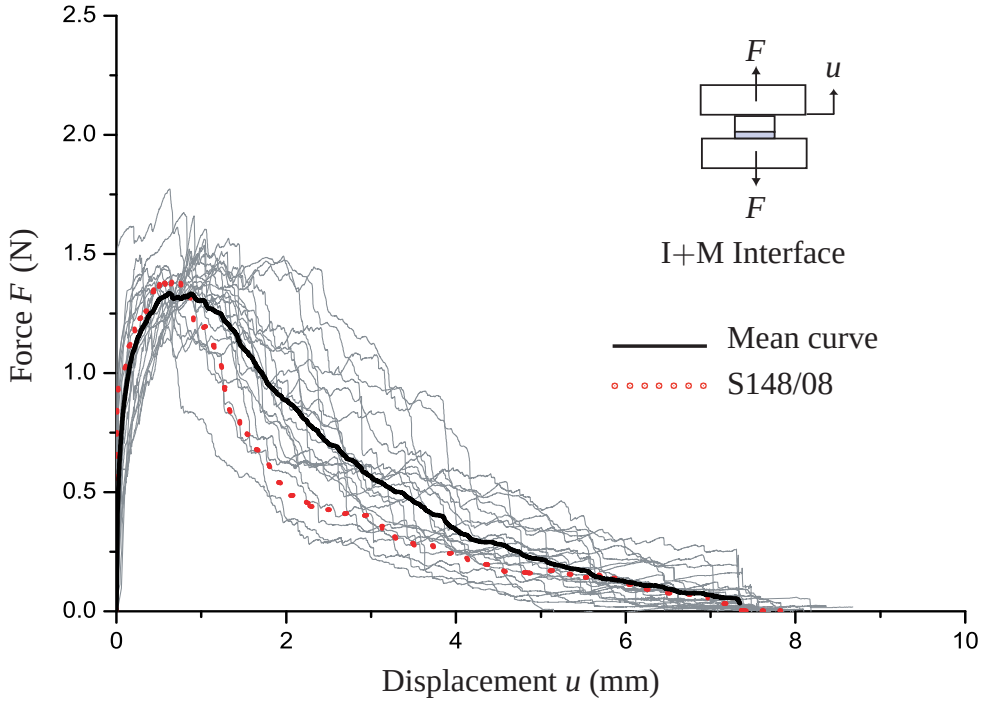

Figure 2.8: Force-displacement responses of all 21 specimens during DT tests of the interface between the intima and media (I+M interface). The mean curve (thick, black and solid) is included and the response of sample S148/08 (thick, red and dotted).

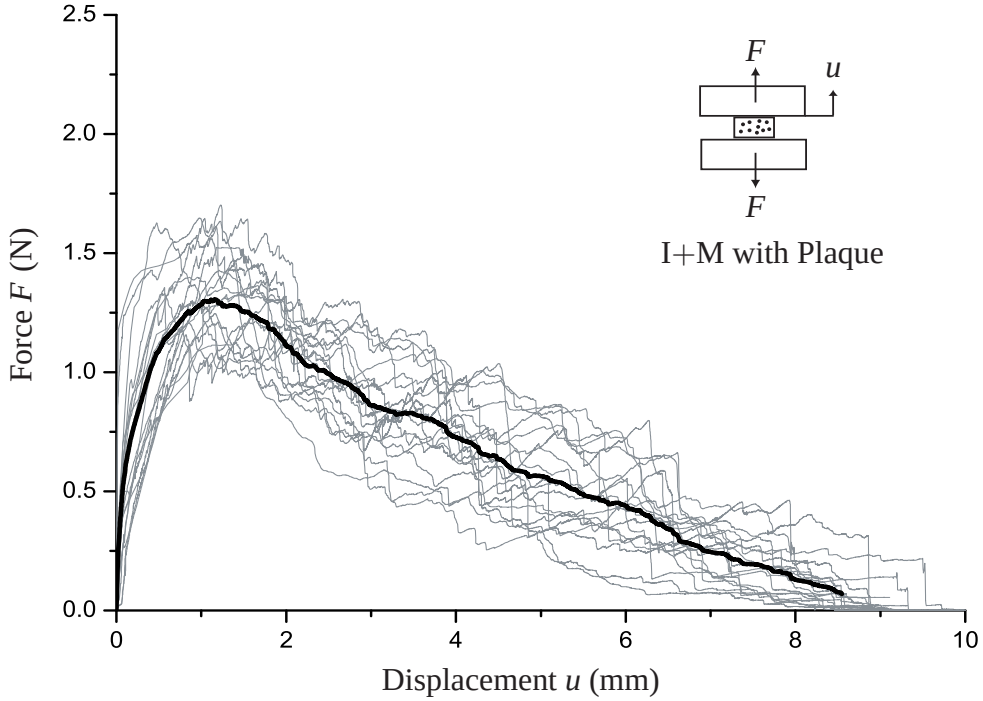

Figure 2.9: Force-displacement responses of all 17 specimens during DT tests of the intima and media, with atherosclerotic plaque (I+M with plaque). The thick curve characterizes the mean response.

Table 2.3: Calculated radial failure stress of the coin-shaped specimen in DT tests.

DT test	*Radial failure stress* $F_{\max}/(d^2\pi/4)$ in kPa	*Displacement u in mm*
A+M interface	132 ± 20	1.0 ± 0.4
Media	124 ± 25	0.4 ± 0.2
I+M interface	110 ± 12	0.6 ± 0.3
I+M with Plaque	104 ± 24	1.1 ± 0.4

Additionally, it is intriguing to investigate the (average) force-displacement behaviors of the specimens in the different regions I, II and III (compare with Fig. 2.3) by calculating the mean curves for each type of DT test (see Figs. 2.10 and 2.11). Note that the atherosclerotic plaque often deposits at certain areas in the region I, the central region of the carotid bifurcation, and in some cases it also deposits in the region II, but plaques are hardly seen in the region III. Consequently, the mean curves only in the regions I and II are shown in Fig. 2.11(b).

2.3.3 Peeling test

Figures 2.12-2.16 show the measured peeling force per width (force/width) in mN/mm versus the path l of the dissection in mm that occurs during the peeling test. The results are shown for strips taken from seven different locations at the bifurcation, see the regions indicated in Fig. 2.4. Each jagged curve (thin and grey) characterizes the resisting performance of the tissue components during a peeling test, and the mean response of the tissue tests is represented by a computed thick black curve. The arithmetic mean values of the force/width F_{pa} and F_{pc} for each type of peeling test are summarized in Table 2.4. The related external work $W_{\mathrm{a}}^{\mathrm{ext}}$ and $W_{\mathrm{c}}^{\mathrm{ext}}$, the elastic energy $W_{\mathrm{pa}}^{\mathrm{elastic}}$ and $W_{\mathrm{pc}}^{\mathrm{elastic}}$, and the dissection energy $W_{\mathrm{pa}}^{\mathrm{dissect}}$ and $W_{\mathrm{pc}}^{\mathrm{dissect}}$ per reference area are summarized in Tables 2.5, 2.6 and 2.7, respectively.

2.3.4 Histology

Two histological images (EvG) of the dissected surfaces between the adventitia-media and the media-intima after DT tests are shown in Fig. 2.17. These images belong to the samples S748/08 and S148/08 for which the related force-displacement responses are shown the thick and dotted red curves in the Figs. 2.7 and 2.8. The morphology of the dissected surfaces and related rupture locations for the circumferential and axial peeling tests at the adventitia-media and media-intima interfaces, and within the media are shown

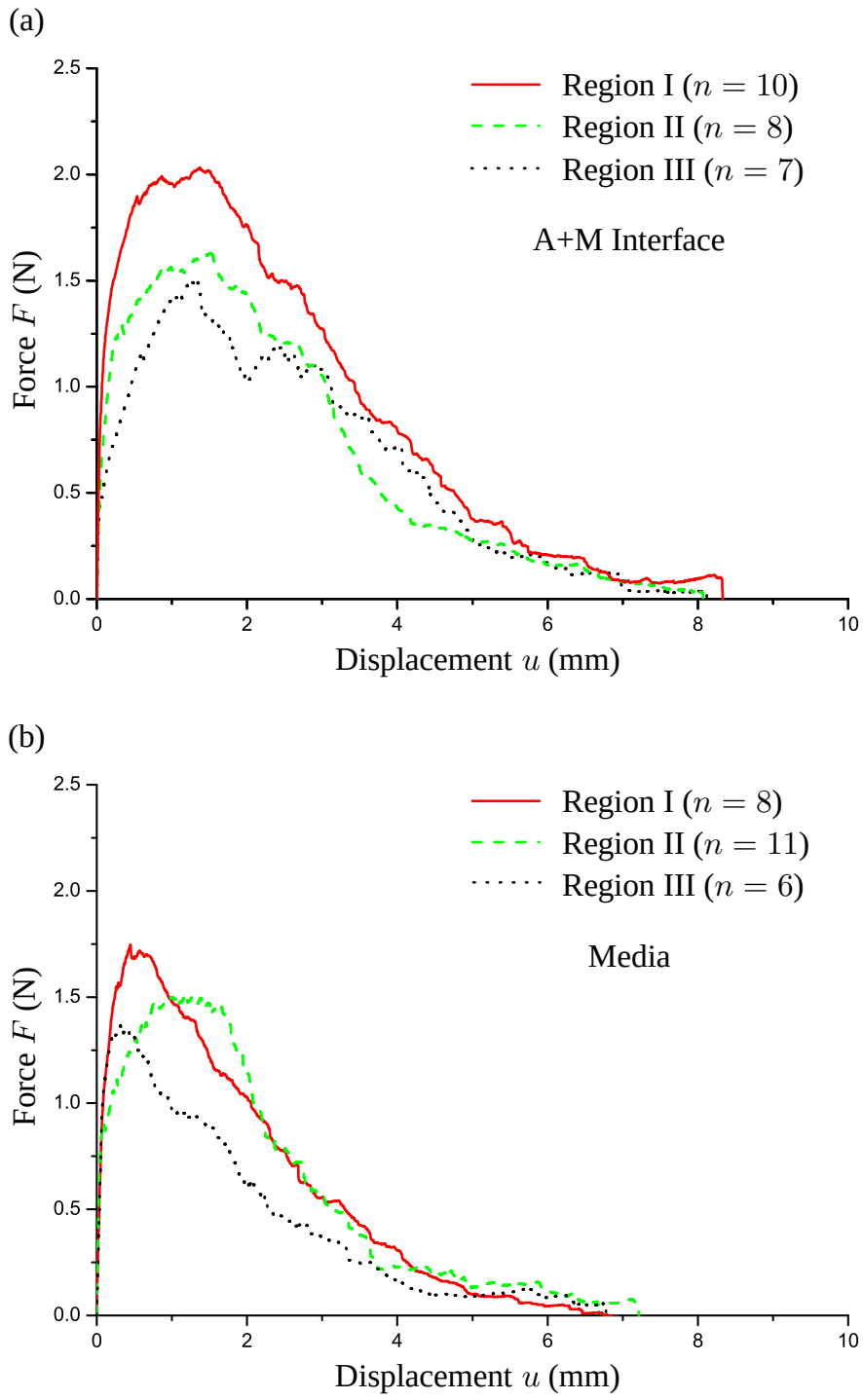

Figure 2.10: Mean force-displacement response of the coin-shaped specimens in the regions I, II and III (compare with Fig. 2.3) during the DT tests of (a) the interface between the adventitia and media, and (b) the media.

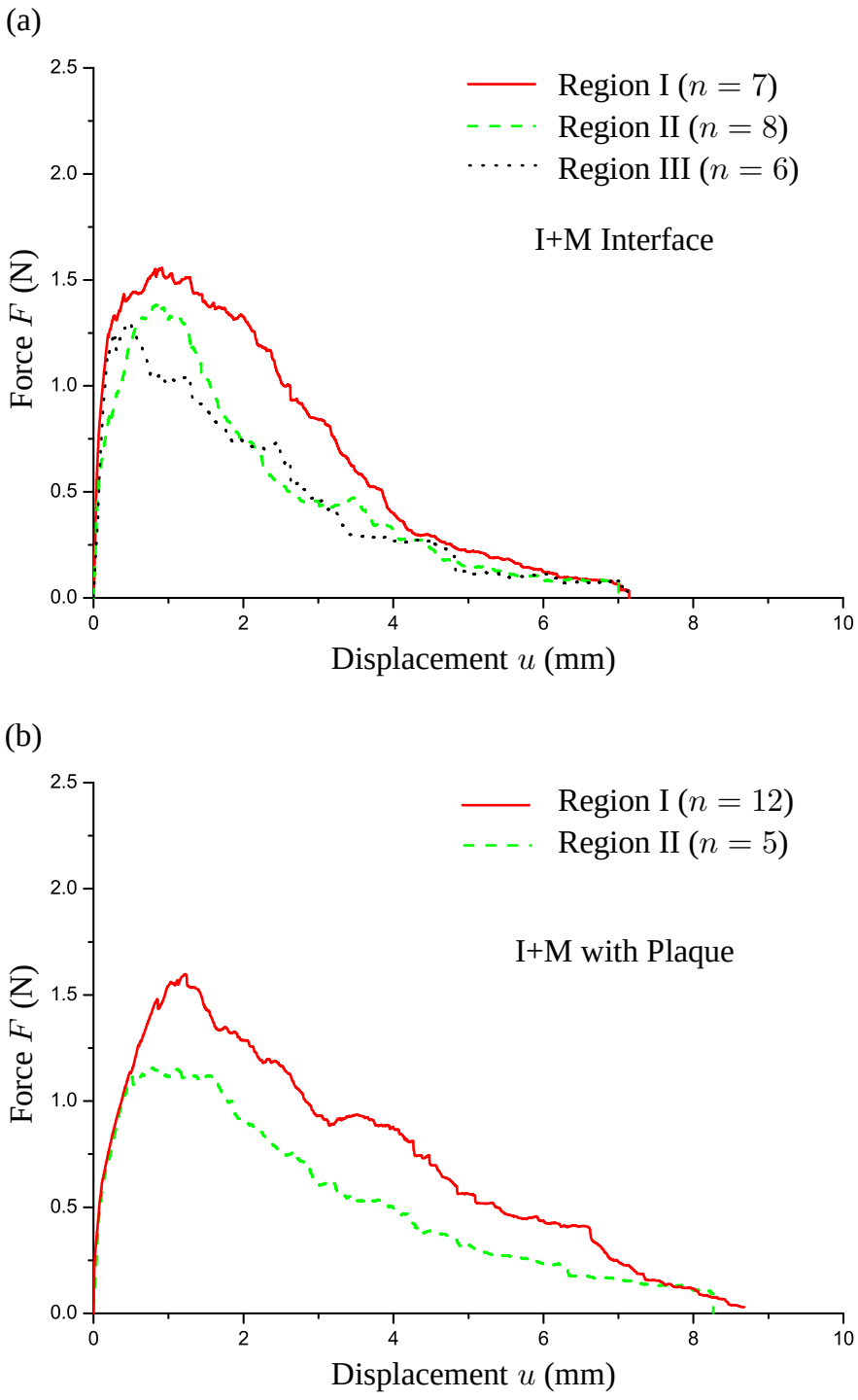

Figure 2.11: Mean force-displacement response of the coin-shaped specimens in the regions I, II and III (compare with Fig. 2.3) during the DT tests of (a) the interface between the intima and media and (b) the intima-media with atherosclerotic plaque.

in Fig. 2.18. The mechanical responses during the peeling tests, in particular the relation between force/width F/w and the path l, of those sample for which the morphology is shown in Fig. 2.18, are indicated by the thick and dotted red curves in the Figs. 2.12-2.16.

2.4 Discussion

All tests were performed with an extension rate of 1.0 mm/min, which may or may not be a physiological value. No clinical or mechanical data regarding the speed with which a dissection propagates in an in vivo situation are yet available. The dissection properties may be rate dependent.

In Fig. 2.7 the steep slope of the mean curve in the initial (first) phase points to an elastic tissue response under the applied extension force until a limit of about 1.1 N. Subsequently, the mechanical response of the tissue components enters into the second phase in which the resisting force continues to increase but strongly nonlinear, and some tissue defects start to generate, mainly on the micro-scale, see MacLean et al. [110] and Makita et al. [114]. In this phase the stiffness decreases gradually with increasing tissue damage [91, 173]. The mean curve goes upwards until the limit force of $F_{\max} = 1.7 \pm 0.3$ N ($n = 25$) is reached which is at the displacement of about $u = 1.0 \pm 0.4$ mm (see Table 2.3). The related radial failure stress may be evaluated as $F_{\max}/(d^2\pi/4) = 132 \pm 20$ kPa ($n = 25$), see also Table 2.3. After reaching the limit force, the mechanical tissue response turns into the third phase characterized by a decreasing force which is accompanied by local dissection until complete tissue failure.

Similar mechanical responses and the same failure mechanism occur during DT tests of the media and the interface between the intima and the media, see Figs. 2.7 and 2.8, respectively. Thereby, the limit force is $F_{\max} = 1.6 \pm 0.3$ N ($n = 25$) which occurs at a displacement of $u = 0.4 \pm 0.2$ mm and the related failure stress of the media is $F_{\max}/(d^2\pi/4) = 124 \pm 25$ kPa ($n = 25$), whereas the failure stress at the interface between the intima and media is $F_{\max}/(d^2\pi/4) = 110 \pm 12$ kPa ($n = 21$) (see Table 2.3), which is significantly lower than for the media ($p = 0.022$; Student's t-test with a p-value less than 0.05 determining significance).

The tested intima-media specimens with atherosclerotic plaques are usually very thick (see Table 2.1) and stiff due to atherosclerotic intimal thickening associated with calcification and a variety of non-atherosclerotic factors (see Glagov et al. [60, 62] and Bots et al. [15]). The mean mechanical response, see Fig. 2.9, shows a nonlinearly dominated increase in the first two phases before the maximum force of $F_{\max} = 1.3 \pm 0.3$ N ($n = 17$) is reached, at which $u = 1.1 \pm 0.4$ mm. The related radial failure stress is estimated as 104 ± 24 kPa ($n = 17$). Subsequently the decreasing force represents continuous dissections of the diseased intima-media until complete tissue separation.

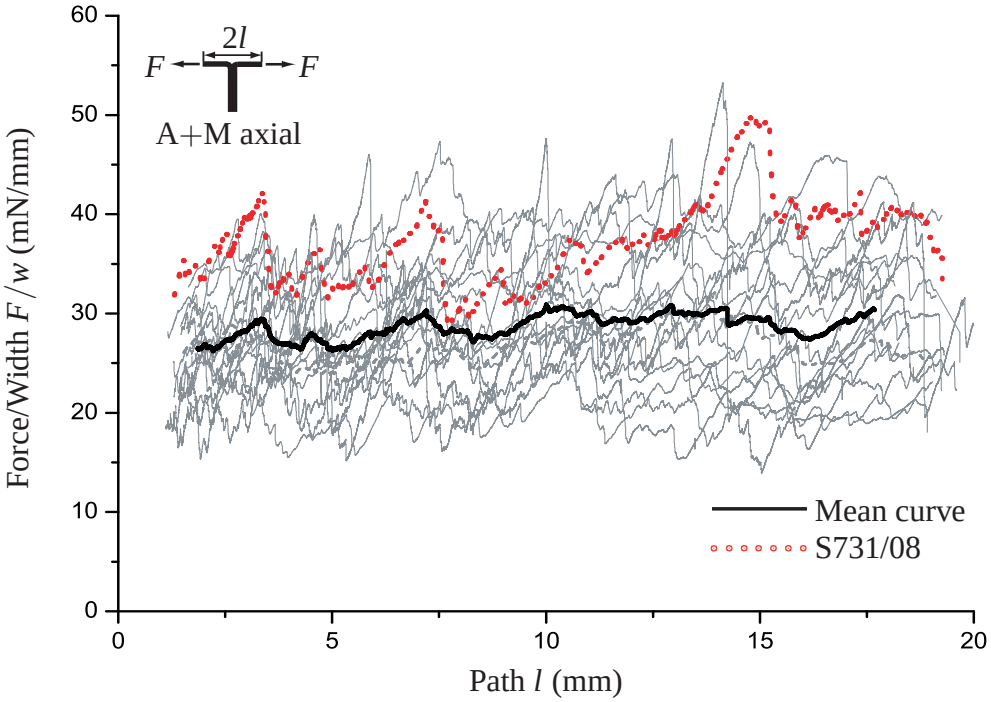

Figure 2.12: Force/Width with respect to the dissection path for all 18 rectangular strips in the axial peeling test of the interface between the adventitia and media. The thick curve represents the mean responses of the individual tissue tests. The red dotted line represents the mechanical behavior of the sample S731/08.

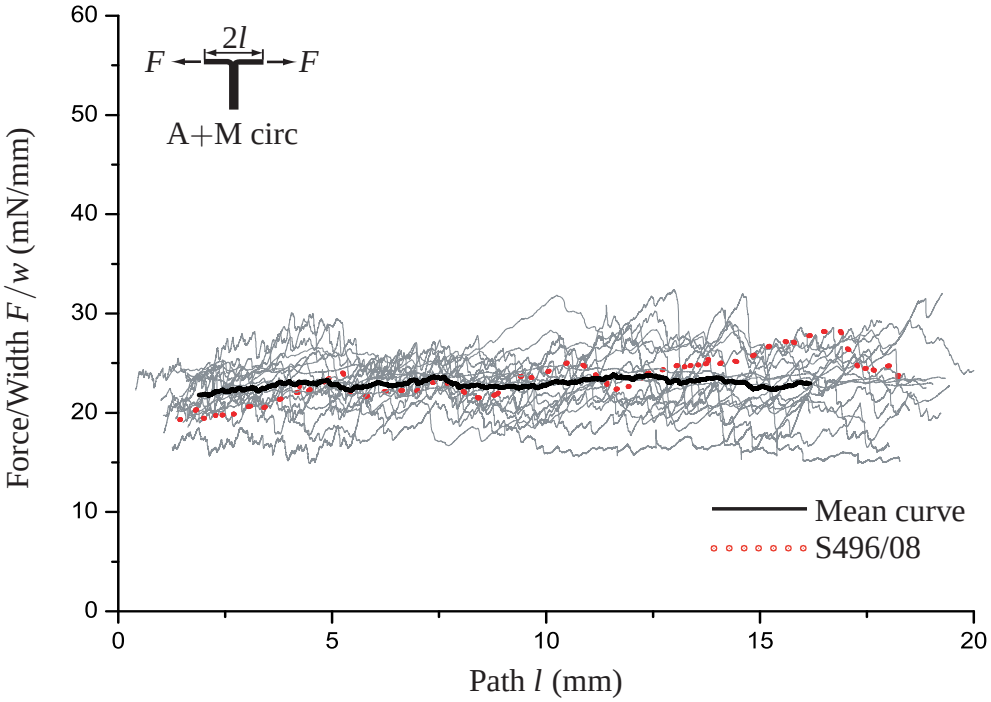

Figure 2.13: Force/Width with respect to the dissection path for the 19 rectangular strips in the circumferential peeling test of the interface between the adventitia and media. The thick curve characterizes the arithmetic mean response. The mechanical behavior of the individual sample S496/08 is indicated by the red dotted line.

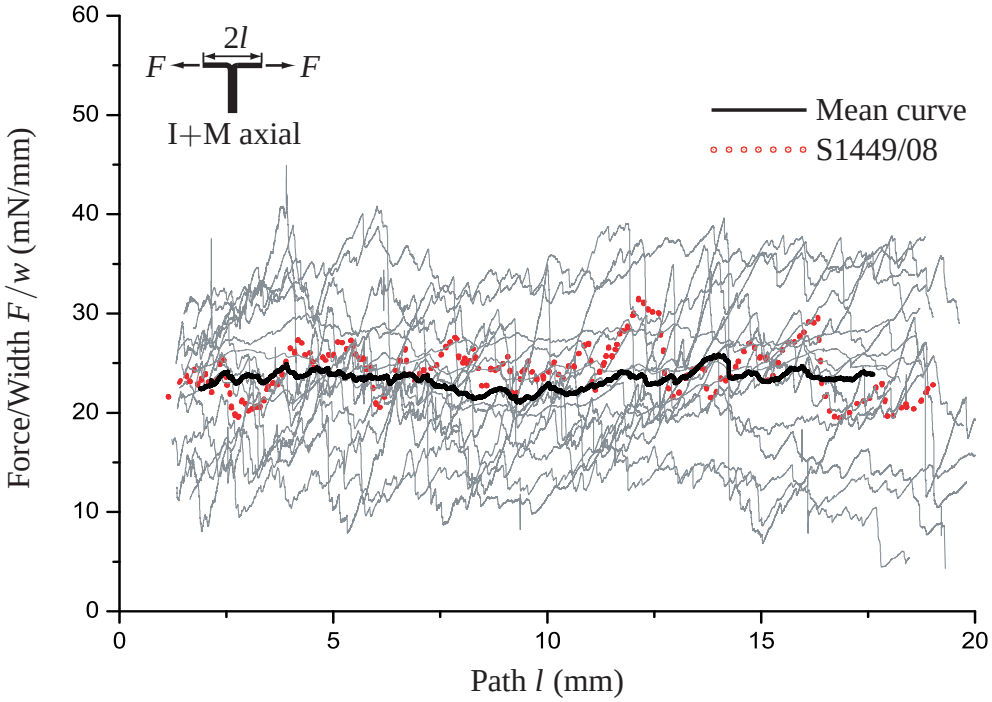

Figure 2.14: Force/Width versus the dissection path for all 17 rectangular specimens in the axial peeling test of the interface between the intima and media. The thick curve captures the mean responses of the individual tissue tests. The red dotted line characterizes the mechanical behavior of the sample S1449/08.

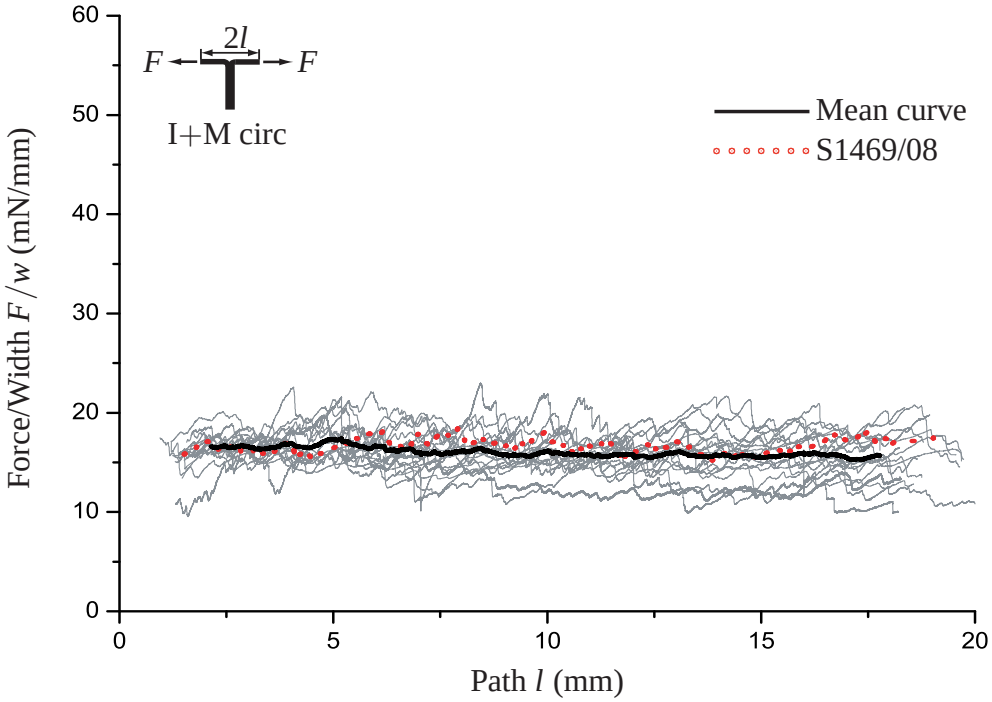

Figure 2.15: Force/Width versus the dissection path for the 18 rectangular strips in the circumferential peeling test of the interface between the intima and media. The arithmetic mean response is characterized by the thick curve. The red dotted line captures the mechanical behavior of the sample S1469/08.

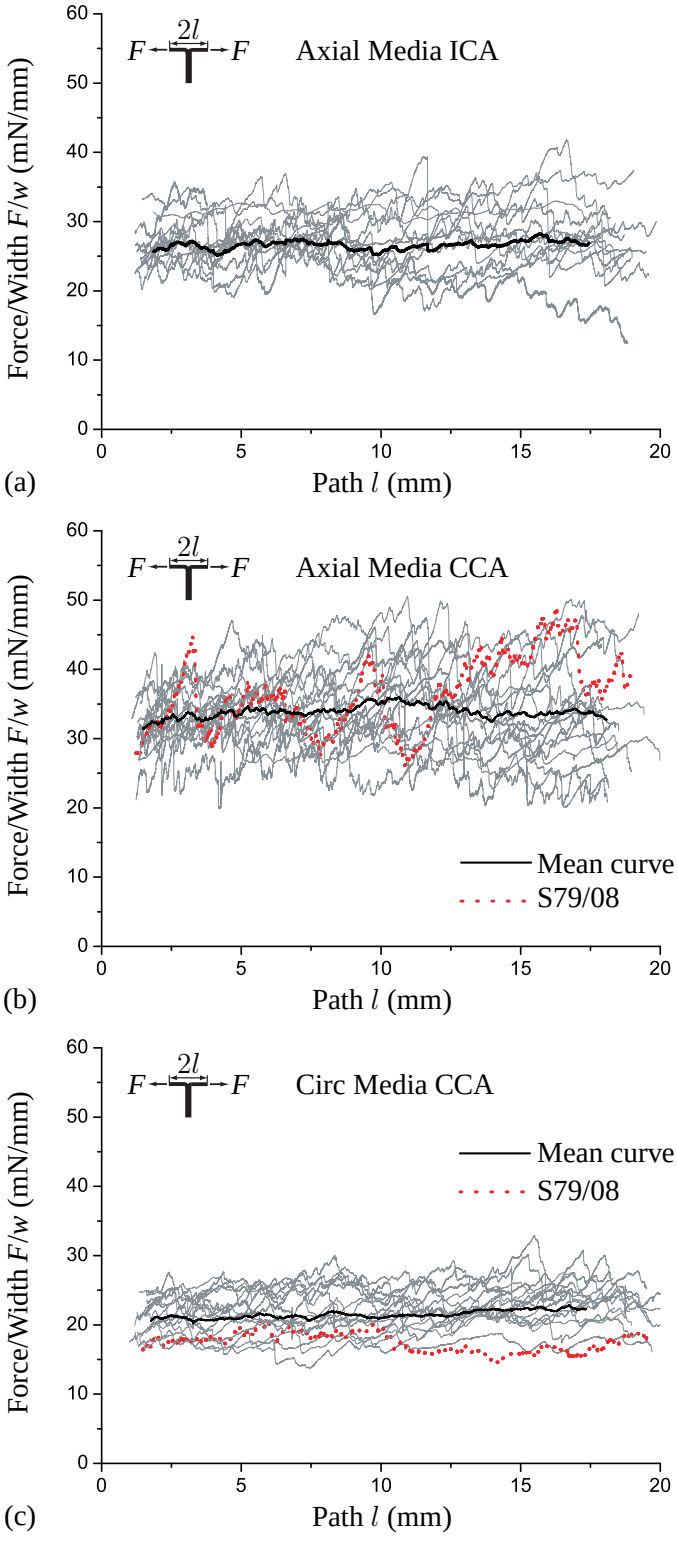

Figure 2.16: Force/Width versus the dissection path for the rectangular strips during the peeling test of (a) the media M 1 in axial direction ($n = 14$), from the ICA, (b) the media M 2 in axial direction ($n = 17$) and (c) the media in circumferential direction from the CCA ($n = 16$). The thick curve in each figure characterizes the arithmetic mean value. For the respective tissue location see Fig. 2.4.

Table 2.4: Mean values of the Force/Width F_{pa} and F_{pc} of all rectangular strips during peeling tests taken from seven different locations, compare with Fig. 2.4. The axial media strip 1 from the ICA and the axial media strip 2 from the CCA are denoted by M 1 and M 2, respectively.

Peeling test	*Force/Width (axial)* F_{pa} in mN/mm	*Force/Width (circumferential)* F_{pc} in mN/mm
A+M Interface	29.1 ± 12.2	22.7 ± 4.5
I+M Interface	23.3 ± 13.8	16.4 ± 3.3
Media	M 1: 26.9 ± 7.1 M 2: 33.7 ± 10.9	21.5 ± 4.2

Table 2.5: External work W_a^{ext} and W_c^{ext} of all rectangular strips during the peeling test. M 1 and M 2 represent the axial media strip 1 from the ICA and the axial media strip 2 from the CCA, respectively; for the specific arterial regions see Fig. 2.4.

External work	*Axial peeling* W_a^{ext} in mJ/mm	*Circumferential peeling* W_c^{ext} in mJ/mm
A+M Interface	1.08 ± 0.46	0.84 ± 0.17
I+M Interface	0.86 ± 0.52	0.61 ± 0.12
Media	M 1: 0.99 ± 0.26 M 2: 1.26 ± 0.41	0.80 ± 0.16

Table 2.6: Elastic energy $W_{pa}^{elastic}$ and $W_{pc}^{elastic}$ stored in the rectangular strips during the different peeling tests. M 1 and M 2 represent the axial media strip 1 from the ICA and the axial media strip 2 from the CCA, respectively; for the specific arterial regions see Fig. 2.4.

Elastic energy	*Axial peeling* $W_{pa}^{elastic}$ in mJ/mm	*Circumferential peeling* $W_{pc}^{elastic}$ in mJ/mm
A+M Interface	0.103 ± 0.043	0.080 ± 0.015
I+M Interface	0.084 ± 0.05	0.053 ± 0.010
Media	M 1: 0.095 ± 0.029 M 2: 0.121 ± 0.035	0.072 ± 0.013

Table 2.7: Dissection energy $W_{pa}^{dissect}$ and $W_{pc}^{dissect}$ per reference area generated by the rectangular strips during the different peeling tests. M 1 and M 2 represent the axial media strip 1 from the ICA and the axial media strip 2 from the CCA, respectively; for the specific arterial regions see Fig. 2.4.

Dissection energy	*Axial peeling* $W_{pa}^{dissect}$ in mJ/cm^2	*Circumferential peeling* $W_{pc}^{dissect}$ in mJ/cm^2
A+M Interface	6.5 ± 2.7	5.0 ± 1.0
I+M Interface	5.2 ± 3.1	3.6 ± 0.72
Media	M 1: 6.0 ± 1.6 M 2: 7.5 ± 2.4	4.8 ± 1.0

Hence, the radial failure stress (mean value) at the interface between the adventitia and the media is the highest among the four types of DT tests. This failure stress is slightly lower than that of the human abdominal aortic media, i.e. $F_{max}/(d^2\pi/4) = 140.1 \pm 15.9$ kPa, where $F_{max} = 1.76 \pm 0.20$ N at $u = 0.85$ mm, see Sommer et al. [173]. There is no significant difference in radial failure stress between the media layer at the carotid bifurcation and the abdominal aortic media [173] ($p = 0.09$) or between the media and the adventitia-media interface of the present study ($p = 0.19$). However, the radial failure stress of the media is remarkably larger than the failure stresses measured in the other two types of DT tests, i.e. healthy intima-media interface ($p = 0.022$) and the diseased intima-media with atherosclerotic plaque ($p = 0.014$). Obviously the mean radial failure stress involved in the diseased intima-media with atherosclerotic plaque is the lowest among all types of DT tests. This suggests that radial rupture within the arterial wall at the carotid bifurcation is more likely to occur for either the atherosclerotic intima-media layer or the interface between the healthy intima and media when compared with the healthy media or the adventitia-media interface (compare with Table 2.3).

Moreover, as can be seen from Figs. 2.10 and 2.11, the maximum average force that can be applied on the specimens from region I (see Fig. 2.3) is significantly larger than those obtained from the other regions, indicating that the radial strength of the tissue in that 'center' of the human carotid bifurcation is higher than elsewhere.

A total of 18 axial and 19 circumferential peeling curves are shown in Figs. 2.12 and 2.13, respectively. The average calculated resisting forces per width of the axial peeling test $F_{pa} = 29.1 \pm 12.2$ mN/mm ($n = 18$) is significantly larger than that of the circumferential strips, i.e. $F_{pc} = 22.7 \pm 4.5$ mN/mm ($n = 19$) ($p = 0.039$). In Addition, as can be seen from these figures, the standard deviation for the resisting force is much higher for axial samples than for circumferential one.

Similar results are obtained for the peeling test of the interface between the intima and the media (see Figs. 2.14 and 2.15). The average peeling force/width of all 17 individual

axially oriented test strips is $F_{pa} = 23.3 \pm 13.8$ mN/mm ($n = 17$), whereas in the circumferential direction this values is much lower, $F_{pc} = 16.4 \pm 3.3$ mN/mm ($n = 18$) ($p = 0.041$). Also here the standard deviation for the resisting force is much higher for axial samples than for circumferential one.

Two axial and one circumferential strip from the media were cut from the carotid bifurcation, see Fig. 2.4. Of interest is that the axially oriented media strip 1, from the ICA, has a lower resisting force/width $F_{pa1} = 26.9 \pm 7.1$ mN/mm ($n = 14$) compared with the axial media strip 2, from the CCA, with $F_{pa2} = 33.7 \pm 10.9$ mN/mm ($n = 17$), see Figs. 2.16(a) and (b). Although the difference between these two values is not so statistically significant ($p = 0.054$), these results clearly indicate that dissection properties of the carotid media vary with location throughout the bifurcation. As for the circumferential media strip, the mean force/width value is $F_{pc} = 21.5 \pm 4.2$ mN/mm ($n = 16$), see Fig. 2.16(c), and is strikingly lower than that of the axial media strip 2 ($p = 0.002$), which indicates the anisotropic dissection properties of the media at the carotid bifurcation. Note that the same point has been reported and highlighted for the human abdominal aortic media by Sommer et al. [173].

Remarkably, Table 2.7 suggests that a lower dissection energy $W_{pa}^{dissect}$, $W_{pc}^{dissect}$ per reference area is required for circumferential peeling tests compared with axial peeling tests. The standard deviation for forces required to peel circumferential strips is much smaller than for related axial strips, and the dissection surfaces for circumferential strips turn out to be much smoother (compare Figs. 2.18(a),(c),(e) with Figs. 2.18(b),(d),(f)).

Moreover, the dissection energy generated by the axial peeling test of the media strip 2 (from the CCA), which is evaluated as $W_{pa}^{dissect} = 7.5 \pm 2.4$ mJ/cm^2 ($n = 17$), see Table 2.7, is almost the same as the dissection energy in the axial peeling test provided by Sommer et al. [173], i.e. $W_{pa}^{dissect} = 7.6 \pm 2.7$ mJ/cm^2 ($n = 7$). Regarding the axial peeling tests of the media strip 1 from the ICA, nevertheless, the related dissection energy reduces to $W_{pa}^{dissect} = 6.0 \pm 1.6$ mJ/cm^2 ($n = 14$), suggesting that a remarkably lower fracture energy is needed to propagate an axial dissection for the media in the ICA than the media in the CCA.

Finally, five axial rectangular strips (not shown in Fig. 2.4) were cut from the CCA to perform peeling tests of the interface between the adventitia and the media. Intriguingly, the results demonstrate that the average peeling force/width, which is evaluated as 34.1 ± 9.2 mN/mm ($n = 5$), is not significantly different ($p = 0.41$) with respect to the mean force/width values of the axial strips, with 29.1 ± 12.2 mN/mm ($n = 18$), that were cut from the ECA.

In the histological analysis we verified that the samples which are considered in the present study were correctly separated. That means, for example, that the media tissue did not contain any parts from the intima or the adventitia and the A+M interface did not contain any parts from the intima.

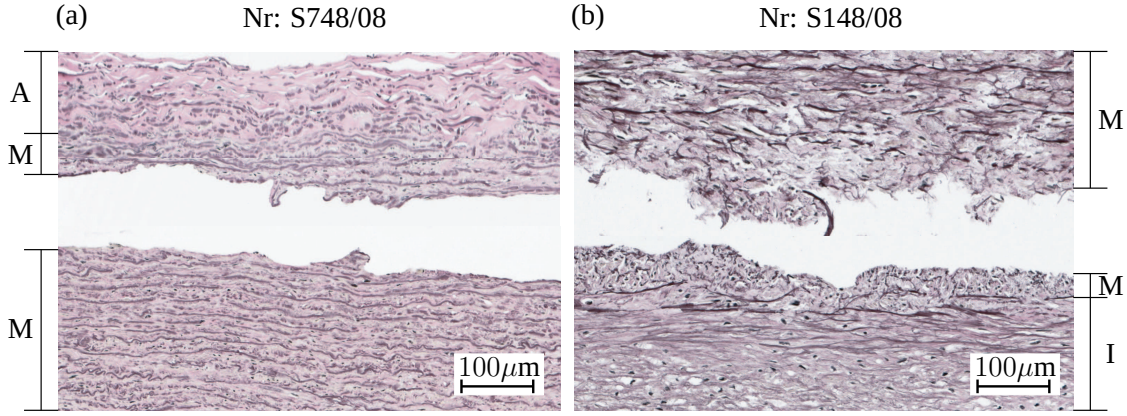

Figure 2.17: Histological images (EvG): morphology of the dissected surfaces between (a) the adventitia and the media, and (b) the media and the intima after DT tests. The related force-displacement responses of these samples are shown by dotted red curves in the Figs. 2.6 and 2.8. A, M and I represent adventitia, media and intima, respectively. Original magnification 20×.

The number of involved elastic lamellae during the dissections that occur due to the peeling tests is in average about 3-4 (see, for example, Fig. 2.18(b)). The interfacial ruptures, including both the adventitia-media and the intima-media interfaces, mainly occur in the media in both the DT and the peeling tests. However, most of these ruptures are quantified to be only about 2-5 elastic lamellae away from the external and internal elastic laminae, which are defined as the two interfaces (boundaries) among the three arterial layers [78,79]. This is reasonable, primarily because the external or internal elastic lamina is just one thin layer within the arterial wall such that an initial cut using a surgical scalpel and our hands in the specimen preparation is almost impossible to be executed exactly at that location. Our study might perhaps be improved by using a microscope, however, executing an initial cut into the interface manually under the microscope would be another challenge. In summary, from a quantitative viewpoint, compared to the thickness of the whole medial layer (approximately 40-50 elastic lamellae), the results of the histological analysis imply that the ruptured locations (2-5 elastic lamellae away from the external and internal elastic laminae, $< 8\%$) are pretty close to the interface.

Microscopical images of the peeling tests indicate that a remarkably rougher dissection surface is generated by peeling axial strips when compared with peeling strips in the circumferential direction (compare the right images in Fig. 2.18 with the left images). Table 2.4 indicates also that there occur much higher resisting forces per width with strikingly higher standard deviations during the axial peeling process when compared to the other direction. More precisely, it illustrates that the dissection in the circumferential direction disseminates mainly along or between elastic laminae, while the axial peeling frequently crosses elastic layers and even some of them cross the external or the internal elastic lam-

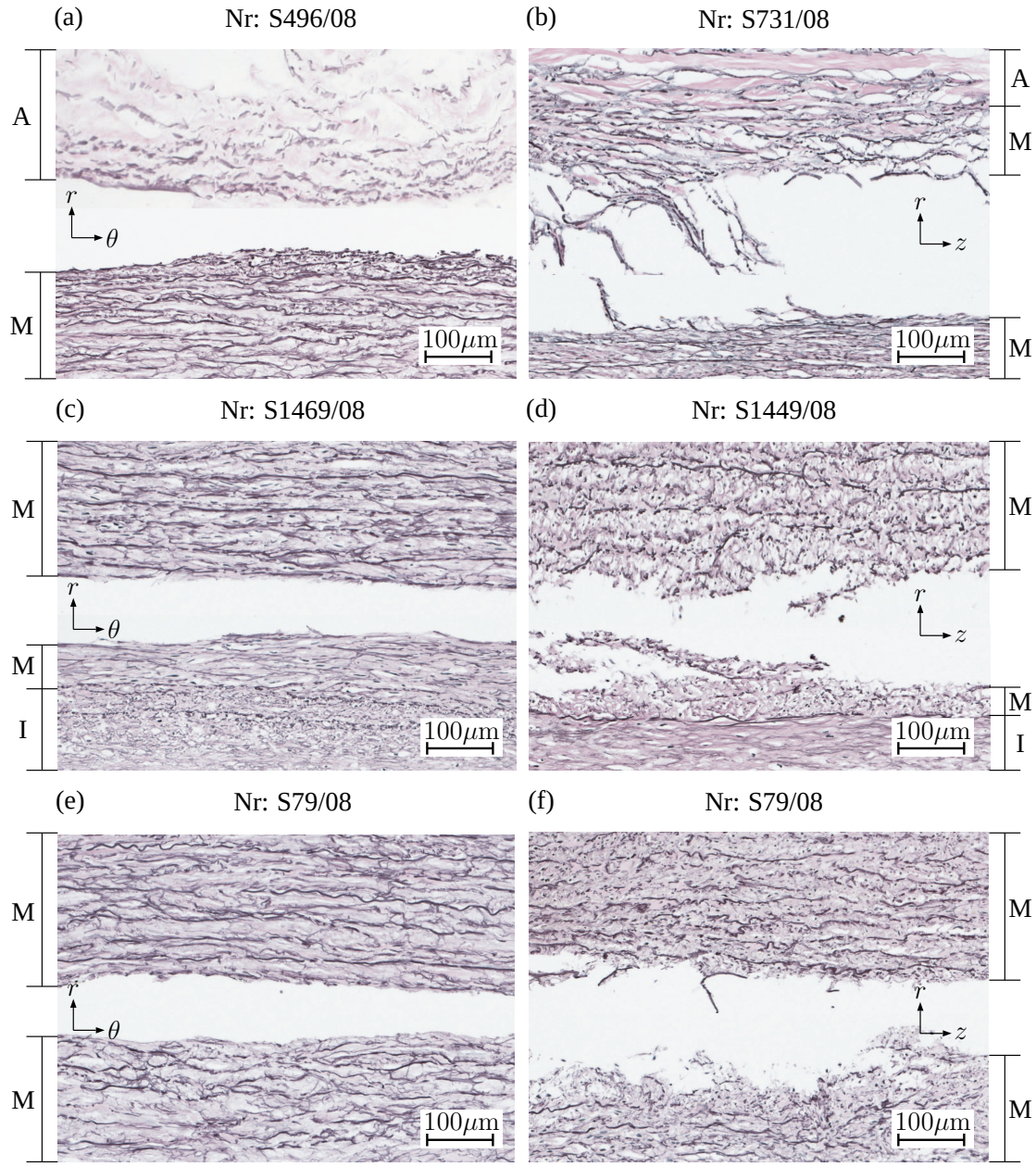

Figure 2.18: Histological images (EvG): morphology of the dissected surfaces and related rupture locations due to peeling tests for circumferential samples (left images) and axial samples (right images). Peeling the adventitia from the media (a),(b), the media from the intima (c),(d) and peeling tests for the media (e),(f) showing a relatively rough dissection surface for strips taken along the axial direction. The related mechanical responses of these samples during the peeling tests are shown by the thick and dotted red curves in the Figs. 2.12-2.16. A, M and I represent adventitia, media and intima, respectively. Original magnification 20×.

ina. Furthermore, for the medial layer the circumferentially-aligned smooth muscle cells and collagen fibers may lead to more resistance to the dissection during the axial peeling test [150, 166, 173].

As for the diseased specimens with atherosclerotic plaque in the DT tests, it is much more difficult to interpret the histology of the dissected surfaces due to several factors such as the used glue, morphologic alterations of elastic fibers, etc. However, we found that some ruptures propagated around the plaque basically following the elastic fibers. A more detailed investigation of the biomechanical properties of human atherosclerotic plaques are described in Shah [169] and Holzapfel et al. [83].

2.5 Conclusion

The results presented in this study demonstrate the dissection properties and radial mechanical strength of arterial wall tissue at human carotid bifurcation, and specifically for the tissue components at and around the interfaces between two arterial layers. This is a first and novel attempt to identify the mechanical strength of human carotid bifurcations. By comparing and analyzing these data, it is suggested that the intima-media interface rather than the adventitia-media interface or the media, is more likely to dissect due to its lower radial failure stress in the DT test and lower dissection energy required in the peeling test. Moreover, the quantified dissection energies per reference area vary for the media from the CCA to the ICA. The anisotropic dissection properties of the media at the carotid bifurcation is also depicted in the present study. Namely, a lower dissection energy is required for circumferential tissue peeling compared with axial peeling.

As we mentioned at the beginning of this work, carotid artery dissections can be caused by a variety of factors, and in several cases the dissection is more complicated than we expect, however, the finding of this study may improve clinical diagnosis and assessment [67], stent-assisted balloon angioplasty [1, 28], relevant medical device design and cardiovascular medicine.

Acknowledgement

The authors would like to thank Lukas Koeltringer, MD and Thomas Pixner for their contribution to specimen collection and histological investigation.

3 EFFECTS OF AGE ON THE ELASTIC PROPERTIES OF THE INTRALUMINAL THROMBUS AND THE THROMBUS-COVERED WALL IN ABDOMINAL AORTIC ANEURYSMS: BIAXIAL EXTENSION BEHAVIOR AND MATERIAL MODELING

Abstract The intraluminal thrombus (ILT) present in the majority of abdominal aortic aneurysms (AAA) plays an important role in aneurysm wall weakening. Studying the age-dependent elastic properties of the ILT and the thrombus-covered wall provides a better understanding of the potential effect of ILT on AAA remodeling. A total of 43 AAA samples (mean age 67 ± 6 yr) including ILT and AAA wall were harvested. Biaxial extension tests on the three individual ILT layers and the thrombus-covered wall were performed. Histological investigations of the thrombi were performed to determine four different age phases, and to correlate with the change in the mechanical properties. A three-dimensional material model was fitted to the experimental data. The luminal layers of the ILT exhibit anisotropic stress responses, whereas the medial and the abluminal layers are isotropic materials. The stresses at failure in the equibiaxial protocol continuously decrease from the luminal to the abluminal side, whereby cracks, mainly oriented along the longitudinal direction, can be observed in the ruptured luminal layers. The thrombi in the third and fourth phases contribute to wall weakening and to an increase of the mechanical anisotropy of their covered walls. The material models for the thrombi and the thrombus-covered walls are in excellent agreement with the experimental data. Our results suggest that thrombus age might be a potential predictor for the strength of the wall underneath the ILT and AAA rupture.

3.1 Introduction

Aortic aneurysms are localized balloon-shaped expansions of the aorta. About 75% of aortic aneurysms are located in the abdomen. Most abdominal aortic aneurysms are asymptomatic, are associated with smoking and high blood pressure and occur primarily in men over age 60. An untreated AAA is at high risk of rupture, which has an overall mortality rate of 90% [200]. Several factors including maximum AAA diameter, expansion rate of AAA [106,177], peak wall stress [106,204], and geometrical factors of the aneurysm [37], were explored to assess the likelihood of rupture. To date still no reliable criterion can predict the risk of AAA rupture in the final clinical decision. However, there is increasing

evidence that patient-specific biomechanical factors may be more reliable in predicting AAA rupture than currently available clinical and biochemical parameters [115].

An intraluminal thrombus (ILT), present in the majority of AAAs, is a three-dimensional fibrin structure incorporated with blood proteins, blood cells, platelets and cellular debris [72]. Many previous studies suggest that the presence of the ILT alters the wall stress distribution and reduces the peak wall stress in AAA [89, 133, 198, 204]. Thus, ILT serves as a mechanical cushion [197, 198, 204] and ILT is usually found at the rupture site of the AAAs [118]. Vorp et al. [199, 202] proposed that the ILT also serves as a barrier to the oxygen supply from the lumen, possibly causing hypoxia of the aortic wall, and local ILT thickness might be a potential predictor of AAA wall strength.

To investigate the influence of ILT on the biomechanics of AAAs, it is pivotal to study and establish its biomechanical behaviors. Wang et al. [203], e.g., carried out uniaxial extension tests to evaluate the mechanical properties of the ILT, and three individual layers (i.e., luminal, medial and abluminal layers) were identified, suggesting that ILT is a heterogeneous, nonlinear elastic and isotropic material. Later biaxial extension tests [193] showed that the luminal layer of the ILT behaves in an isotropic manner, which was consistent with the finding of previous uniaxial extension tests. Other recent mechanical studies focus on a variety of aspects regarding the ILT and correlation between the ILT and aneurysm wall weakening [93, 194]. However, the role of ILT in a rupture risk assessment of AAAs is still elusive and relevant data are lacking. Moreover, available experimental data show the biomechanical properties of the aneurysm wall [192], however, it is not clear if the wall was covered with thrombus or not.

There are three aims of the present study. The first aim is to systematically investigate the biomechanical properties of the ILT and the AAA wall underneath the thrombus via biaxial extension tests. Such experimental data lead to a better and more comprehensive understanding of the complex structure of the ILT and its potential influence on growth and remodelling of AAAs. Based on these data, the development of more appropriate 3D material models, which are able to characterise the mechanical and growth (remodelling) behaviours of the ILT and the AAA wall, is then feasible, which is the second aim. The third aim is that we seek to identify the thrombus age by means of histology, which seems to be a first attempt within AAA research.

3.2 Materials and Methods

3.2.1 Material and specimen preparation

In total, 43 AAA samples (mean age 67 ± 6 yr) including ILT and AAA wall were harvested from open surgical aneurysm repairs at the department of vascular surgery, Medical University Graz, Austria. Use of AAA material from human subjects was approved by

the Ethics Committee. The maximum AAA diameters of these patients were mostly above 5.5 cm, which is the most commonly used criterion to assess increased risk of AAA rupture [103] by clinicians. All samples, primarily from the anterior portion of the aneurysm, were stored in Dulbecco's Modified Eagle's Medium (DMEM) and tested within 6 h after retrieval. Square specimens, approximately 2×2 cm, were cut from the thickest part of the ILT sample and the corresponding AAA wall, where the local longitudinal direction was marked with a colored thread sewn by surgeons. The mean thickness of each specimen was measured using the same method as by Sommer et al. [173].

ILT heterogeneity has been reported and highlighted by several representative studies [193, 203]. In this study, for most ILT samples three individual layers (luminal, medial, abluminal) could easily be distinguished and peeled off, see Fig. 3.1. Four nylon sutures were fixed to each side of the square specimen with fish hooks and four markers were placed in a distance of approximately 6 mm from each other at the center of the specimen forming a diamond, see Fig. 3.2(a).

3.2.2 Biaxial extension tests

Square specimens were mounted in a biaxial testing device via connecting four carriages by hooked nylon sutures (Fig. 3.2(b)), and were then submerged into a bath filled with DMEM and maintained at 37.0 ± 1.0C by a heater-circulation unit (Ecoline E 200; LAUDA, LAUDA-Königshofen, Germany). The initial lengths between the two markers in each direction were also measured by a CCD camera before the start of the biaxial extension tests.

A stress-driven protocol was used during the testing procedure, where the engineering stresses (i.e. the first Piola-Kirchhoff stresses) served as a measure [76]. The non-zero stresses have the form

$$P_{\theta\theta} = \frac{f_\theta}{TX_L}, \qquad P_{LL} = \frac{f_L}{TX_\theta}, \tag{3.1}$$

where f_θ and f_L denote the measured forces in each direction, T is the mean thickness in the unloaded configuration, and X_θ and X_L are the initial dimensions of the square specimen, i.e. 2 cm, see Fig. 3.2. In this study the shear deformation was treated as negligible [80]). Each specimen was tested using the following protocols: $P_{\theta\theta} : P_{LL} = 1 : 1$, $0.75 : 1$, $1 : 0.75$, $0.5 : 1$, $1 : 0.5$, $0.25 : 1$, $1 : 0.25$ and $1 : 1$. For each protocol the ratio between the applied engineering stresses $P_{\theta\theta} : P_{LL}$ remained constant. We started with 15 kPa to do the biaxial protocol for the luminal, medial and abluminal layers, while the initially applied stress was determined to be 150 kPa for the degenerated AAA wall. Each time the load level increased by 5 kPa for the ILT and 50 kPa for the AAA wall, based on the previous stress values until mechanical ruptures occurred. Throughout the test 2 kPa/sec and 20 kPa/sec were maintained during the loading cycle for the ILT and the AAA wall,

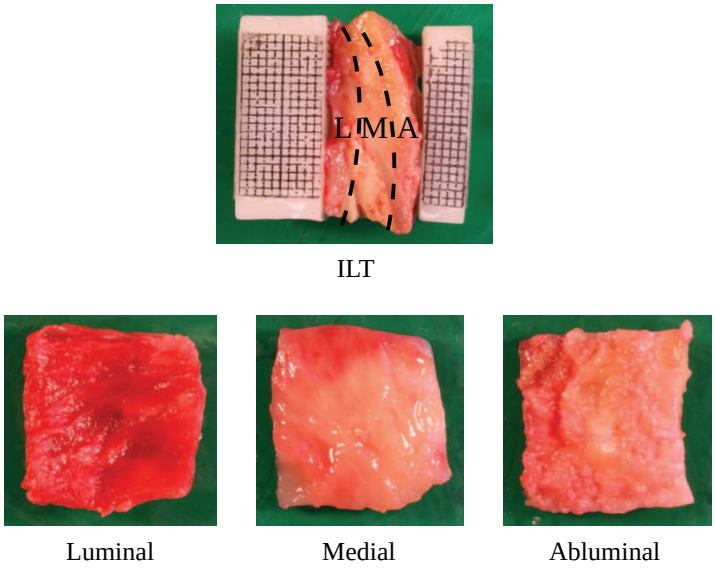

Figure 3.1: Representative photographs of cross-section of a square ILT specimen (top) and its three individual layers: luminal (L), medial (M) and abluminal (A) (bottom).

respectively. The testing was performed with ten loading and unloading cycles for each stress ratio, and the last (tenth) cycle was used for subsequent analysis.

3.2.3 Data analysis

The Cauchy stress σ and stretch λ were computed to quantify the biaxial biomechanical response of the tissue. With negligible shear components, the Cauchy stresses were determined as

$$\sigma_{\theta\theta} = \frac{f_\theta}{t x_L}, \qquad \sigma_{LL} = \frac{f_L}{t x_\theta}, \tag{3.2}$$

where t is the mean thickness of the tissue in the current configuration, and x_L and x_θ indicate the current dimensions of the square specimen along the longitudinal and circumferential directions, respectively. The assumption of incompressibility then gives $t x_L x_\theta = T X_L X_\theta$ and the Cauchy stresses can be rewritten as

$$\sigma_{\theta\theta} = \frac{f_\theta \lambda_\theta}{T X_L}, \qquad \sigma_{LL} = \frac{f_L \lambda_L}{T X_\theta}, \tag{3.3}$$

where $\lambda_\theta = x_\theta / X_\theta$ and $\lambda_L = x_L / X_L$ represent the tissue stretches in each direction, which are measured at the markers.

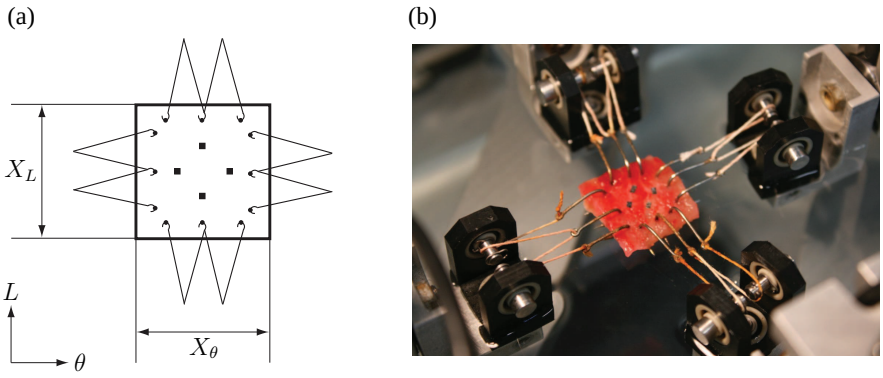

Figure 3.2: Schematic sketch of a square specimen fixed by four-sided nylon sutures associated with four markers (a); representative image of the specimen mounted in a biaxial tensile testing device (b).

3.2.4 Biaxial mechanical evaluation

For the equibiaxial stress-controlled protocol ($P_{\theta\theta} : P_{LL} = 1 : 1$), the mean peak stretch (MPS) values ($\lambda_{\theta,\max}$, $\lambda_{L,\max}$) for the three individual ILT layers and the thrombus-covered AAA walls in the circumferential and longitudinal directions were recorded and compared using paired *t*-test. The maximum tangential modulus (MTM) in the equibiaxial stress-controlled protocol was also calculated to assess stiffness, at $P_{\theta\theta} = P_{LL} = 20\,\text{kPa}$ for the thrombus and at $P_{\theta\theta} = P_{LL} = 150\,\text{kPa}$ for the AAA wall. The applied engineering stress values, which caused the specimens to rupture for the equibiaxial protocol, were averaged for each tissue type. The cracks of the ruptured specimens after biaxial testing were studied in order to summarize some key features in this regard, specifically for the ILT. All values were statistically expressed as mean $\pm$ SD.

3.2.5 Material model

To model the mechanical characteristics of both ILT and thrombus-covered wall, we used a strain-energy function Ψ which is based on a model developed for arterial walls [79, 82], i.e.

$$\Psi = \mu(I_1 - 3) + \frac{k_1}{k_2}(\exp\{k_2[(1-\rho)(I_1-3)^2 + \rho(I_4-1)^2]\} - 1), \tag{3.4}$$

where $\mu > 0$ and $k_1 > 0$ are stress-like parameters with dimension (kPa), and $\rho \in [0,1]$ and $k_2 > 0$ are dimensionless. By neglecting shear deformations the invariants I_1 and $I_4 > 1$

can be written as

$$I_1 = \lambda_\theta^2 + \lambda_L^2 + \lambda_r^2, \qquad I_4 = \lambda_\theta^2 \cos^2\varphi + \lambda_L^2 \sin^2\varphi, \tag{3.5}$$

where λ_θ, λ_L, λ_r in Eq. $(3.5)_1$ are the principal stretches in the circumferential, longitudinal and radial directions, respectively. Both the ILT and the thrombus-covered wall samples are assumed to be incompressible, which requires that $\lambda_r\lambda_\theta\lambda_L = 1$. In Eq. $(3.5)_2$, φ is a geometrical parameter that represents the angle between some fiber reinforcement and the circumferential direction; here φ is treated as a phenomenological variable.

The Cauchy stresses in the circumferential and longitudinal directions are $\sigma_{\theta\theta} = \lambda_\theta \partial\Psi/\partial\lambda_\theta$, $\sigma_{LL} = \lambda_L \partial\Psi/\partial\lambda_L$. Hence, with (3.5) and the incompressibility we get [80]

$$\sigma_{\theta\theta} = 2(\lambda_\theta^2 - \lambda_\theta^{-2}\lambda_L^{-2})\psi_1 + 2\lambda_\theta^2 \cos^2\varphi\,\psi_4, \tag{3.6}$$

and

$$\sigma_{LL} = 2(\lambda_L^2 - \lambda_L^{-2}\lambda_\theta^{-2})\psi_1 + 2\lambda_L^2 \sin^2\varphi\,\psi_4, \tag{3.7}$$

where the abbreviation $\psi_i = \partial\Psi/\partial I_i$, $i = 1,4$, has been used. Note that the stress relations (3.6) and (3.7) are valid for zero shear deformation. The related shear stress $\sigma_{\theta L}$ then has the form $\sigma_{\theta L} = \lambda_\theta\lambda_L \sin 2\varphi\,\psi_4$, see Holzapfel and Ogden [80].

The data from the five biaxial protocols ($P_{\theta\theta} : P_{LL} = 1:1$, $0.75:1$, $1:0.75$, $0.5:1$, $1:0.5$) for each ILT and wall specimen associated with the circumferential and longitudinal directions were simultaneously fit to the material model (3.4) by using the optimization toolbox 'lsqnonlin' in Matlab 7.0. Consequently, the five parameters $(\mu, k_1, k_2, \varphi, \rho)$ were obtained. To measure the 'goodness of fit' the square of the Pearson correlation coefficient was computed for both the circumferential and the longitudinal Cauchy stresses.

3.2.6 Histology

After mechanical testing the specimens were fixed in 10% neutral-buffered formalin (pH 7.4), embedded in paraffin using standard techniques and prepared for histological investigations. Consecutive histological sections were cut at 4 μm and stained with Hematoxylin and Eosin (HE), Prussian blue (PB), Elastica van Gieson (EvG), Gömöri methenamine Silver stain (G) or Mallory-Cason Trichrome (also known as SFOG) to determine different specimen compositions. Subsequently, the sections were examined under a light microscope to study the thrombus compositions with regard to presence or absence of erythrocytes (SFOG), vital lymphocytes (HE) remaining from the blood stream, macrophages (HE), iron deposits (PB) from degraded erythrocytes, reticulin fibers (G), collagen fibers (G and EvG) and fibrin compositions (SFOG) with morphological differentiation between loose fibrin network or homogenized fibrin and other homogenized proteins. Statistical

analysis was then performed to quantify the relative percentage of cellular contents for each specimen. We postulate a four-phase thrombus evolution within the AAA; phase I (very fresh), phase II (young), phase III (intermediate), phase IV (old).

3.3 Results

In total 33 luminal, 22 medial, 12 abluminal layers and 14 thrombus-covered walls were tested and analyzed. The mean (outer) diameter of the AAA samples was 6.0 ± 0.9 cm ($n = 43$) with a mean patient age of 67 ± 6 yr. The mean measured thicknesses for the individual luminal, medial and abluminal layers were 2.53 ± 0.45 mm, 2.86 ± 0.37 mm and 2.15 ± 0.29 mm, respectively. The thickness of the AAA wall under the thrombus was 2.27 ± 0.23 mm. Highly degraded abluminal layers were often found to be very weak, greatly increasing the possibility of mechanical failure even at a very low load level. Clinical data of 36 patients are summarized in Table 3.1.

3.3.1 Biaxial mechanical response

Intraluminal thrombus (ILT). The MPS and MTM values in the equibiaxial stress-controlled protocol ($P_{\theta\theta} = P_{LL} = 20$ kPa) for the luminal, medial, abluminal layers and the fresh thrombi are summarized in Table 3.2. There is a clear indication of mechanical anisotropy for several luminal layers ($n = 10$), where the MPS $\lambda_{\theta,\max}$ and $\lambda_{L,\max}$ for the equibiaxial stress-driven protocol were 1.17 ± 0.03 and 1.09 ± 0.02, respectively ($p < 0.01$). The MPS $\lambda_{L,\max}$ was found to be significantly smaller than for samples which behaved isotropically ($p = 0.01$), whereas there was no significant difference in $\lambda_{\theta,\max}$ between both groups ($p = 0.25$). For the medial ($n = 22$) and abluminal ($n = 12$) layers, there was no significant difference in both MPS and MTM values in the circumferential and the longitudinal directions. Furthermore, the MPS for the abluminal layers were found to be significantly larger than those of both luminal and medial layers at the same stress level (all p values less than 0.01), suggesting a continuous increase in extensibility and decrease in stiffness from the luminal to the abluminal side in the biaxial mechanical behavior of the ILT. The Cauchy stress-stretch plots in Fig. 3.3 show the biaxial data (symbols) of the different ILT tissues.

Fresh thrombus. In this study 4 pieces of dark-red fresh thrombi harvested from four different patients (66 ± 3.6 yr, 4 males) were tested. The mean thickness was 6.87 ± 0.51 mm. Intriguingly, they were all not layer specific and homogeneous; they behaved isotropically under biaxial loading. Their biaxial mechanical behaviors were quite similar to the abluminal layers of old thrombi, see Figs. 3.3(g),(h), and subsequent Fig. 3.6.

Table 3.1: Clinical data of 36 patients whose AAA samples were succeeded in testing.

No.	Age (yr)	Gender	Max. D (cm)	Thromb. Age (phases)	Approx. time (from CT to OP)	TC (G/l)	CRP (mg/l)	FIB (mg/l)	Status
14	64	M	5	II	$>$ 3 months	199	32.9/+	695/+	a
15	53	M	8	IV	1 day	274	86.1/+	709/+	s
16	67	M	5.8	II	1 month	276	5.9	464/+	a
17	60	M	6	(–)	2 weeks	246	2.8	410/+	a
18	67	M	6.5	I, II, IV	4 days (Rup)	212	114.9/+	553/+	s
20	71	M	6.5	II	$>$ 1 month	272	11.3/+	574/+	a
21	69	M	7.8	I, III	1 month	194	21.8/+	624/+	a
22	63	F	5.5	II	$>$ 6 months	280	5.1	271	a
23	73	M	6.5	III	1 day	299	24.1/+	590/+	a
24	68	M	5.3	II	$>$ 3 months	192	$<$ 1.0	239	a
25	69	F	5	(–)	$>$ 1 month	209	6.1	461/+	a
26	66	M	6	II	$>$ 1 month	294	3.8	433/+	a
27	74	M	6	III	6 days	134/-	1.1	237	s
28	68	M	6.6	IV	5 days	171	3.0	481/+	s
29	67	M	6	III	1 week	278	18.2/+	570/+	s
31	59	M	6	(–)	1 week	249	3.8	318	a
32	64	M	6	II	$>$ 2 months	184	3.0	384	a
34	61	M	5.5	I, II	$>$ 3 months	168	1.8	364	a
35	66	M	6	II	2 weeks	225	4.7	327	a
37	69	M	5	IV	6 days	161	$<$ 1.0	299	a
38	63	M	5.3	II	2 months	284	5.1	401/+	a
39	68	M	5	(–)	3 months	203	$<$ 1.0	358	a
40	71	M	5	II	5 months	184	15.6/+	543/+	a
41	68	M	7	II	12 days	187	1.9	334	a
42	75	M	4.2	(–)	$>$ 2 months	251	$<$ 0.6	353	a
43	72	F	7	IV	3 days	222	9.3/+	403/+	a
44	65	M	6.6	II	1 month	234	2.0	383	a
46	71	M	7.5	III	1 week	210	5.9	359	a
47	50	M	6	II	1 month	228	4.7	441/+	a
50	59	M	7.5	IV	5 days	293	1.4	425/+	a
51	69	M	5.7	(–)	$>$ 1 month	290	11.0/+	381	a
53	79	M	6.5	II	$>$ 1 month	137/-	7.6	398	a
54	67	M	5.0	II	2 months	215	4.7	346	a
55	66	M	5.6	III	1 week	192	2.2	371	s
57	56	M	6.2	(–)	1 month	140	5.8	379	a

Max. D, maximum diameter; Thromb. Age in terms of phases I, II, III, IV, i.e. very fresh, young, intermediate, old thrombus; (–) means no thrombus in this patient or age determination failed; CT, X-ray computed tomography; OP, operation; (Rup) means ruptured aneurysm; TC, preoperative count of thrombocyte (normal value: $140 - 440$ G/l); preoperative CRP, C-reactive protein (normal value: -8.0 mg/l); /+ and /- denote values out of normal range; preoperative FIB, fibrinogen (normal value: $210 - 400$ mg/l); s, symptomatic; a, asymptomatic status of patient.

Thrombus-covered AAA wall. Our experimental results demonstrated that the thrombus-covered AAA walls ($n = 14$) exhibit an anisotropic exponential response associated with

Table 3.2: MPS and MTM values (Mean ± SD) in the equibiaxial stress-controlled protocol ($P_{\theta\theta} = P_{LL} = 20$ kPa) for the anisotropic luminal ($n = 10$), isotropic luminal ($n = 23$), medial ($n = 22$), abluminal layers ($n = 12$) and the fresh thrombi ($n = 4$). NS denotes no significant difference.

ILT	$\lambda_{\theta,\max}$	$\lambda_{L,\max}$	$p(\lambda)$	MTM$_\theta$ (kPa)	MTM$_L$ (kPa)	p (MTM)
Luminal (Aniso)	1.17 ± 0.03	1.09 ± 0.02	< 0.01	208 ± 55	291 ± 69	0.02
Luminal (Iso)	1.15 ± 0.05	1.13 ± 0.04	0.14	189 ± 48	206 ± 71	0.35
Medial	1.21 ± 0.03	1.20 ± 0.04	0.35	137 ± 39	145 ± 47	0.54
Abluminal	1.25 ± 0.04	1.27 ± 0.05	0.29	108 ± 31	102 ± 23	0.59
Fresh thrombus	1.29 ± 0.04	1.27 ± 0.03	0.45	90 ± 24	97 ± 19	0.66

a larger circumferential stiffness, see the symbols in Fig. 3.4. In the equibiaxial protocol ($P_{\theta\theta} = P_{LL} = 150$ kPa), the MPS and MTM values in the circumferential direction were significantly larger than those in the longitudinal direction, see Table 3.3.

Rupture stresses and cracks. The engineering stresses that caused the specimens to rupture for the luminal, medial and abluminal layers were 60.5 ± 6.2, 41.2 ± 6.5 and 27.9 ± 4.5 kPa, respectively. For the thrombus-covered walls, the mean stress leading to the mechanical failure was 356.6 ± 54.7 kPa. Interestingly, cracks were more often found along the longitudinal direction at the center of the specimens, for approximately 70% of the luminal layers in the phases II and III, see Fig. 3.5. This kind of crack was found to be independent of the hooks. However, there was no clear tendency of the cracks for the medial and abluminal layers, as well as the thrombus-covered walls, where ruptures were more likely initiated by the hooks, see also Fig. 3.5.

3.3.2 Material model

The material model (3.4) was able to fit the three individual layers of the ILT very well, with a mean R^2 of 0.92 ± 0.05, 0.93 ± 0.04, 0.93 ± 0.04 and 0.94 ± 0.03 for the luminal, medial, abluminal layers and the fresh thrombus, respectively. The model results of the ILT are shown in Fig. 3.3 as solid curves, and the related parameters μ, k_1, k_2, φ and ρ are summarized in Table 3.4.

The model (3.4) was also appropriate to characterize the biaxial mechanical responses of the thrombus-covered walls with a 'goodness of fit' R^2 of 0.93 ± 0.04. Figure 3.4 shows the analytical results predicted by the model as solid curves, and the related parameters are summarized in Table 3.5. In order to find a correlation between thrombi and the thrombus-covered walls, the wall specimens were classified in two types, i.e. (i) walls covered by the younger thrombi (phase II) and (ii) walls covered by the intermediate and old thrombi (phases III and IV), see also Table 3.5. The material model parameters for each group were then used to predict the mean stress-stretch responses of the ILT and the thrombus-covered wall, see Figs. 3.6 and 3.7, respectively.

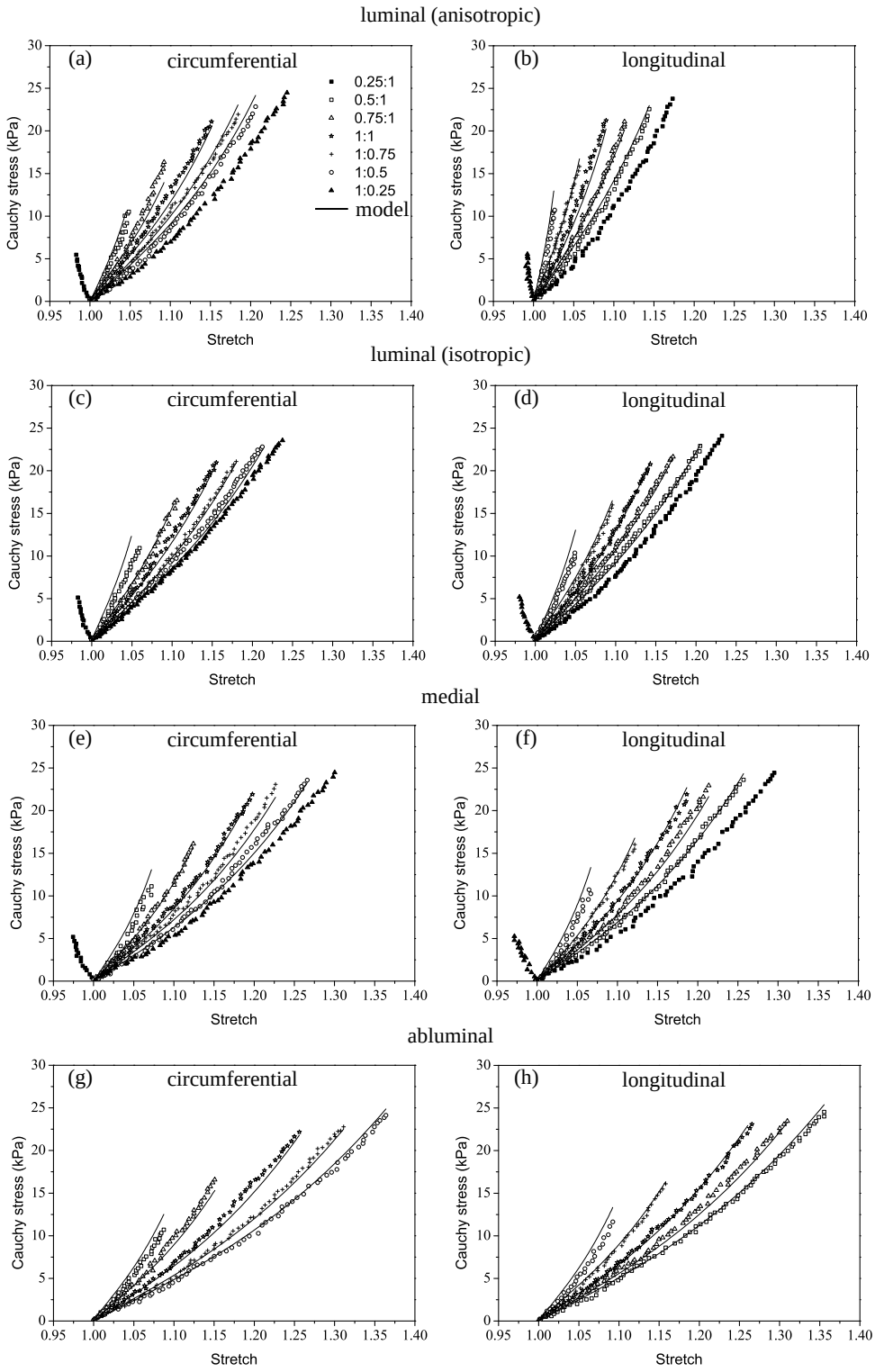

Figure 3.3: Experimental data (symbols) with corresponding material model (solid curves) for (a)-(d) the anisotropic and isotropic luminal layers, (e)-(f) the medial layers, and (g)-(h) the abluminal layers of ILT specimens (patient No. 18) in the circumferential and longitudinal directions. The legend in plot (a) applies also to all others.

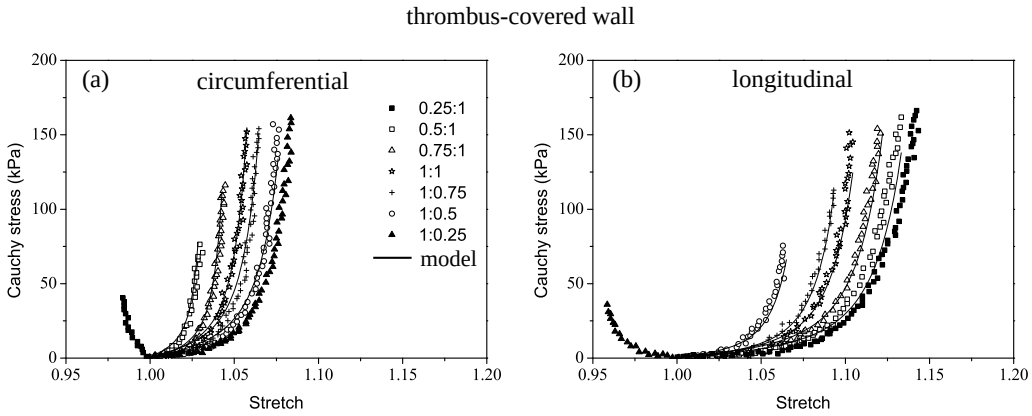

Figure 3.4: Experimental data (symbols) for a thrombus-covered wall during biaxial extension tests with corresponding material model (solid curves) in (a) the circumferential and (b) the longitudinal directions (patient No. 22). The legend in plot (a) applies also to (b).

3.3.3 Histology

In the current study, 32 ILT samples succeeded in the age determination by histology. In general, the thrombi within the AAAs mainly consisted of four types of components including erythrocytes, loose fibrin network with thin bundles, fibrin network with thick bundles and homogenized proteins. During all stages neither reticulin, fibrotic fibers nor capillaries were detected, which is completely different from the thrombi in small veins and arteries [90]. Moreover, neither collagenous nor elastic fibers were existent in the ILT.

Based on the above-mentioned preliminary investigations, a four-phase thrombus evolution within AAA seems to be meaningful. In phase I (very fresh), the thrombus initially formed with almost only the erythrocytes from the blood stream. It might contain some other components, such as loose fibrin network, leucocytes, or thrombocytes, but they were all in low percentages. In phase II (young), fibrin network started to grow in a very loose manner and caught erythrocytes in between. During this phase, the thrombi had a large percentage of loose fibrin network (thin bundles) combined with relatively lower percentages of both erythrocytes and fibrin networks with thick bundles. In phase III (intermediate), the erythrocytes disrupted and proteins were washed out of the fibrin network, in which fibrin network remained and became more condensed with thick bundles. In the subsequent phase IV (old), fibrin networks disrupted and residue small proteins were more condensed as compared to the previous phase. Representative histological images and statistical quantification of the relative percentage of cellular contents in each phase are shown in Figs. 3.8(a)-(d) and Fig. 3.9, respectively. In a few cases the aneurysm wall was also available for histological examination. Elastica van Gieson (EvG) stained sections of the thrombus-covered wall showed a complete loss of elastic fibers and a loss of myocytes,

Table 3.3: MPS and MTM values (Mean ± SD) in the equibiaxial stress-controlled protocol ($P_{\theta\theta} = P_{LL} = 150$ kPa) for the thrombus-covered (TC) wall ($n = 14$).

	$\lambda_{\theta,\max}$	$\lambda_{L,\max}$	$p(\lambda)$	MTM_θ (MPa)	MTM_L (MPa)	p (MTM)
TC wall	1.07 ± 0.03	1.11 ± 0.04	0.01	8.7 ± 1.7	6.6 ± 2.7	0.02

whereas relatively more collagen fibers were clear to discern in the media, see Fig. 3.8(e). Figure 3.8(f) shows the morphological characteristics of thick and thin bundles of fibrin network.

By comparing MTM values of all specimens at the same stress level of 20 kPa, it is found that the stiffness of the thrombotic material continuously increases with thrombus age for each individual ILT layer. Simultaneously, the luminal layer may become anisotropic during this aging process, see Fig. 3.10. A strongly positive correlation between the ILT thickness and the thrombus age is also observed, see Fig. 3.11.

3.4 Discussion

In previous studies the ILT was identified as an isotropic and heterogeneous material [193, 203] by using both uniaxial and biaxial extension tests. For several luminal layers we found, however, a clear indication of mechanical anisotropy. Hence we conclude that the luminal layer of the ILT is, in general, not an isotropic tissue. We analyzed that the stiffness of the anisotropic luminal layers in the longitudinal direction is (much) larger with respect to that in the circumferential direction or to the luminal layers, which behaved isotropically, see, e.g., Fig. 3.3. However, the circumferential stiffness at $P_{\theta\theta} = P_{LL} = 20$ kPa is not significantly different for both groups. Moreover, our experimental results suggest that both medial and abluminal layers are isotropic. To the authors' knowledge no biaxial data are available in this regard prior to this study. The computed mean rupture stresses indicated that the stiffness of ILT tissues continuously decrease from the luminal to the abluminal side. It should be noted that the rupture stresses obtained in this study may not represent the stress level at which ILT rupture actually occurs. This is primarily due to the fact that a number of ruptures, specifically for the degenerated medial and abluminal layers, are initiated by the hooks on the edges, see Fig. 3.5. About 70% of the cracks in the luminal layers in phases II and III were found along the longitudinal direction. This particular crack morphology is closely related to the pore orientations, shapes and protein bonds between two neighboring pores within the fibrin networks, which prevail as a typical component in these two phases. In addition, our investigations suggest that fresh thrombi have very unique characteristics, which are, as stated previously, not layer specific and homogeneous, and which is in contrast with the old and more organized thrombi.

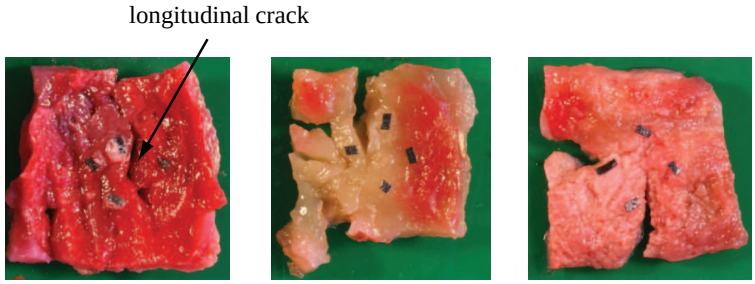

Figure 3.5: Representative images of ruptured luminal, medial and abluminal layers, where a crack along the longitudinal direction of the luminal layer is clearly indicated.

The importance of the aneurysm wall strength regarding AAA rupture assessment has been stressed by several prior studies [120, 195, 201, 204]. Our result is basically in agreement with an early study by Vande Geest et al. [192]. Compared to the normal aorta, the wall stiffening can be attributed to destruction of the long half-life elastin and failure of the collagen cross-linkage. [32] In addition, by comparing the stress-stretch responses between the aneurysm walls covered with younger thrombi (phase II) and with intermediate and old thrombi (phases III and IV) our study verifies that there is an increase in the wall anisotropy when the thrombus gets older, see Fig. 3.7. Thereby, a weakening of the wall occurs in the longitudinal direction. That may also imply that the older thrombi are related to aneurysm wall weakening.

As can be seen from Table 3.4, the model parameters μ, k_1 and k_2 continuously decrease from the luminal to the abluminal layer. In addition, both stiffness parameters μ and k_1 are highest for the anisotropic luminal and lowest for the abluminal layers, respectively. There is no significant difference in each material parameter between the abluminal layer and the fresh thrombus (all p values are larger than 0.05). This indicates that in both (low and high) loading domains the stiffness of the ILT continuously decreases from the luminal to the abluminal side, whereas the biaxial mechanical response of the fresh thrombus is quite similar to the abluminal layer. For the luminal, medial and abluminal layers, the mean values of φ approach 90°, however, as previously stated, φ is here not treated as a fiber angle. As a measure of mechanical anisotropy, ρ is significantly larger for the anisotropic luminal layers than for the isotropic ILT layers as well as the fresh thrombi (all p values are less than 0.01).

In contrast with the ILT, the thrombus-covered wall has much higher values of the stiffness parameters k_1 and k_2, representing its significant load-bearing capacity in the high loading domain. Moreover, in regard to Table 3.5, a significantly smaller value of k_2 (responsible for the higher loading domain) and a larger value of ρ indicate that walls covered by an intermediate or old thrombus, Type (ii), are much weaker in the high loading domain and more mechanically anisotropic when compared with walls covered by a young thrombus,

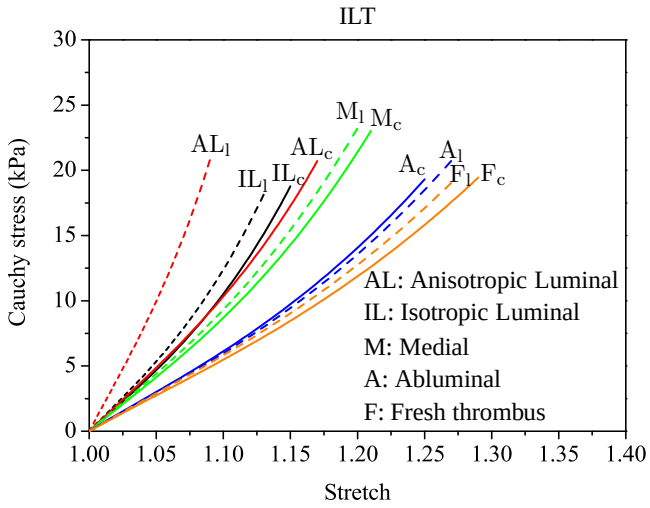

Figure 3.6: Average stress-stretch model responses of anisotropic (AL) and isotropic (IL) luminal, medial (M), abluminal (A) layers and fresh thrombus (F) for the equibiaxial protocol using the mean model parameters of Tables 3.4, where $()_c$ and $()_l$ denote circumferential (solid curves) and longitudinal (dashed curves) directions, respectively.

Type (i). Prior to the current study, several material models regarding the ILT and the AAA wall have been proposed [146, 153, 192, 193, 203]. Nevertheless, some of these models were either derived from uniaxial extension tests or were based on two-dimensional strain-energy functions, which are less appropriate to characterize the mechanical responses of three-dimensional AAA tissues.

Table 3.4: Model parameters (Mean $\pm$ SD) for the anisotropic luminal ($n = 10$), isotropic luminal ($n = 23$), medial ($n = 22$), abluminal layers ($n = 12$) and the fresh thrombi ($n = 4$), see Eqs. (3.6)-(3.7).

ILT	μ (kPa)	k_1 (kPa)	k_2 (–)	φ (°)	ρ (–)	R^2
Luminal (Aniso)	9.7 ± 1.5	15.9 ± 4.3	2.7 ± 1.4	84.1 ± 10.7	0.33 ± 0.07	0.93 ± 0.04
Luminal (Iso)	8.2 ± 1.7	12.3 ± 3.7	0.6 ± 0.3	89.3 ± 2.3	0.03 ± 0.02	0.92 ± 0.05
Medial	7.1 ± 1.9	6.0 ± 2.2	0.07 ± 0.1	86.7 ± 7.5	0.05 ± 0.05	0.93 ± 0.04
Abluminal	5.1 ± 1.1	2.9 ± 1.0	0.03 ± 0.01	89.1 ± 1.1	0.05 ± 0.01	0.94 ± 0.03
Fresh thrombus	4.9 ± 0.7	2.1 ± 0.4	0.02 ± 0.01	88.9 ± 0.3	0.04 ± 0.01	0.94 ± 0.02

Data of thrombus age is very much lacking in the literature, especially for the ILT within AAAs. To further interpret the change in the mechanical properties, there is a need to classify all tested specimens within different age phases. All fresh thrombi belong to phase I and almost all isotropic luminal layers are of phase II, however, anisotropic luminal layers are either of phase III or IV. Medial layers cover phases II–IV, while abluminal layers belong mainly to phases III and IV. For each individual ILT sample, the luminal and medial

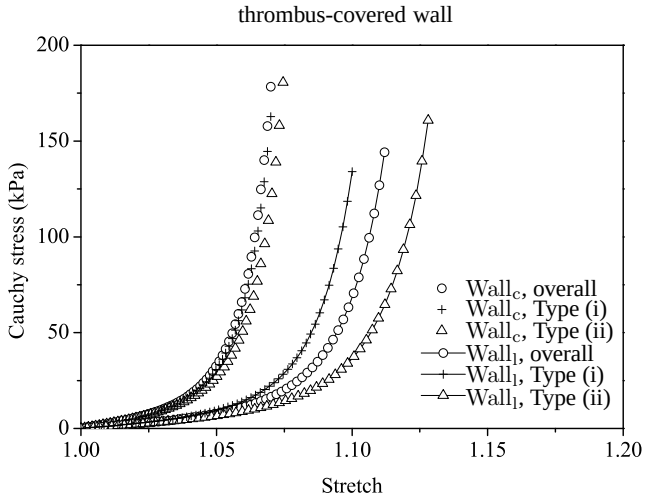

Figure 3.7: Circumferential and longitudinal mean stress-stretch responses of the thrombus-covered walls using the mean model parameters from Table 3.5. $()_c$ and $()_l$ denote circumferential and longitudinal directions; overall, Type (i) and Type (ii) denote all thrombus-covered walls, walls covered by the younger thrombi (phase II) and by the intermediate and old thrombi (phases III and IV), respectively.

Table 3.5: Model parameters (Mean $\pm$ SD) for the thrombus-covered wall ($n = 14$).

Wall type	μ (kPa)	k_1 (kPa)	k_2 (–)	φ ($^\circ$)	ρ (–)	R^2
Type (i)	6.0 ± 3.2	97.4 ± 26.6	173.7 ± 64.7	35.8 ± 6.0	0.25 ± 0.08	0.94 ± 0.04
Type (ii)	7.1 ± 4.6	61.0 ± 35.4	114.7 ± 60.4	31.9 ± 4.1	0.32 ± 0.09	0.95 ± 0.02

layers usually have the same age phase. Initially, the thrombotic materials are very compliant and isotropic (phase I). Starting from phase II, they become stiffer due to the formation of the loose fibrin network. In this situation, the thrombi are sponge-like materials with fluid inside and they are mechanically isotropic. During phase III, the thrombi become much stiffer as the fibrin networks are composed of much thicker bundles. The thrombotic material can be either isotropic or anisotropic for different individual ILT layers. As a consequence of the fibrin network disruption and more condensed residue proteins, the thrombi are much stiffer in phase IV, comprising the anisotropic luminal and the isotropic medial and abluminal layers.

One possible explanation for the mechanical isotropy of the luminal and medial layers in the phases II and III is that the fibrin network plays a dominant role in the biaxial stretching as compared to erythrocytes or other degraded proteins during the younger phases. Importantly, fibrin polymers have a large extensibility and elasticity when compared with other protein polymers [18, 108]. Factors to trigger the mechanical anisotropy of several luminal layers in the phases III and IV can be summarized as follows. First, differences between

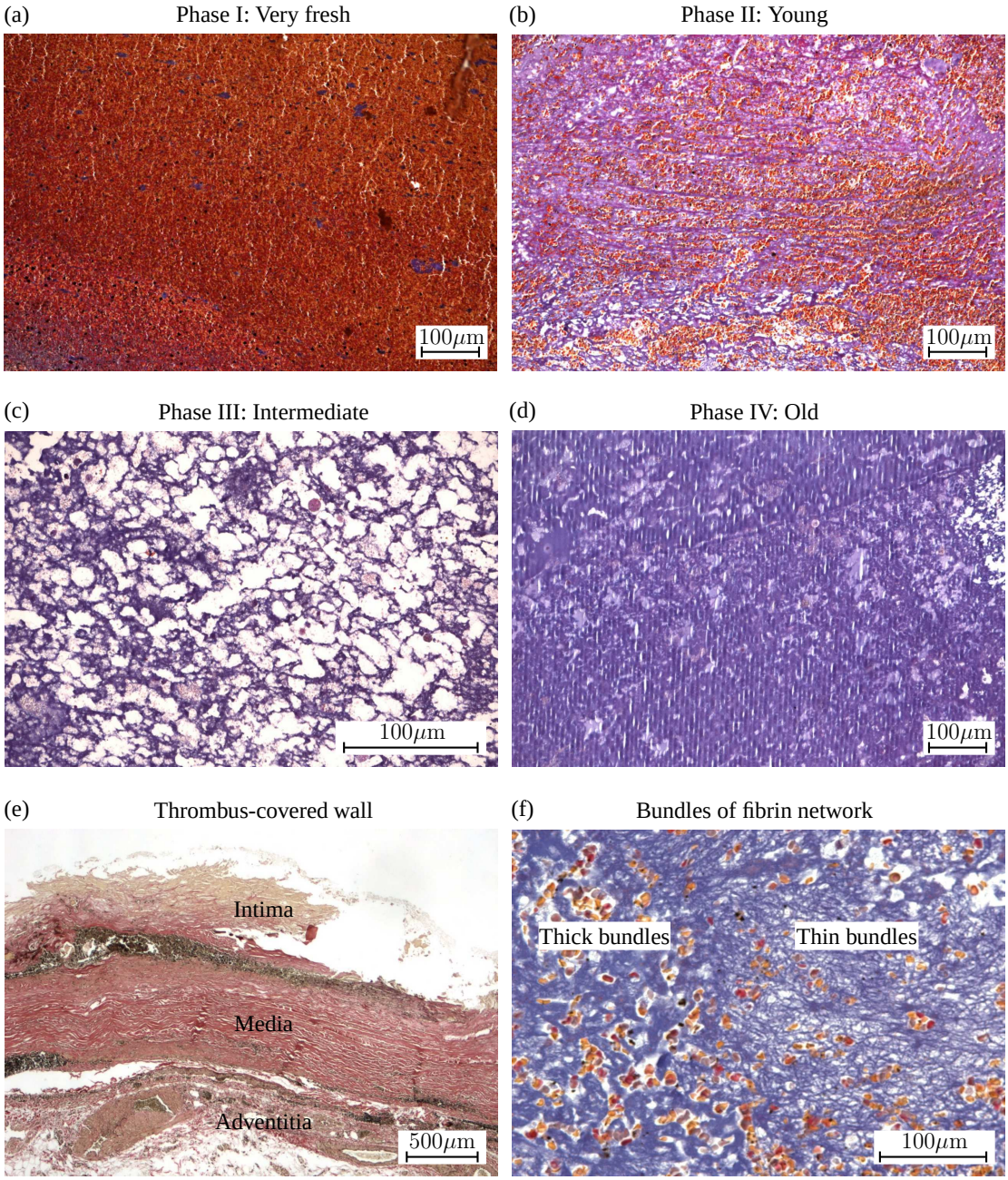

Figure 3.8: Representative histological images characterizing the morphology of the thrombotic material in four age phases: (a) very fresh, (b) young, (c) intermediate and (d) old. Original magnification 10×. Histological images of (e) the thrombus-covered wall consisting of three individual layers (original magnification 4×) and (f) the fibrin network mixed with both thick and thin bundles highlighting their distinct morphological characteristics (original magnification 40×).

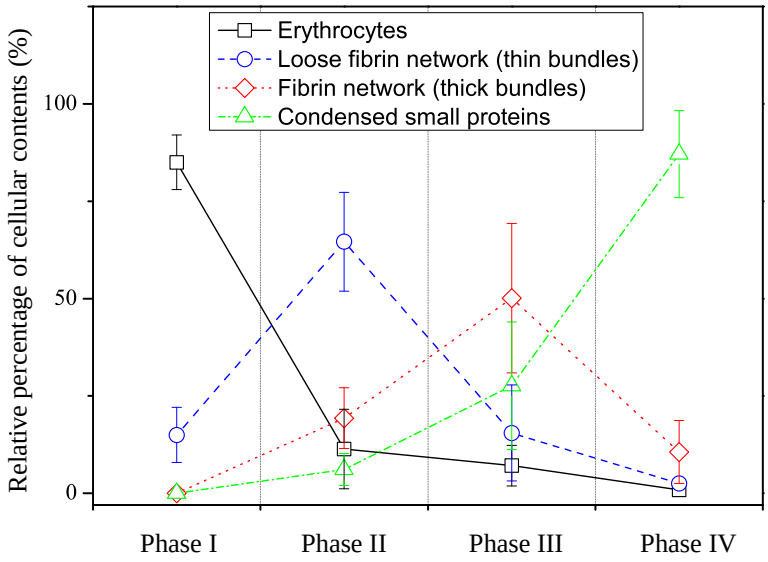

Figure 3.9: Relative percentage of cellular contents of the thrombotic material in the age phases I-IV.

the thick and thin bundles within the fibrin network, evident from histology, may lead to different mechanical properties during biaxial stretching. The microstructure might be a factor for the mechanical anisotropy of the thrombotic material, which needs to be further investigated. Second, as a scaffold, pore densities, shapes and orientations of the fibrin network in the younger phase may considerably influence the distributions and depositions of residue small proteins in the later phases. Thus, the older thrombotic material may exhibit mechanical anisotropy probably due to unequal distributions of residue proteins. Finally, shear stresses due to the blood stream should also be, to some extent, taken into account in such a complex and potentially dynamic environment.

All laboratory data given were sampled 4-48 hours prior to surgery. All patients suffered from hypertension, whereas diabetes were only found in 7 (19%) of 36 patients. In 30 (83%) patients, aneurysms are asymptomatic. Smoking statistics show that 85% of the patients are active smokers or smoked previously. Further, we roughly estimated the thrombus age for each patient by integrating age information of the three individual ILT layers, see Table 3.1. Note, however, that a few specimens with success in mechanical testing failed in the determination of the thrombus age. Approximate time from preoperative X-ray computed tomography (CT) to operation (OP) for the patients whose thrombi are in the phases III and IV (these are 12 patients) are equal or less than 1 week (3.7 ± 2.1 days, mean $\pm$ SD) except for patient No. 21 (1 month). In 10 (80%) of these 12 patients, maximum diameters are equal to or larger than 6 cm. By contrast, patients with a younger thrombus (phase II), which are 17, hold a much longer time from CT to OP; at least 1 month for 14 patients (82%) out of these 17.

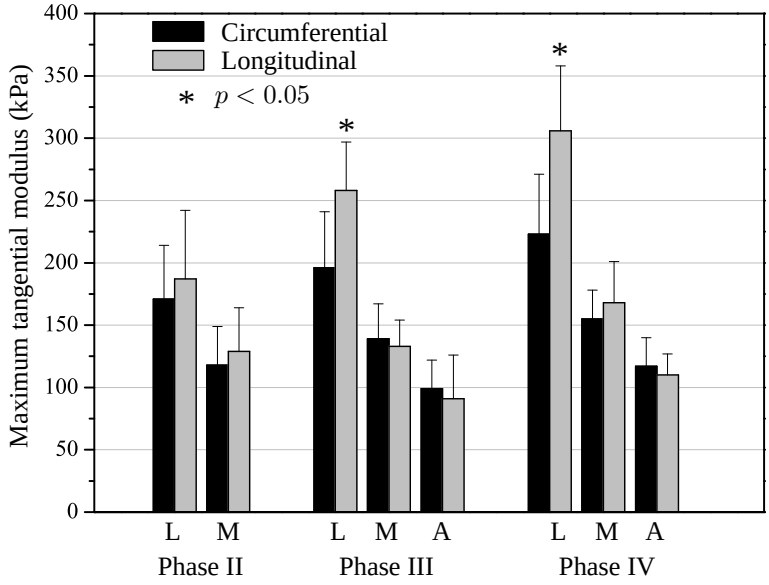

Figure 3.10: Maximum tangential modulus (MTM) at a stress level of 20 kPa versus relevant thrombus age phases for individual luminal (L), medial (M) and abluminal (A) layers. Abluminal layers are only identified in phases III and IV. A significant difference is noted for the longitudinal MTM values of the luminal layer in both phases III and IV with respect to phase II.

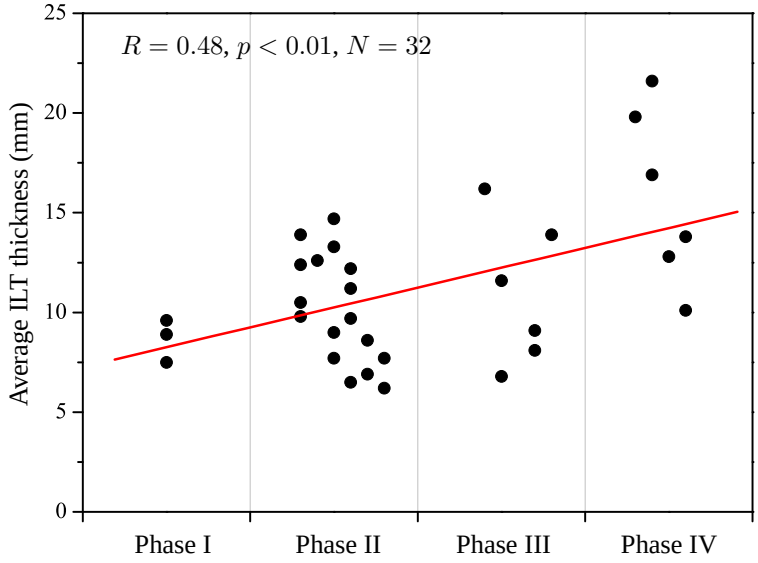

Figure 3.11: Average ILT thickness versus relevant thrombus age phases for 32 specimens whose ages are histologically determined.

As an inflammatory indicator, preoperative CRP values are outside the normal range for 7 (60%) of 12 patients whose thrombi are in the phases III and IV. Meanwhile, 70% of these 12 patients have larger values of preoperative fibrinogen over the normal range. It is well known that fibrinogen is a critical index to evaluate the fibrin content of the thrombi, since it is essential for coagulation of blood and fibrin formation [36]. Preoperative values of thrombocyte count for most patients (91%) are within the normal range. Moreover, patient No. 18 is the only one whose aneurysm ruptured before surgery. It should also be noted that this patient is the only one who showed three different types of ILT, including fresh, young and old thrombi (phases I, II and IV). This indicates that the ILT can be a complex structural material with different biomechanical properties even in the same AAA sample.

Peak wall stress and wall strength are two major potential predictors of AAA rupture [48, 106, 147, 195, 200]. In fact previous studies have substantiated that the ILT plays an important role in the AAA wall weakening [2, 93]. Therefore, more investigative attention should be given to the wall strength underneath the ILT, which is of crucial interest to the assessment of AAA rupture. Vande Geest et al. [195] first developed a noninvasive technique to evaluate AAA wall strength *in vivo*. The present study suggests that the thrombus age is a critical factor to examine the strength of its covered wall. Consequently, the thrombus age, combined with other key predictor variables such as maximum diameter, peak wall stress and wall strength, may give a more comprehensive consideration on AAA rupture assessment. The corresponding mathematical model, if developed, would be a promising technique to link patient-specific ILT properties to the AAA wall strength.

There are also some limitations in the present work. The proposed age determination of thrombus does not provide the actual number of days for the specimens but rather the relative age phases. The main reason is that there is no cellular reaction (inflammatory response) for the ILT to organize the thrombotic material, which differs from thrombi in small arteries and veins. A full transversal section of the thrombus from the lumen to the ablumen, however, may be helpful to explore more morphological characteristics in histology and to further analyze the microstructure of ILT with thrombus aging. Although, biaxial extension tests can essentially characterize the biaxial mechanical behaviors of both ILTs and wall tissues, the ultimate tensile strength for both tissue types can not be measured by carrying out this experimental method. It would also be good to compare the failure properties of ILTs with different ages and the walls that they cover.

3.5 Conclusion

The main finding of this paper is that the luminal layer of the ILT may not be an isotropic material. Compared to isotropic luminal layers, anisotropic samples have remarkably larger

longitudinal stiffnesses and are frequently associated with highly degraded medial and abluminal layers. Moreover, it appears that the present biaxial study is the first one which documents that the mechanical behaviors of fresh thrombi are quite similar to those of the abluminal layers in old (laminated) thrombi.

Another key finding in this study is that we may determine the relative age phases of the thrombi, which are critically important and novel in AAA research. Further investigations show that the mechanical properties of the thrombotic material may change significantly with the thrombus age, and, remarkably, the older thrombi are related to aneurysm wall weakening. These findings provide us with an additional perspective into the initiation and progression of the ILT in the biomechanical AAA environment. It is, therefore, concluded that the thrombus age is a potential predictor for the strength of the wall underneath the ILT as well as AAA rupture.

Acknowledgement

We acknowledge Dr. Gerhard Sommer from the Institute of Biomechanics at Graz University of Technology for his help during the experimental tests.

4 VARIATIONS OF DISSECTION PROPERTIES AND MASS FRACTIONS WITH THROMBUS AGE IN HUMAN ABDOMINAL AORTIC ANEURYSMS

Abstract Thrombus age is an important factor helping to better explore the influence of intraluminal thrombus (ILT) on the biomechanical properties of abdominal aortic aneurysm (AAA). Experimental studies indicate a correlation between the relative thrombus age and the mechanical properties of aneurysmal tissues. On 32 AAA samples we performed peeling tests with the aim to dissect the material (i) through the ILT thickness, (ii) within the individual ILT layers and (iii) within the aneurysm wall underneath the thrombus by using two extension rates (1 mm/min, 1 mm/sec). Histological investigations and mass fraction analysis were performed to characterize the dissected morphology, to determine the relative thrombus age, and to quantify dry weight percentages of elastin and collagen in the AAA wall. A remarkably lower dissection energy was needed to dissect within the individual ILT layers and through the thicknesses of old thrombi. With increasing ILT age the dissection energy of the underlying intima-media composite continuously decreased and the anisotropic dissection properties for that composite vanished. The quantified dissection properties were rate dependent for both tissue types (ILT and wall). Histology showed that single fibrin fibers or smaller protein clots within the ILT generate smooth dissected surfaces during the peeling. There was a notable decrease in mass fraction of elastin within the thrombus-covered intima-media composite with ILT age ($11.8\% \pm 4.5\%$ to $4.1\% \pm 3.9\%$; $p < 0.001$), whereas no significant change was found for that of collagen ($22.4\% \pm 5.1\%$ to $17.6\% \pm 5.3\%$; $p = 0.11$). These findings suggest that Intraluminal thrombus aging leads to a higher risk of dissection initiation for the ILT and the intima-media composite of the aneurysmal wall.

4.1 Introduction

An abdominal aortic aneurysm (AAA) is a vascular pathology associated with permanent and irreversible localized dilations. Rupture of an AAA is a mechanical failure of the aneurysm wall, which occurs when the peak wall stress exceeds the local strength of the aortic tissue. In order to seek a more reliable criterion for the AAA rupture assessment, the majority of recent studies have focused on the development of non-invasive methods to predict the rupture risk of patient-specific AAA models on a computational basis [113, 151, 195, 204, 210]. Detailed information of patient-specific geometries of the

intraluminal thrombus (ILT) and the wall, and advanced models for the anisotropic wall and the interaction between the fluid and the structure have improved the reliability of finite element simulations to a great extent. Aneurysmal degeneration, from a pathohistological point of view, is mainly attributed to loss of elastin and collagen remodeling within the aortic wall [23, 33, 162]. As a key issue, rupture locations of AAA have been identified by several studies [38, 39, 64] using experimental techniques and computational validations. For example, Doyle et al. [39] reported the rupture site of a silicon rubber AAA model, i.e. at the inflection point, which is in agreement with the peak stress regions as numerically predicted. In addition to that, they continuously measured the internal rupture pressures of experimental AAA models manufactured by different silicon materials [38]. Another representative work in characterizing rupture sites was conducted by Raghavan and colleagues [144]. Based on whole ruptured AAA specimens harvested from fresh cadavers, they suggested that primary rupture sites were on the lateral quadrants and were longitudinally oriented.

Despite these new findings, understanding of the intrinsic AAA rupture mechanisms and patterns remain poor. In particular, the aneurysmal aortic dissection, which may exist and play a key role in the AAA rupture initiation and progression, was seldom considered in previous research. It has long been suggested that bleeding into the ILT caused by fissures is frequently associated with AAA rupture [6, 125, 155] and fissure creation is most probably a consequence of ILT dissection during the AAA expansion [155]. Recently Pasta et al. [138] reported a set of mechanical dissection data of ascending thoracic aortic aneurysm. However, relevant experimental data based on the tissue within the AAA are not yet available in the literature. Owing to the wall weakening effect of the ILT [2, 84, 93, 199, 202], there is also a pressing need to explore how much ILT aging can potentially affect the dissection properties of aneurysmal tissues. An advanced understanding of the underlying relationships is of essential importance for gaining more insights in pathological progressions and rupture mechanisms of AAAs.

In the present study, we quantitatively assess the dissection properties of the degenerated thrombus-covered aortic tissues and the related ILTs. Since the ILT is heterogeneous [184, 193, 203] we investigate the dissection properties of the three individual ILT layers (luminal, medial, abluminal). Peeling tests [173, 187] were performed to measure the dissection energy that is needed to propagate a dissection within the tissue. In addition, the relative thrombus age was histologically determined according to the methodology proposed in our recent study [184], and was then correlated with the changes in the dissection properties of the ILT and the aortic wall tissue covered by the thrombus. Finally, mass fraction analyses were performed to quantify the corresponding dry weight percentages of elastin and collagen within the thrombus-covered walls and to explore their variations with the ILT age.

4.2 Materials and Methods

4.2.1 Material and specimen preparation

In total, 32 AAA samples (patients' mean age 70 ± 10 yr) consisting of ILTs and AAA walls were harvested from open surgical aneurysm repairs. Use of the material was approved by the Ethics Committee, Medical University Graz, Austria. All samples were procured from the anterior portion of the aneurysm and stored in Dulbecco's Modified Eagle's Medium (DMEM). The ILT heterogeneity has been reported by previous studies [184,193,203], in which three individual ILT layers, i.e. luminal, medial and abluminal, were introduced.

For executing peeling tests through the ILT thickness a prismatic-shaped specimen was first cut from the thickest part of the ILT sample, as shown in Fig. 4.1. In addition, circumferential and longitudinal rectangular strips through the thickness of the ILT (two pieces in each direction, illustrated by the dashed lines in Fig. 4.1) were obtained by gently cutting them from the prismatic-shaped specimen. The lengths of the rectangular strips varied a lot due to the different thicknesses of the ILT. For the remaining part of the ILT sample, the individual layers were separated, and strips were then cut from the separated ILT layers in the circumferential and longitudinal directions, respectively (see also Fig. 4.1). The dimension of each rectangular strip was here about 18.0×6.0 mm (length $\times$ width).

Due to the size of the thrombus-covered wall specimens, two adjacent rectangular strips were cut in the circumferential and longitudinal directions, respectively (see specimens 1 and 2 in Fig. 4.1). Further separation was performed to remove the adventitia from the intima-media composite for each strip. Finally, we cut a small (rectangular) piece of aortic wall tissue from the remaining material as representatively shown by specimen 3 in Fig. 4.1, on which we performed the mass fraction analysis.

Details of the specimen preparation for the peeling test have been described in previous studies by our lab [173, 187]. In brief, each rectangular strip was given an initial cut (incision of about 2.0-3.0 mm in length) using a surgical scalpel in order to better control the initiation of the tissue failure. Hence, two 'tongues' were obtained for mounting them into the testing machine. To avoid slippage of the specimens during loading, rectangular pieces of sandpaper were glued with superadhesive gel at both sides of the 'tongues'. A prepared ILT specimen for the peeling test is shown in Fig. 4.2.

4.2.2 Testing protocols

For the peeling through the ILT thickness, the obtained rectangular strips were labeled as C(T) in the circumferential and L(T) in the longitudinal directions; (T) represents through the thickness. The rectangular strips used for the peeling within the individual luminal layer

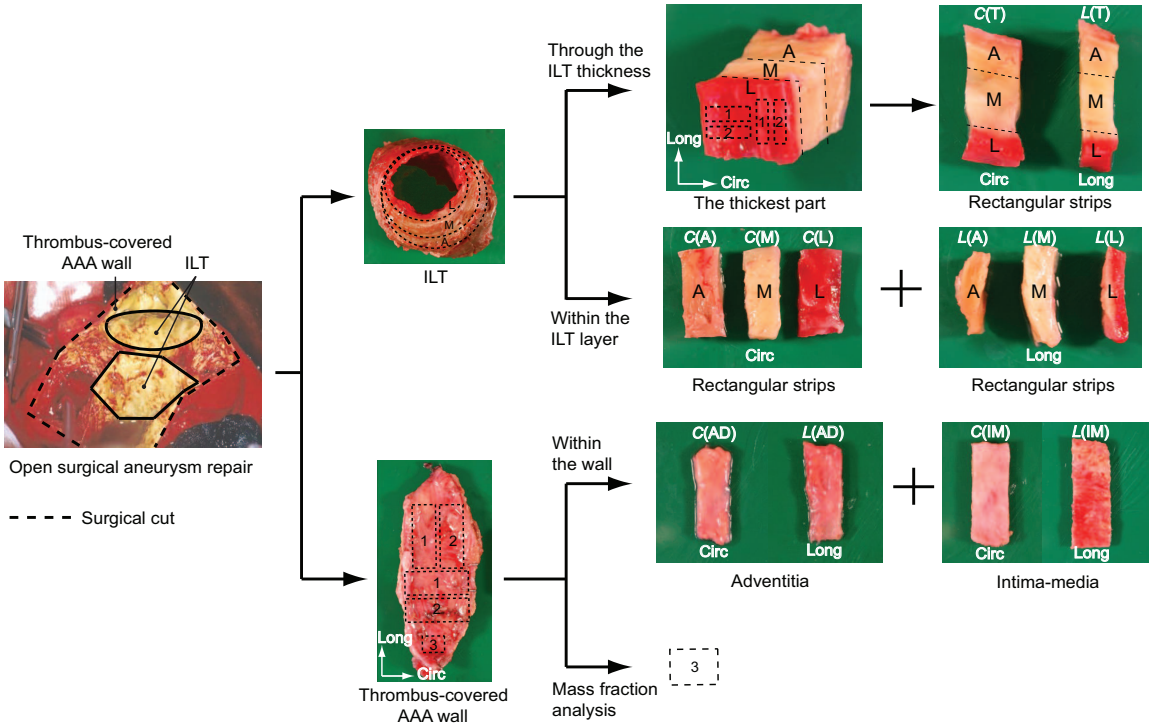

Figure 4.1: Schematic illustration of specimen cutting and anatomical separation of the ILT and the thrombus-covered wall. Test samples for peeling through the ILT thickness, within the ILT layer and within the wall; one sample for mass fraction analysis. Circ and Long represent circumferential and longitudinal directions, respectively; L, M, A denote the three layers of the ILT, which are luminal (L), medial (M) and abluminal (A); the labeling of the individual samples is stated in Section 4.2.2.

were denoted as *C*(L) in the circumferential and *L*(L) in the longitudinal directions. In an analogous manner, the strips cut from the medial and the abluminal layers were labeled as *C*(M), *L*(M) and *C*(A), *L*(A), respectively; (L), (M) and (A) represent luminal, medial and abluminal layers of the ILT. Compared to a healthy human aorta, the degenerated aneurysm wall is usually associated with atherosclerosis so that the intima and the media cannot be separated due to the lack of the layer-specific arterial structure. Therefore, in the current study the peeling tests were performed on the intima-media composite and the remaining adventitia. Similarly, the rectangular intima-media and adventitia strips were labeled as *C*(IM), *L*(IM) and *C*(AD), *L*(AD), as previously done for the ILT samples; (IM) and (AD) represent intima-media composite and adventitia of the aneurysmal wall.

For each type of peeling test, the rectangular strip specimens in each direction were peeled off under different extension rates, i.e. 1 mm/min and 1 mm/sec, respectively. This allows us to examine whether the protocol-controlled AAA tissue dissection is rate dependent, which is not discussed in our previous related studies [173, 187]. It should also be em-

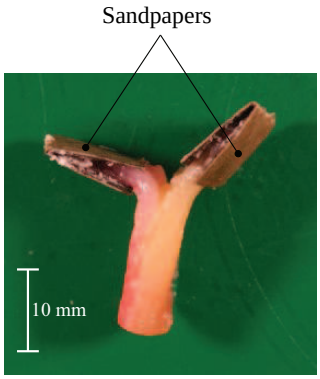

Figure 4.2: Representative photograph of a prepared luminal strip before the peeling test.

phasized that the strips were cut from neighboring regions of the same sample in order to minimize regional variations or sample differences in the subsequent comparison of extension rate effects.

4.2.3 Test setup and procedure

The experimental setup has been introduced through similar tests [82, 173]. The prepared specimens were moistened with phosphate buffered saline (PBS) solution until testing. Once both 'tongues' of the prepared specimen were clamped in the testing machine, the individual peeling test was carried out under the prescribed extension rate. Note that all peeling tests were executed in PBS solution at $37.0 \pm 1.0^{\circ}$C. After mechanical testing, the strip samples were inserted into neutral buffered formaldehyde solution (pH 7.4) for fixation and sent off for further histological investigations.

4.2.4 Dissection energy and data analysis

The force/width values, denoted by F_{pc} and F_{pl}, were measured and averaged for the circumferential and longitudinal strips, respectively. The dissection energy per reference area [173, 187], say W^{dissect}, during the (circumferential c and longitudinal l) peeling (p) was quantified by subtracting the elastic energy W^{elastic} from the external work W^{ext}, i.e.

$$W_{\mathrm{pc}}^{\mathrm{dissect}} = (W_{\mathrm{c}}^{\mathrm{ext}} - W_{\mathrm{pc}}^{\mathrm{elastic}})/L_{\mathrm{pc}}, \qquad W_{\mathrm{pl}}^{\mathrm{dissect}} = (W_{\mathrm{l}}^{\mathrm{ext}} - W_{\mathrm{pl}}^{\mathrm{elastic}})/L_{\mathrm{pl}}, \tag{4.1}$$

where L_{pc} and L_{pl} denote the reference lengths of the strips in the circumferential and longitudinal directions, respectively. All quantitative results in the current study are reported as mean $\pm$ SD. The Shapiro-Wilk and the Kolmogorov-Smirnov tests were utilized to determine the data normality. Comparisons of the force/width values or the dissection energy

either between different sample groups or between different thrombus age phases were performed by using the Student's *t*-test.

4.2.5 Histology

To investigate the morphology of the dissected surfaces, the tested specimens were fixed in neutral buffered formalin with pH 7.4, and then embedded in paraffin. The paraffin blocks were sectioned at 4-5 μm and stained with Mallory-Cason Trichrome (known as SFOG), Prussian blue (PB) and Hematoxylin and Eosin (HE) to investigate the morphology of the dissected surfaces. Details of the methods for thrombus age determination within the AAA have been described in a recent paper [184].

4.2.6 Mass fraction analysis

With the mass fraction analysis we quantitatively determined dry weight of elastin and collagen within the intima-media and the adventitia. AAA tissues were frozen in liquid nitrogen and homogenized by grinding in a mortar with a pistil. The wet and dry weights after reaching constant weight by drying for 3 to 4 days at 105°C of the homogenate were determined, respectively; for details regarding elastin quantitation and collagen analysis see a recent study. [186]

4.3 Results

4.3.1 Peeling tests

All reported statistical values and representative curves in the following three individual parts (i.e. peeling through the ILT thickness, peeling within individual ILT layers and peeling of the thrombus-covered walls) were obtained from peeling tests with the extension rate 1 mm/min.

Peeling through the ILT thickness. A total of 25 ILT samples including 21 *C*(T) and 23 *L*(T) rectangular strips were tested and analyzed. The peeling through the different ILT thicknesses are shown in the representative Figs. 4.3(a) and 4.3(b). Column plots of the dissection energy W^{dissect} through the ILT thickness with respect to the thrombus age phases II, III and IV for the individual ILT layers are shown in Figs. 4.4(a)-(c), and the statistical results are summarized in Table 4.1.

Peeling within individual ILT layers. A total of 52 luminal (25 *C*(L) and 27 *L*(L) strips), 55 medial (28 *C*(M) and 27 *L*(M) strips) and 20 abluminal (11 *C*(A) and 9 *L*(A) strips)

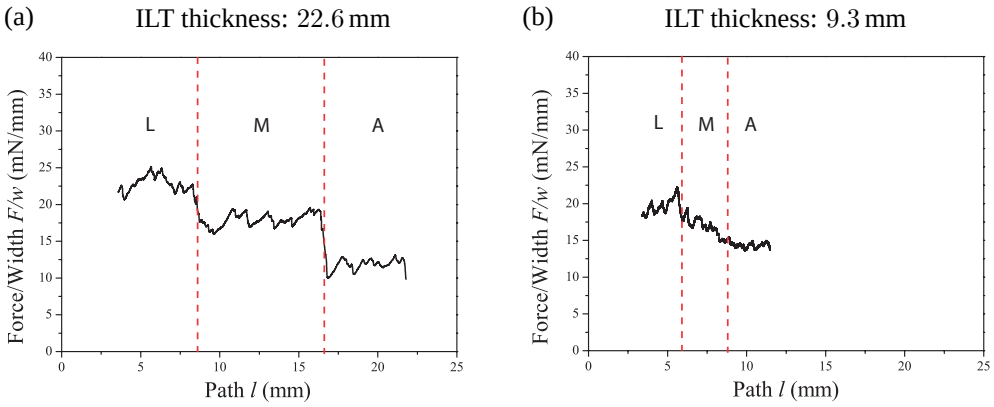

Figure 4.3: Representative plots of force/width versus the dissection path for two ILT samples during the peeling through different ILT thicknesses, i.e. (a) 22.6 mm and (b) 9.3 mm. Three regions, denoted by (L) luminal, (M) medial and (A) abluminal layers, are distinguished by two dashed lines.

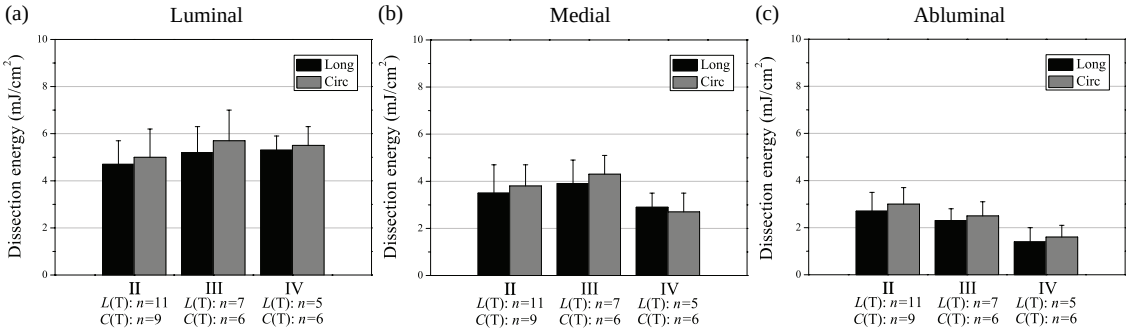

Figure 4.4: Column plots (mean values and standard deviations) of dissection energy W^{dissect} through the ILT thickness with respect to the thrombus age phases II (young), III (intermediate) and IV (old) for the individual ILT layers. Long and Circ denote longitudinal and circumferential directions, respectively. For the labeling see Fig. 4.1.

specimens were studied. Representative curves regarding the peeling within the three individual ILT layers are shown in Figs. 4.5(a)-(c). Column plots of the dissection energy W^{dissect} within the three individual ILT layers versus the thrombus age phases II-IV are shown in Fig. 4.6, and relevant quantitative values are summarized in Table 4.1.

Peeling of the thrombus-covered walls. A total of 48 thrombus-covered wall specimens for the adventitia (25 *C*(AD) and 23 *L*(AD) strips) and 53 specimens for the intima-media composite (27 *C*(IM) and 26 *L*(IM) strips) were studied. Changes in the dissection energy W^{dissect} with the thrombus age for the adventitia and the intima-media composite are shown in Fig. 4.7. The computed dissection energy values are summarized in Table 4.1.

Comparison of different extension rates. Figure 4.8 shows comparisons of the test results with two different extension rates, in which mean force/width values through the ILT thickness (Fig. 4.8(a)), within the individual ILT layers (Fig. 4.8(b)-(d)) and within the thrombus-covered walls (Fig. 4.8(e),(f)) are shown. Note that the dissection path through the ILT thickness varies due to different sample thicknesses (see, for example, the ILT curves in Figs. 4.3(a) and (b)). Here we show a box-whisker plot for each ILT layer through the thickness, see Fig. 4.8(a).

4.3.2 Histology

Representative images of the morphology of the dissected surfaces during the peeling tests of the ILT and the thrombus-covered aortic wall tissues are shown in Fig. 4.9. Due to the characteristics of the microstructural morphology in the thrombus tissue, thrombus age was determined as four relative age phases, namely phase I (very fresh), phase II (young), phase III (intermediate), phase IV (old); the relevant histological characteristics for each age phase are summarized in a previous study. [184] In the current study the thrombus age of 29 ILT samples was determined by histology: 13 were classified as young, 9 as intermediate and 7 as old thrombi.

4.3.3 Mass fraction

Mass fractions of elastin and collagen within the thrombus-covered adventitia in the relative thrombus age phases II, III and IV are shown in Fig. 4.10. The relevant values for the elastin and collagen within the thrombus-covered intima-media with respect to ILT ages are represented in Fig. 4.11. Figure. 4.12 indicates the variations of the mass fraction ratios between elastin and collagen from thrombus age phase II to IV.

4.4 Discussion

In this study, one goal was to explore the dissection properties of ILT tissues and thrombus-covered walls and, specifically, to establish the correlations between the dissection properties of aneurysmal tissues and thrombus ages. For the peeling through the ILT thickness, Fig. 4.3 clearly demonstrates that there is a continuous decrease of the force/width value through the three distinctive regions; from the luminal to the abluminal layer. From a quantitative point of view, the mean force/width value continuously decreases from the luminal to the medial layer by approximately 12% (SD 5%), and from the medial to the abluminal layer by about 28% (SD 9%).

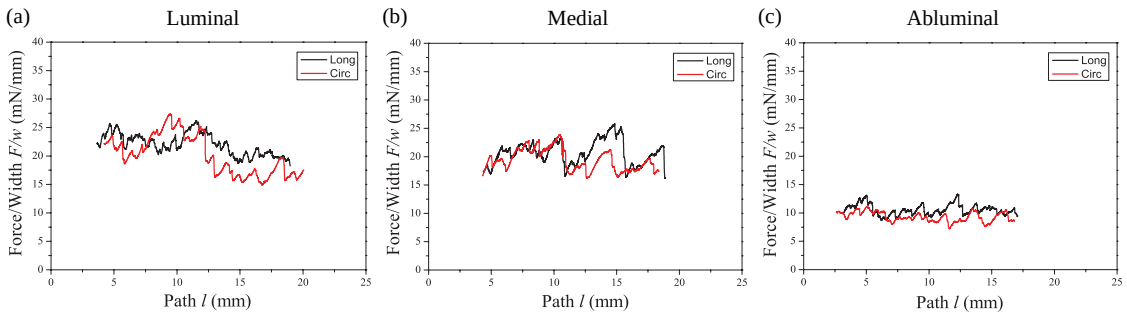

Figure 4.5: Representative plots of force/width versus the dissection path for the individual ILT layers during the peeling test within the layer. Long and Circ indicate longitudinal and circumferential directions, respectively. Both luminal and medial layers are in the thrombus age phase III, whereas the abluminal layer is in the thrombus age phase IV.

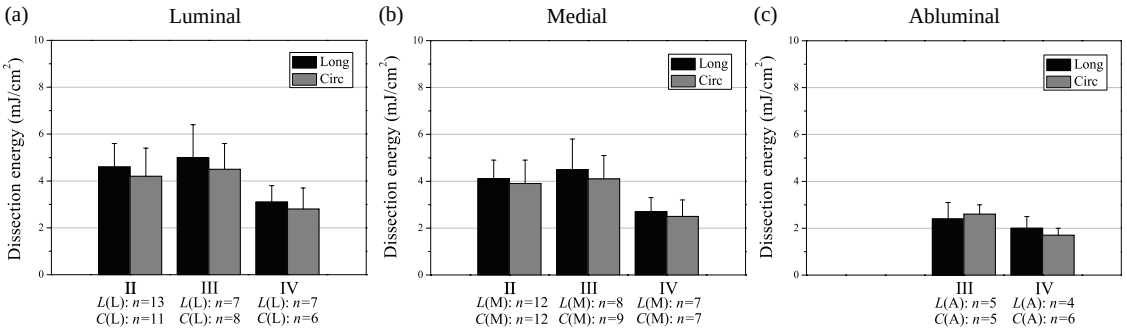

Figure 4.6: Column plots (mean values and standard deviations) of dissection energy W^{dissect} for the individual ILT layers with respect to the thrombus age phases II (young), III (intermediate) and IV (old). Long and Circ denote longitudinal and circumferential directions, respectively. Peeling tests within the abluminal layer are available mainly for the thrombi in the age phases III and IV. No fresh thrombus (age phase I) was considered. For the labeling see Fig. 4.1.

Moreover, the effects of thrombus age on the dissection energy W^{dissect} were also investigated. Intriguingly, the three individual ILT layers show different variations with respect to the ILT age (Fig. 4.4). For the luminal layer, the dissection energy slightly increases from the age phase II to III and IV, whereas the dissection energy through the medial thickness increases from the age phase II to III but then it is followed by a noticeable decrease from III to IV. In contrast, the dissection energy through the thickness of the abluminal layer continuously decreases with ILT age. These findings suggest that a remarkably lower dissection energy is needed to dissect through the medial and abluminal thicknesses of the old thrombi. Hence, an increased ILT age may lead to a higher risk of dissection initiation through its thickness. Within the same ILT age, the dissection energy is found to be

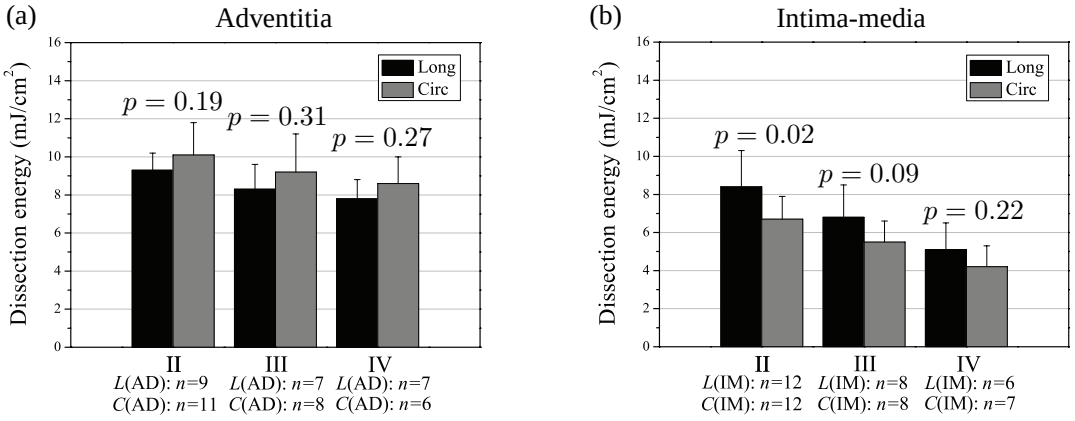

Figure 4.7: Column plots (mean values and standard deviations) of dissection energy W^{dissect} with respect to the thrombus age phases II (young), III (intermediate) and IV (old) for the adventitia and the intima-media for the thrombus-covered wall. Long and Circ denote longitudinal and circumferential directions, respectively. The p values indicate statistical comparisons of the dissection energy between the longitudinal and circumferential directions for each thrombus age phase. For the labeling see Fig. 4.1.

progressively decreasing from the luminal to the abluminal side (see Figs. 4.4(a)-(c), and Table 4.1). Thus, there is also a potential risk of dissection through the ILT thickness for each ILT age phase.

Regarding the peeling within the ILT layers, our findings reveal that the mean circumferential and longitudinal force/width values to dissect within the luminal layers were quite close to those of the medial layers, but significantly larger than those within the abluminal layers ($p = 0.01$ in the circumferential, $p = 0.02$ in the longitudinal directions), see Figs. 4.5 and 4.6. There is no significant difference in the force/width value between the circumferential and longitudinal directions for each individual ILT layers. It should be mentioned that due to material weakness only a very few peeling data within the abluminal layers were obtained from thrombotic materials in the age phase II; thus they were not considered for a statistical comparison. By correlating the computed dissection energy with the thrombus age, it appears that the luminal and medial layers share the same variation trend with ILT age, in which the dissection energy slightly increases from age phase II to III but significantly decreases from age phase III to IV (circumferential $p = 0.008$, longitudinal $p = 0.013$ for luminal; circumferential $p = 0.005$, longitudinal $p = 0.003$ for medial), see Fig. 4.6. A comparison is possible for the abluminal layers between the age phases III and IV (circumferential $p = 0.02$, longitudinal $p = 0.36$). Fibrin network in the ILT changing from thin to thick bundles may lead to a higher resistance to the dissection during the peeling test, which could explain the (slight) increase of the dissection energy from age phase II to III. Likewise, the subsequent significant decrease of the dissection

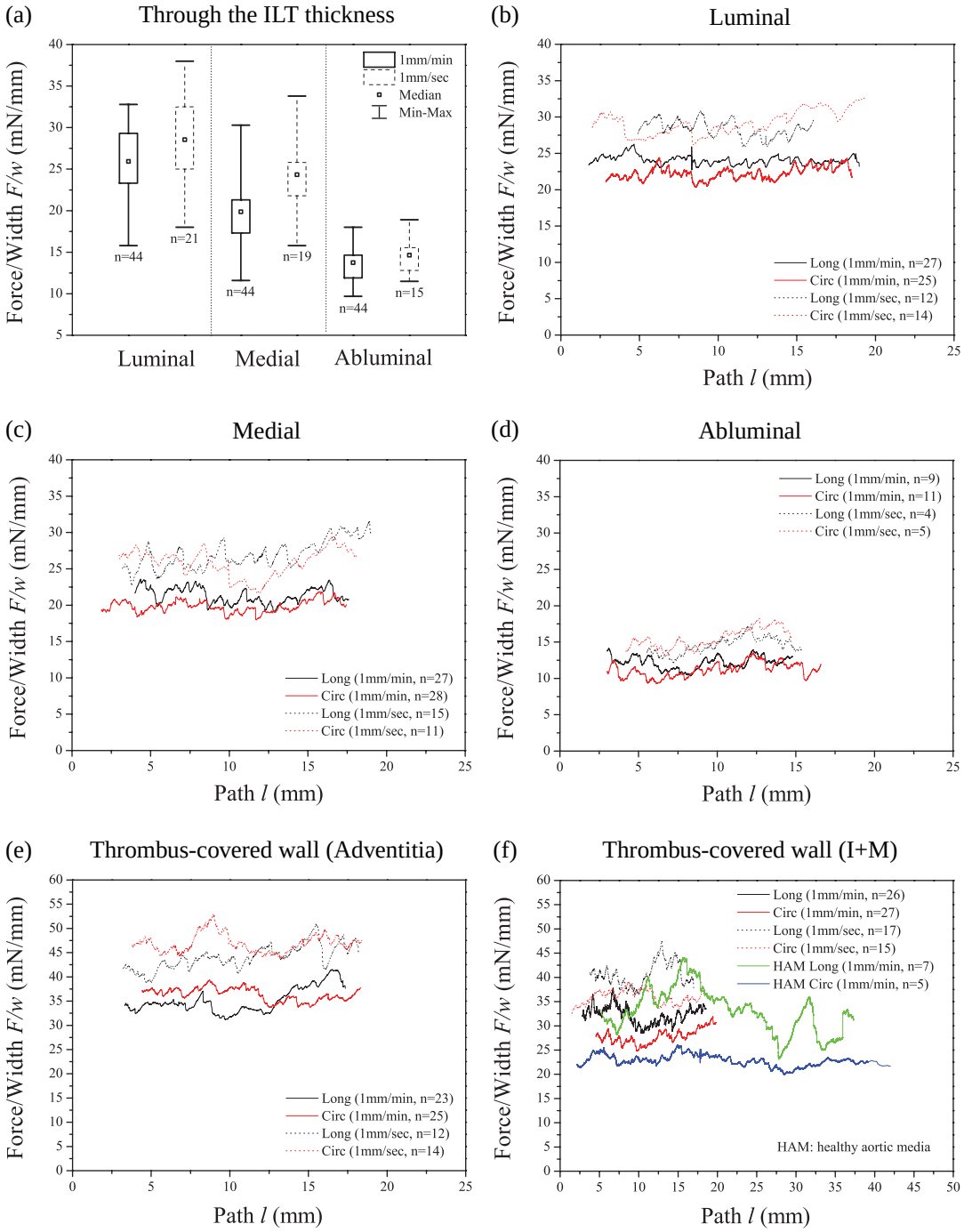

Figure 4.8: Mean force/width responses through the ILT thickness, within the individual ILT layers and within the thrombus-covered walls with two peeling extension rates, i.e. 1 mm/min (solid boxes in (a) and solid curves in (b)-(f)) and 1 mm/sec (dashed boxes in (a) and dashed curves in (b)-(f)). Mean force/width responses of the healthy aortic media (HAM) [173] with the rate of 1 mm/min are also shown by green and blue curves in (f).

Table 4.1: Computed dissection energy W^{dissect} (mJ/cm^2) for the thrombus age phases II, III and IV during the peeling tests with 1 mm/min through the ILT thickness, within the individual ILT layers and within the adventitia and the intima-media composite (I+M) of the thrombus-covered walls. Dissection energy (mJ/cm^2) of the healthy aortic media with a rate of 1 mm/min, documented by a previous experimental study [173]. The circumferential and longitudinal directions are denoted by c and l, respectively.

			Dissection energy W^{dissect} (mJ/cm^2)		
			Age phase II	Age phase III	Age phase IV
Through the ILT thickness	Luminal	c	5.0 ± 1.2	5.7 ± 1.3	5.5 ± 0.8
		l	4.7 ± 1.0	5.2 ± 1.1	5.3 ± 0.6
	Medial	c	3.8 ± 0.9	4.3 ± 0.8	2.7 ± 0.8
		l	3.5 ± 1.2	4.0 ± 1.0	2.9 ± 0.6
	Abluminal	c	3.0 ± 0.7	2.5 ± 0.6	1.6 ± 0.5
		l	2.7 ± 0.8	2.3 ± 0.5	1.4 ± 0.6
Within the ILT layers	Luminal	c	4.2 ± 1.2	4.5 ± 1.2	2.8 ± 0.9
		l	4.6 ± 1.0	5.0 ± 1.4	3.1 ± 0.7
	Medial	c	3.9 ± 1.0	4.1 ± 1.0	2.5 ± 0.7
		l	4.1 ± 0.8	4.5 ± 1.3	2.7 ± 0.6
	Abluminal	c		2.6 ± 0.4	1.7 ± 0.3
		l		2.4 ± 0.7	2.0 ± 0.5
Thrombus-covered wall	Adventitia	c	10.1 ± 1.7	9.2 ± 2.0	8.6 ± 1.4
		l	9.3 ± 0.9	8.3 ± 1.3	7.8 ± 1.0
	I+M	c	6.7 ± 1.2	5.5 ± 1.1	4.2 ± 1.1
		l	8.4 ± 1.9	6.8 ± 1.7	5.1 ± 1.4
			Dissection energy W^{dissect} (mJ/cm^2)		
Healthy abdominal aorta [173]	Media	c		5.1 ± 0.6	
		l		7.6 ± 2.7	

energy can be attributed to microstructural changes of the ILT from age phase III to IV, in which fibrin networks disrupt, and residue small proteins become the main component. If multi-axial loading conditions within the AAA are considered, the *in vivo* ILT dissection could be a combination of both (tested) scenarios (i.e. through the thickness and within the layers).

Wall dissection is a potential risk factor to initiate AAA rupture, however, to the authors' knowledge, no relevant quantitative data have been measured prior to the current study, particularly for the wall segment underlying the ILT, which has a decreased tensile strength due to a higher degree of proteolysis and infiltration of inflammatory cells [53, 93, 94, 155, 199]. The adventitia, in general, shows the higher mean force/width values in both the circumferential and longitudinal directions when compared to the associated intima-media composite. As shown in Fig. 4.7(a), there is no significant difference in force/width value between circumferential and longitudinal directions for the adventitia for all ILT age

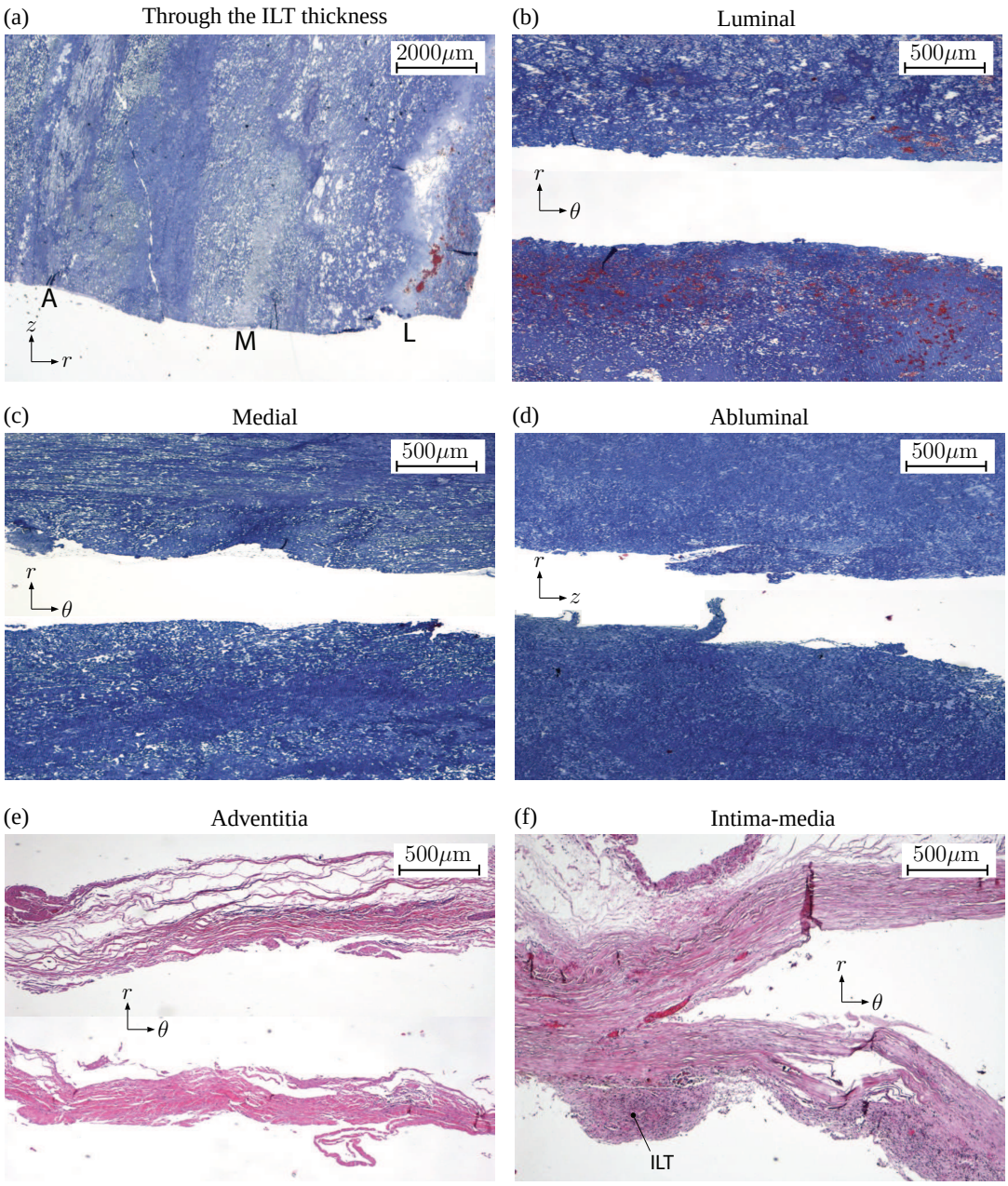

Figure 4.9: Histological images (SFOG) characterizing the dissected morphology during the peeling tests (a) through the ILT thickness (original magnification 10×) and within (b) luminal, (c) medial and (d) abluminal ILT layers (original magnification 40×). L, M, A in image (a) represent luminal, media, abluminal layers, respectively. Histological images (HE) of (e) the adventitia and (f) the intima-media showing morphology of the dissected surfaces within the thrombus-covered wall (original magnification 40×). All thrombi are in age phase III. The coordinates r, θ and z refer to the radial, circumferential and longitudinal direction, respectively.

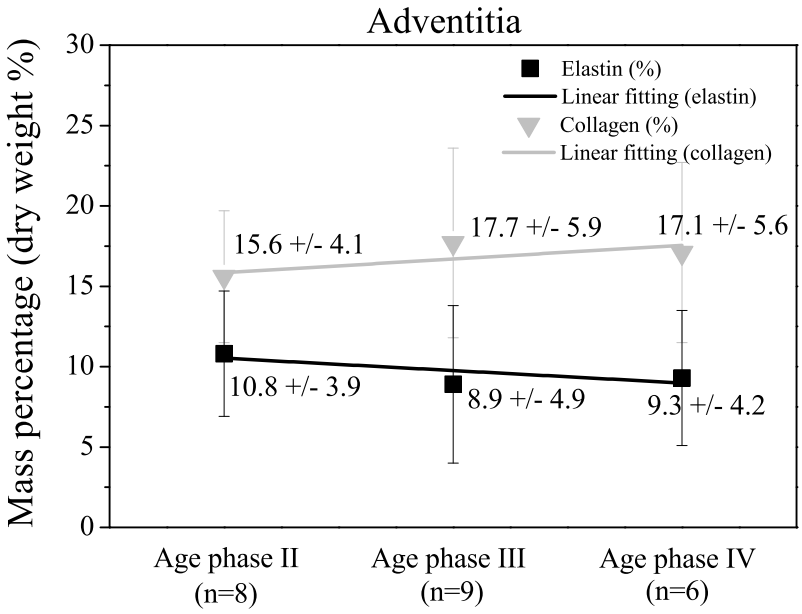

Figure 4.10: Mass fractions of elastin and collagen within the thrombus-covered adventitia in relative thrombus age phases II, III and IV.

phases, however, the intima-media composite (Fig. 4.7(b)) illustrates anisotropic dissection properties in age phase II in which the longitudinal force/width value is significantly larger than in the circumferential direction. This could partially be due to the collagen fibers generally oriented closer to the circumferential direction in the media [163]. However, the anisotropic dissection properties for that composite vanish progressively from age phase III to IV suggesting a more disorganized microstructure probably due to varying distributions and realignment of the aged collagen [23, 126]. A wall weakening effect of the ILT has been stressed by numerous previous studies [2, 84, 93, 184, 199, 202]. Our findings suggest that such a weakening effect is also represented by noticeable changes of the dissection properties of the wall tissue underneath the ILT, but it is mainly present for the intima-media composite. We further propose that with an increased ILT age the dissection through the intima-media composite may not be able to propagate also through the adventitia, as more dissection energy is needed (compare relevant values between the adventitia and the intima-media in Fig. 4.7 and Table 4.1).

Another goal of the current study was to examine whether the results of the protocol-controlled dissection test are rate dependent or not. Figure 4.8 demonstrates that the force/width values with the extension rate of 1 mm/sec are in average 18% (SD 7%) higher for the ILT when compared to 1 mm/min; the values are about 28% (SD 9%) higher for the diseased aortic wall. These findings suggest that the dissection properties of both the ILT and the thrombus-covered walls are rate dependent. Under the same extension rate of 1 mm/min, the mean force/width values for the diseased aortic intima-media are higher in

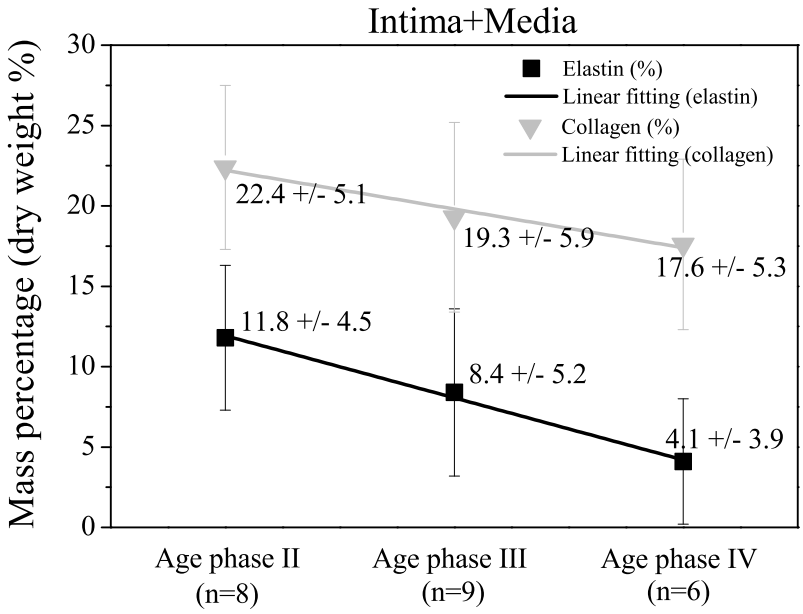

Figure 4.11: Mass fractions of elastin and collagen within the thrombus-covered intima-media composite in relative thrombus age phases II, III and IV.

the circumferential but lower in the longitudinal directions when compared to the healthy aortic media (HAM) [173] (Fig. 4.8(f)). Note also that the two speeds used in the current study may or may not be within the physiological domain since to our knowledge no clinical or mechanical data regarding the dissection propagation speed within the AAA *in vivo* are available. Hence, the two extension rates, i.e. 1 mm/min and 1 mm/sec, just represent very slow and very fast velocities.

Histological investigations show that the dissected surfaces during the peeling through the ILT thickness (Fig. 4.9(a)) and within the ILT layers (Figs. 4.9(b)-(d)) are quite smooth for most specimens. A few large fiber-like protein clots, generated from the surface, are also observed for the dissected thrombotic material (see, for example, the abluminal layer in Fig. 4.9(d)). As can be seen from the Figs. 4.9(e) and (f), the peeling within either the adventitia or the intima-media composite cause (much) rougher dissected surfaces due to the rupture of collagen fibers. This histological observation suggests that single fibrin fibers or smaller protein clots within the ILT structure are not strong enough to disrupt the surface unevenly during the peeling process when compared with collagen fibers within the aortic wall.

Dry weight percentage of elastin in the adventitia of the thrombus-covered wall decreases slightly from $10.8\% \pm 3.9\%$ to $9.3\% \pm 4.2\%$ ($p = 0.50$) from thrombus age phase II to IV, see Fig. 4.10. In contrast, the related value for collagen slightly increases from $15.6\% \pm 3.3\%$ to $17.1\% \pm 4.8\%$ ($p = 0.47$) as the ILT becomes older. The slight variations indicate that mass fractions of elastin and collagen within the thrombus-covered adventitia keep

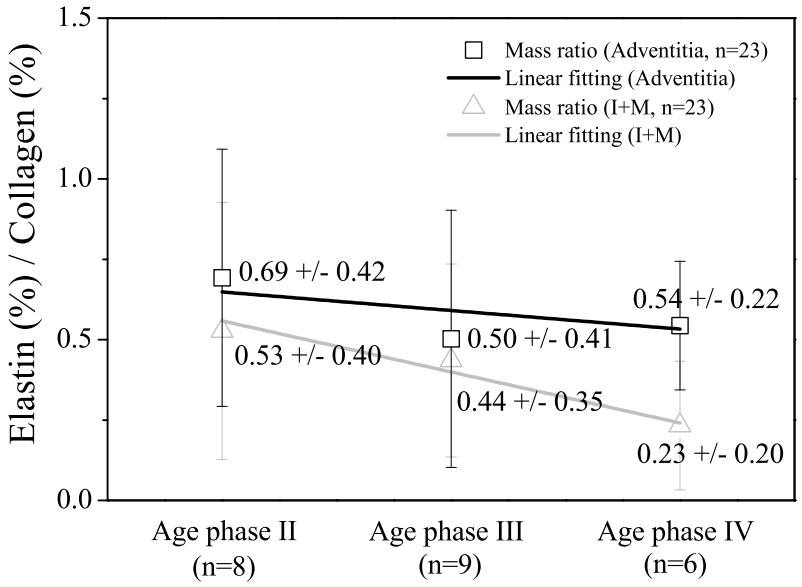

Figure 4.12: Mass fraction ratio between elastin and collagen within the thrombus-covered adventitia and intima-media (I+M) with respect to the relative thrombus age phases II, III and IV.

almost constant, and thus are hardly influenced by ILT age. Both elastin and collagen within the intima-media composite decrease in their mass fractions, as shown in Fig. 4.11, and, in particular, the mass loss of elastin is by a significant decrease from $11.8\% \pm 4.5\%$ in age phase II to $4.1\% \pm 3.9\%$ in age phase IV ($p = 0.01$). Despite the decrease in mass fraction from $22.4\% \pm 5.1\%$ in age phase II to $17.6\% \pm 5.3\%$ in age phase IV, the mass content of collagen did not change significantly ($p = 0.11$). By considering the mass ratio of elastin to collagen, linear fittings in Fig. 4.12 indicate that the ratios decrease for both the adventitia and the intima-media composite during the aging of ILT. The intima-media composite has a lower mass ratio than that of the adventitia probably due to a pronounced elastin loss within that composite. Note that the presented mass fraction data should not be mixed up with volume fractions reported in earlier studies such as He and Roach [73].

In terms of limitations we note that the *in vivo* cyclic pulsatile pressure was not taken into account during the protocol-controlled experimental tests, which, in the authors' opinion, may affect both the dissection propagation and the ILT failure. However, implementation of such a mechanical environment in the experimental tests is not so straightforward, but could possibly be done by using computational techniques.

4.5 Conclusion

Intraluminal thrombus aging leads to microstructural changes and to a higher risk of dissection initiation for the ILT and the intima-media composite of the aneurysmal wall. For each thrombus age phase, a dissection may propagate through the ILT thickness due to a continuous decrease of the dissection energy from the lumen to the ablumen side, although there is no evidence that fissures created by the tissue dissection can reach the underlying wall. According to our data, a dissection through the intima-media needs a higher energy value for a continuation in the adventitia. Moreover, it appears that the present study is the first which documents layer-specific mass fractions of the elastin and collagen within the AAA wall and correlates their variations with ILT ages. A pronounced decrease in mass fraction for elastin with an increasing ILT age was only found within the intima-media composite. The findings presented in this work may better explain fissure creation and propagation within the ILT structure and provide a basis for a refined understanding of the dissection-induced ILT failure and the related AAA rupture mechanism.

Acknowledgement

The authors particularly thank Britta Obrist from the Medical University of Graz for her help during the mass fraction analysis.

5 GENDER DIFFERENCES IN BIOMECHANICAL PROPERTIES, THROMBUS AGE, MASS FRACTION AND CLINICAL FACTORS OF ABDOMINAL AORTIC ANEURYSMS

Abstract The main purpose of the present study is the investigation of gender differences in the biomechanical properties, thrombus age, mass fraction and key clinical factors of abdominal aortic aneurysms (AAAs). A total of 90 AAA samples (78 males and 12 females) were harvested from open surgical aneurysm repairs. Biaxial extension and peeling tests were performed to characterize the biaxial mechanical responses and to determine dissection properties of both the intraluminal thrombi (ILT) and the thrombus-covered walls. Relative thrombus age was determined by characterizing the ILT histological microstructure. Mass fraction analyses quantified dry weight percentages of elastin and collagen within the AAA walls. Moreover, we statistically compared some key clinical factors between male and female. The luminal layers of the female thrombi and the female AAA walls showed a significantly lower tissue stiffness (modulus) in the longitudinal direction when compared to males. Gender differences were also shown in the dissection properties of the intima-media composite within the AAA walls, in which a statistically significantly lower energy to propagate a dissection was quantified for females than males. Moreover, 82% of female thrombi were relatively older thrombi (ILT age phases III and IV), twofold that of the male thrombi (43%). A pronounced lower elastin content was identified for the intima-media composites of the male AAA walls, whereas female AAA walls had significantly lower dry weight percentages of collagen. Regarding clinical factors, nicotine pack years, serum creatinine and AAA expansion rate were found to be much higher for male patients. These findings may help to explain higher risks for AAA growth in males and the ruptures of smaller sized AAAs in females.

5.1 Introduction

Gender differences in abdominal aortic aneurysms (AAAs) have been extensively investigated and discussed by a variety of previous studies [66, 70, 139, 172]. It is well known that male gender is more susceptible to developing an AAA, with a prevalence of 4:1 male to female ratio [171]. However, females have significantly faster growth rates [128, 172] and greater proportional dilatations [54] when compared with males. Reasons for gender-related differences remain unclear [87]. A rodent experimental model [3] implied that the

estrogen-mediated reduction in macrophage matrix metalloproteinase (MMP)-9 production in females was a main trigger for the disparity. Many studies also focused on the effect of gender on the risk of AAA rupture indicating that females had three to four times higher risks of aneurysm rupture than men [19, 20], as well as a higher proportion of ruptured versus elective repair [19, 167].

Recently, finite element analysis [101] was used to compute peak wall stress (PWS) and peak wall rupture risk (PWRR) with a gender perspective showing that PWRR is slightly higher in females. To date, a few studies describe the influence of gender on the biomechanical properties of AAA. The first and the only paper in this field was conducted by Vande geest et al. [190] The authors performed uniaxial extension tests to investigate the ultimate tensile strength of AAA wall tissue between different genders suggesting that there was a trend toward a decrease in wall strength of females as compared to males. However, information was lacking about the orientations of their rectangular specimens and more importantly, the mechanical behaviors of AAA wall tissue under multi-axial loading conditions for males and females remained unknown. Recently, the intraluminal thrombus (ILT) has received more attention in numerous AAA studies [84, 184, 193, 199, 204]. In particular, relative thrombus age first proposed by our lab [184], is an important factor to assess the strength of the wall underneath the ILT. This motivates our effort to explore gender differences in the biomechanical properties of tissues considering thrombus age. Moreover, there is a need to quantitatively determine the mass fraction of elastin and collagen within the male and female AAA walls.

The present study focuses on four aims: (i) we explore the influence of gender on the biaxial mechanical responses and the dissection properties of both the ILT and the thrombus-covered wall; (ii) we focus on the distributions of the relative thrombus age for male and female patients; (iii) we investigate gender differences with respect to mass fractions of elastin and collagen within AAA wall tissues; (iv) we compare some key clinical factors between male and female patients in order to examine whether gender difference matters or not.

5.2 Materials and Methods

5.2.1 Patient population

This study included 90 patients (mean age 69 ± 13 yrs, 78 males and 12 females) who underwent open surgical aneurysm repairs from November 2008 to March 2012 at the clinical department of vascular surgery, LKH Graz, Austria. Note that 61 male and 9 female aneurysms (out of a total of 90) were asymptomatic and 5 male aneurysms were ruptured. Use of the material was approved by the Ethics Committee, Medical University

Graz, Austria. All samples including the ILT and the thrombus-covered wall were procured from the anterior portion of the aneurysm and stored in Dulbecco's Modified Eagle's Medium (DMEM) after retrieval. The maximum AAA diameters were obtained from CT scan images. The maximum ILT thicknesses were measured at three different locations of the thickest part for each ILT sample and then averaged. The mean wall thicknesses were quantitatively measured by a PC-controlled videoextensometer.

5.2.2 Biomechanical tests

Details of specimen preparations and the experimental protocols for biaxial extension and peeling tests have been described in the previous studies by Tong et al. [184, 187]. Peeling tests quantitatively determine energy required to propagate a dissection in a tissue [187]. Briefly, rectangular strips were cut with a uniform dimension of 18.0×6.0 mm (length $\times$ width) and were further given an initial cut (incision of about 2.0-3.0 mm in length) using a surgical scalpel in order to better control the initiation of the tissue failure. Hence, two 'tongues' were obtained for mounting them into a PC-controlled, screw-driven high-precision tensile testing machine. The tests were executed in phosphate buffered saline solution at $37.0 \pm 1.0^{\circ}$C and the extension rate of 1 mm/min was maintained throughout the test. In the current study peeling tests were performed to dissect the material (i) within the individual ILT layers, (ii) through the ILT thickness and (iii) within the aneurysm wall underneath the thrombus. For more details of the protocol see the relevant sections in a very recent study [185], which provides the quantified dissection data for the current work..

5.2.3 Biomechanical data analysis

The Cauchy stress σ and the stretch λ were computed to quantify the biaxial biomechanical responses of the tissue. The mean peak stretch (MPS) values ($\lambda_{\theta,\max}$, $\lambda_{L,\max}$) for the three individual ILT layers and the thrombus-covered AAA walls in the circumferential and longitudinal directions were recorded. The maximum tangential modulus (MTM), defined as the slope of the nonlinear stress-stretch curve at the maximum load, was calculated for each patient and further averaged to assess stiffness at $P_{\theta\theta} = P_{LL} = 20$ kPa for the ILT and at $P_{\theta\theta} = P_{LL} = 150$ kPa for the AAA wall. For the peeling test, the force/width values denoted by F_{pc} and F_{pl} were measured and averaged for the circumferential and longitudinal strips, respectively. Further, the dissection energy per reference area, say W^{dissect}, during the (circumferential c and longitudinal l) peeling (p) was quantified by subtracting the elastic energy W^{elastic} from the external work W^{ext}, i.e. $W_{\mathrm{pc}}^{\mathrm{dissect}} = (W_{\mathrm{c}}^{\mathrm{ext}} - W_{\mathrm{pc}}^{\mathrm{elastic}})/L_{\mathrm{pc}}$ and $W_{\mathrm{pl}}^{\mathrm{dissect}} = (W_{\mathrm{l}}^{\mathrm{ext}} - W_{\mathrm{pl}}^{\mathrm{elastic}})/L_{\mathrm{pl}}$, where L_{pc} and L_{pl} denote the reference lengths of the strips in the circumferential and longitudinal directions, respectively. The way how the elastic energy and the external work during the peeling are computed has been described in a previous study [187].

5.2.4 Thrombus age determination and mass fraction analysis

Current techniques of thrombus age determination within the AAA are used to characterize microstructural changes in histology; for details of the methods see the related studies [84, 184].

The mass fraction analysis in the current study quantitatively determined dry weight of elastin and collagen within the intima-media and the adventitia of the AAA wall. Tissues were frozen in liquid nitrogen and homogenized by grinding in a mortar with a pistil. The wet and dry weight after reaching constant weight by drying for 3 to 4 days at 105°C of the homogenate were determined, respectively.

Elastin quantitation was performed with the fastin elastin assay (Biocolor, Carrickfergus, UK) following the manufacturer's instructions. Essentially, elastin was extracted three times from the dried tissue homogenates with 100°C hot 0.25 M oxalic acid for one hour. Elastin precipitated by trichloroacetic and hydrochloric acid was bound to the dye 5, 10, 15, 20-tetraphenyl-21H,23H-porphine tetra-sulfonate and resolubilized in guanidine HCl for spectroscopic analysis at 513 nm. Elastin amounts were calculated from a standard curve determined by co-processing elastin standards of 12.5, 19, 25, 35 and 50 μg.

Collagen analysis was performed by following published procedures [149]. Essentially, collagen was hydrolyzed by 2 M NaOH for 20 min at 121°C in an autoclave. Released hydroxyproline was oxidized by Chloramine-T. Addition of Ehrlich's reagent resulted in a chromophore that was analyzed by spectroscopy at 550 nm. Hydroxyproline amounts were calculated from a standard curve determined by co-processing hydroxyproline standards of 0-20 μg. Collagen amounts were calculated from its hydroxyproline content of 12.5% [41].

5.2.5 Clinical factors

The study included 90 patients undergoing open abdominal aneurysm repair. All patients had a preoperative abdominal aortic computed tomography (CT) scan. Patients' data were collected prospectively after being admitted. Information which entered into the database included patients demographics, body mass index, history including nicotine use, comorbidities including hypertension, diabetes mellitus, and renal dysfunction, preoperative clinical data and results from the computed tomography.

5.2.6 Statistical analysis

All results were statistically reported as mean $\pm$ SD. The Shapiro-Wilk and the Kolmogorov-Smirnov tests were utilized to determine the data normality. Comparisons of the quantita-

tive values between males and females were performed by using the Student's t-test and Chi-squared test. A p-value of less than 0.05 determined significant.

5.3 Results

5.3.1 Patient data

Comparisons of age, maximum AAA diameter, maximum ILT thickness and wall thickness between 78 male and 12 female patients are documented in Table 5.1. Males were significantly younger ($p = 0.01$) and had larger AAA diameters ($p = 0.03$) than females. No significant difference was found in either the maximum ILT thickness ($p = 0.21$) or the wall thickness ($p = 0.11$) between male and female.

Table 5.1: Data for age, maximum AAA diameter, maximum ILT thickness and wall thickness for male ($n = 78$) and female ($n = 12$) patients.

	Male ($n = 78$)	Female ($n = 12$)	p-value
Age (years)	66 ± 11	75 ± 6	0.01
Max. diameter (cm)	5.9 ± 0.9	5.3 ± 0.6	0.03
Max. ILT thickness (cm)	2.3 ± 0.8	2.0 ± 0.5	0.21
Wall thickness (mm)	2.6 ± 0.6	2.3 ± 0.4	0.11

5.3.2 Biomechanical properties

The Shapiro-Wilk and the Kolmogorov-Smirnov tests showed that the MPS and MTM values and the dissection energy were normally distributed.

Biaxial mechanical responses

For that part a total of 45 male and 7 female samples were tested and analyzed. The mean biaxial mechanical responses of the luminal, medial, abluminal layers and the thrombus-covered walls considering gender differences are shown in Fig. 5.1. The relevant MPS and MTM values in the circumferential and longitudinal directions for males and females are summarized in Table 5.2. The circumferential and longitudinal MPS of both luminal and medial layers and the longitudinal MPS of the thrombus-covered wall were significantly larger for females than those of males (all p values less than 0.05). The luminal layers of the female thrombi and the female AAA walls showed a significantly lower MTM ($p = 0.04$ vs. 0.03) in the longitudinal direction when compared to males.

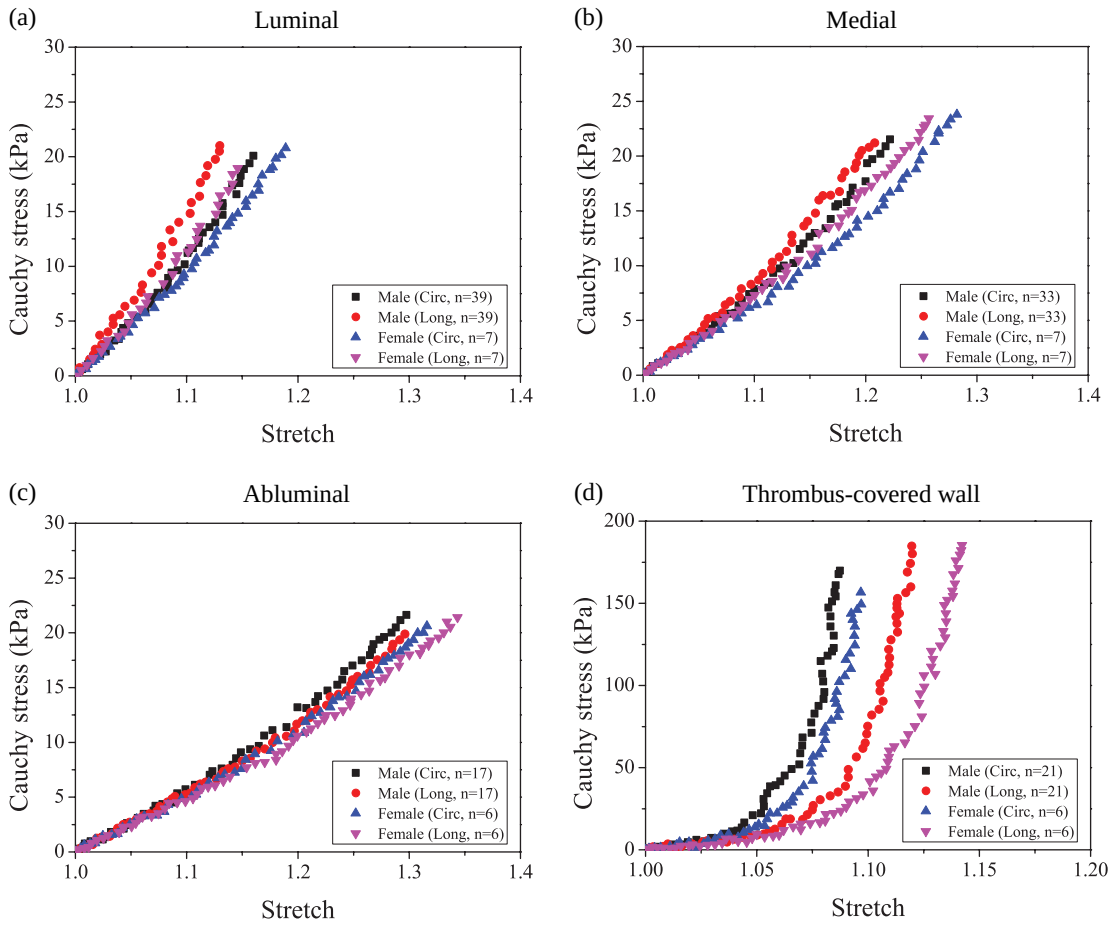

Figure 5.1: Gender differences for the mean biaxial mechanical responses of the luminal, the medial, the abluminal layers and the thrombus-covered walls. Circ and Long represent circumferential and longitudinal directions, respectively.

Dissection properties

We performed peeling tests to dissect 33 male and 5 female samples. Gender differences in dissection energy of the individual ILT layers, through the ILT thickness and within the thrombus-covered walls are shown by column plots in Figs. 5.2, 5.3 and 5.4, respectively. The computed dissection energy values for males and females are summarized in Table 5.3. No significant difference was found in the energy between male and female to dissect the individual ILT layers. A statistically significantly lower energy to propagate a dissection (subsequently called ‘fracture energy’) was quantified to dissect within the intima-media composite for female when compared to males (circumferential: $p = 0.01$; longitudinal: $p = 0.04$).

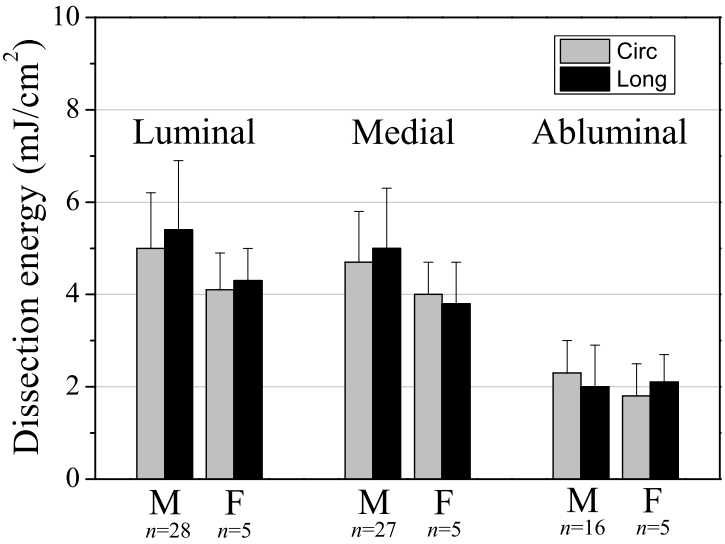

Figure 5.2: Gender differences in the dissection energy during the peeling within the individual ILT layers, i.e. luminal, medial and abluminal. Circ and Long represent the circumferential and longitudinal directions, respectively. Male and female are represented by M and F, respectively.

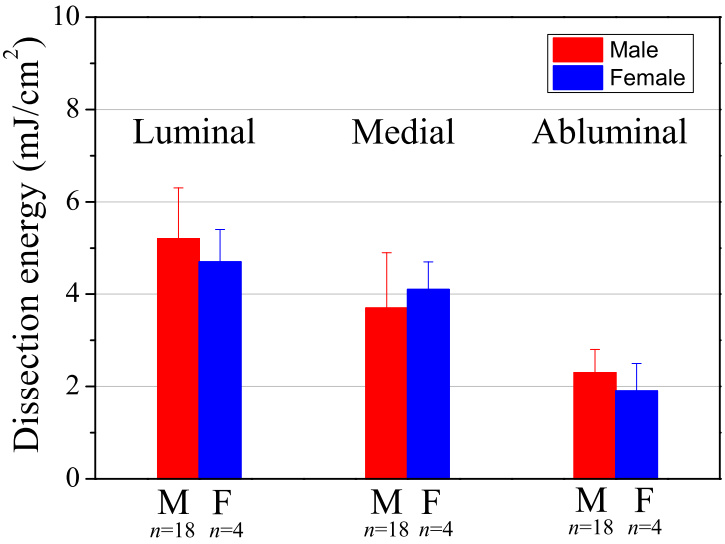

Figure 5.3: Gender differences in the dissection energy during the peeling through the ILT thicknesses. Male and female are represented by M and F, respectively.

Table 5.2: Mean peak stretch ($\lambda_{\theta,\max}$, $\lambda_{L,\max}$) and maximum tangential modulus (MTM) values (Mean $\pm$ SD) between male and female for the equibiaxial stress-controlled protocol ($P_{\theta\theta} = P_{LL} = 20\,\text{kPa}$) for the luminal ($n = 46$), medial ($n = 40$), abluminal layers ($n = 23$) and for the equibiaxial stress-controlled protocol ($P_{\theta\theta} = P_{LL} = 150\,\text{kPa}$) of the thrombus-covered walls ($n = 27$).

		Male ($n = 39$)	Female ($n = 7$)	p-value
Luminal	$\lambda_{\theta,\max}$	1.16 ± 0.05	1.20 ± 0.03	0.04
	$\lambda_{L,\max}$	1.12 ± 0.03	1.15 ± 0.02	0.02
	MTM_θ (kPa)	196 ± 48	161 ± 31	0.07
	MTM_L (kPa)	290 ± 52	246 ± 39	0.04
		Male ($n = 33$)	Female ($n = 7$)	p-value
Medial	$\lambda_{\theta,\max}$	1.23 ± 0.04	1.27 ± 0.03	0.02
	$\lambda_{L,\max}$	1.20 ± 0.05	1.25 ± 0.03	0.02
	MTM_θ (kPa)	143 ± 35	125 ± 29	0.21
	MTM_L (kPa)	158 ± 41	130 ± 32	0.10
		Male ($n = 17$)	Female ($n = 6$)	p-value
Abluminal	$\lambda_{\theta,\max}$	1.28 ± 0.04	1.30 ± 0.03	0.28
	$\lambda_{L,\max}$	1.30 ± 0.05	1.33 ± 0.03	0.18
	MTM_θ (kPa)	110 ± 33	101 ± 21	0.54
	MTM_L (kPa)	105 ± 25	93 ± 18	0.29
		Male ($n = 21$)	Female ($n = 6$)	p-value
Thrombus-covered wall	$\lambda_{\theta,\max}$	1.08 ± 0.03	1.10 ± 0.02	0.14
	$\lambda_{L,\max}$	1.11 ± 0.04	1.15 ± 0.02	0.03
	MTM_θ (MPa)	8.8 ± 2.5	6.7 ± 1.8	0.07
	MTM_L (MPa)	6.3 ± 2.1	4.1 ± 1.6	0.03

5.3.3 Thrombus age

Four relative thrombus age phases, namely phase I (very fresh), phase II (young), phase III (intermediate), phase IV (old), were proposed to describe the ILT evolution within the AAA; relevant histological characteristics for each age phase were summarized in a previous study [184]. In the current study the thrombus ages of 78 ILT samples were determined by histology, which consist of 4 fresh, 36 young, 22 intermediate and 16 old thrombi. Within each thrombus age phase, the number of patients and their percentages with respect to the total number of male and female are shown in Fig. 5.5. Approximately 82% of female thrombi were relatively old thrombi (ILT age phases III and IV), twofold that of the male thrombi (43%).

5.3.4 Mass fraction

Mass fractions of elastin and collagen within the thrombus-covered intima-media composite and the adventitia for male and female patients are shown in the Figs. 5.6 and 5.7, re-

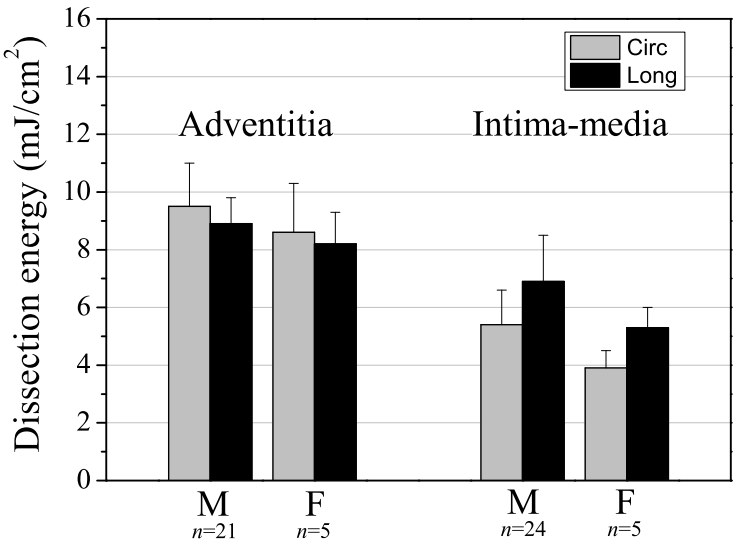

Figure 5.4: Gender differences in the dissection energy during the peeling within the adventitia and the intima-media composite of the thrombus-covered walls. Circ and Long represent the circumferential and longitudinal directions, respectively. Male and female are represented by M and F, respectively.

spectively. Within the thrombus-covered intima-media composite, a mass fraction analysis shows that males have a significantly lower dry weight percentage of elastin than females (male: $4.8\% \pm 3.4\%$ vs female: $8.9\% \pm 2.9\%$; $p = 0.04$), see Fig. 5.6. However, the dry weight percentage of collagen in that composite is significantly higher for males when compared to females (male: $25.6\% \pm 5.9\%$ vs female: $18.3\% \pm 5.1\%$; $p = 0.03$). For the thrombus-covered adventitia, there is no significant difference in the mass fraction of the elastin between male and female (male: $8.7\% \pm 3.5\%$ vs female: $10.6\% \pm 3.1\%$; $p = 0.33$), see Fig. 5.7. However, males have a statistically significantly higher dry weight percentage of collagen than females (male: $21.5\% \pm 6.3\%$ vs female: $13.8\% \pm 4.5\%$; $p = 0.03$).

5.3.5 Clinical factors

The data of clinical presentation, nicotine abuse, body mass index, concomitant diabetes mellitus, renal function, chronic obstructive pulmonary disease, hypertension, AAA shape and expansion rate are shown in Table 5.4. All patients had a history of hypertension. There was no significant difference between male and female patients regarding the clinical status of the aneurysm at the time of operation, body mass index, presence of concomitant diabetes mellitus, chronic obstructive pulmonary disease, hypertension and AAA shape. However, male patients showed significantly higher nicotine abuse represented by pack

Table 5.3: Gender differences in the computed dissection energy (mJ/cm^2) during the peeling tests within the individual ILT layers ($n = 33$), through the ILT thickness ($n = 22$) and within the thrombus-covered walls ($n = 29$). The circumferential and longitudinal directions are denoted by c and l, respectively.

			Dissection energy (mJ/cm^2)		
			Male ($n = 28$)	Female ($n = 5$)	p-value
Within the ILT layers	Luminal	c	5.0 ± 1.2	4.1 ± 0.8	0.12
		l	5.4 ± 1.5	4.3 ± 0.7	0.12
	Medial	c	4.7 ± 1.1	4.0 ± 0.7	0.18
		l	5.0 ± 1.3	3.8 ± 0.9	0.08
	Abluminal	c	2.3 ± 0.8	1.8 ± 0.7	0.23
		l	2.0 ± 0.9	2.1 ± 0.6	0.82
			Male ($n = 18$)	Female ($n = 4$)	p-value
Through the ILT thickness	Luminal		5.2 ± 1.1	4.7 ± 0.7	0.39
	Medial		3.7 ± 1.2	4.1 ± 0.6	0.53
	Abluminal		2.3 ± 0.5	1.9 ± 0.6	0.23
			Male ($n = 24$)	Female ($n = 5$)	p-value
Within the thrombus-covered wall	Adventitia	c	9.5 ± 1.5	8.6 ± 1.7	0.25
		l	8.9 ± 0.9	8.2 ± 1.1	0.15
	Intima-media	c	5.4 ± 1.2	3.9 ± 0.6	0.01
		l	6.9 ± 1.6	5.3 ± 0.7	0.04

years ($p = 0.03$), value of serum creatinine ($p = 0.002$) and AAA expansion rate ($p = 0.026$).

5.4 Discussion

Data in Table 5.1 clearly indicate that the age of female patients is significantly higher than that of males. However, the maximum AAA diameters were statistically significantly smaller for females when compared to males. With a gender perspective, a lower AAA diameter did not indicate a relatively lower risk for female patients in determining elective surgical repairs since normal aortic diameter of females is in average 2 mm smaller than that of males [102, 174]. Instead, the relative AAA diameter, which is defined as maximum AAA diameter versus normal aortic diameter, was suggested as a geometrical factor for the rupture risk assessment [100]. There was no significant difference in either the maximum ILT thickness or the wall thickness between male and female. Note, however, that the AAA has a significant regional variation in wall thickness [145]. Since the wall samples in the current study were obtained from the thrombus-covered regions, our results cannot be applied to the whole AAA.

For the biaxial mechanical responses of the luminal layers, the circumferential and longitu-

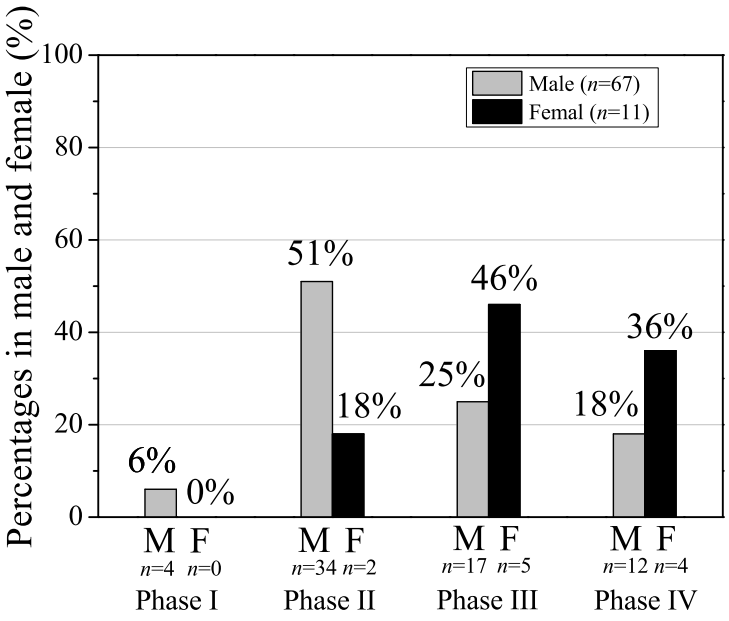

Figure 5.5: Comparisons of the number of patients and their percentages with respect to the total number of male and female within each thrombus age phase. Male and female are represented by M and F, respectively.

dinal MPS $\lambda_{\theta,\max}$ and $\lambda_{L,\max}$ of females were significantly larger than those of males (see Table 5.2). The MTM in the longitudinal direction was found to be significantly smaller for females when compared to males. These results suggest that the luminal layers of the female thrombi are more extensible during biaxial extension and generally weaker in the longitudinal direction as compared to males. Although the MPS of the medial layers in the circumferential and longitudinal directions are significantly larger for females, there was no significant difference in MTM values between genders. A continuous increase in the extensibility and a decrease in the stiffness from the luminal to the abluminal side were observed in the biaxial mechanical behaviors of the ILT [184]. As the weakest layer in material stiffness, the MPS and MTM values of the abluminal layers in the circumferential and the longitudinal directions are not influenced by gender. For the thrombus-covered walls, it appears that females had a statistically significantly larger value $\lambda_{L,\max}$ but a significantly lower value MTM_L when compared to males, suggesting that aneurysmal wall strength in the longitudinal direction is (much) weaker for female than for male. In contrast, gender differences were not observed in the mechanical responses of the aneurysmal wall tissue in the circumferential direction. These results imply that the male and the female thrombi might have different wall weakening effects, which needs further investigations.

As can be seen from the Figs. 5.2, 5.3 and the Table 5.3, no significant difference was found in the energy between male and female to dissect the individual ILT layer (i.e. luminal, medial and abluminal) and through the ILT thickness. Moreover, the dissection

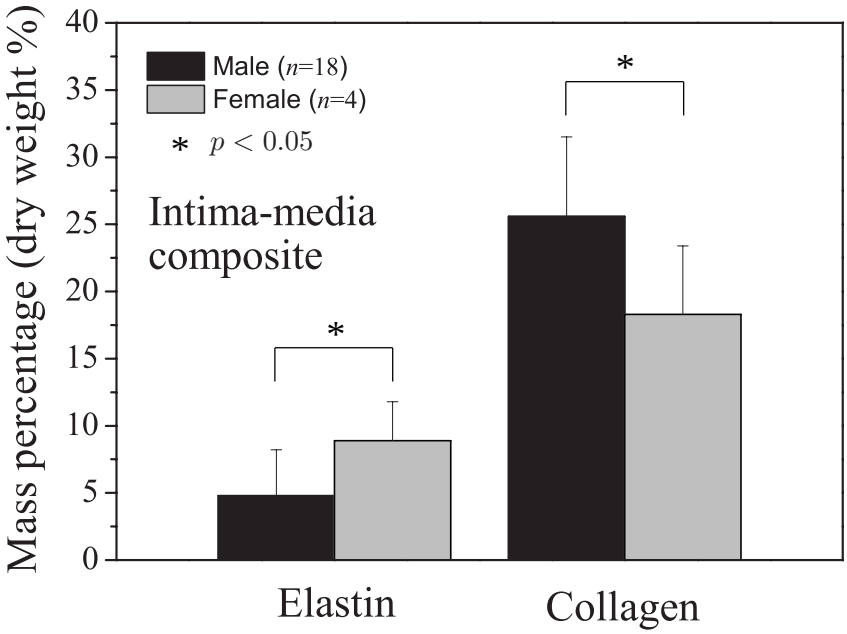

Figure 5.6: Mass fractions of elastin and collagen within the thrombus-covered intima-media composite for male and female patients. Significant differences are noted for the dry weight percentages of both elastin and collagen between male and female.

properties of the ILT are not direction-dependent for male and female. Based on these experimental data, it is, therefore, suggested that gender differences are not shown in the ILT dissection properties. It should also be emphasized that the *in vivo* ILT dissection occurs in a more complex and potentially dynamic mechanical environment. Many factors may directly (or indirectly) influence the dissection initiation and propagation of the ILT within the AAA, and hence the gender differences might exist. Although there is no significant difference in the dissection properties of the thrombus-covered adventitia between male and female in both circumferential and longitudinal directions, a statistically significantly lower fracture energy can be quantified to dissect within the intima-media composite for female, as compared to male (see Fig. 5.4 and Table 5.3). Despite a more disorganized aortic structure compared to the healthy aorta [23, 84, 126, 185], the dissection properties of the intima-media composite for the male and the female AAAs are generally anisotropic, which means that more resistance would be given to tissue dissection along the longitudinal direction.

Further, we compare the relative thrombus age between 67 male and 11 female patients. Since current techniques in the relative thrombus age determination do not provide actual number of days or other time units, the main focus here is to statistically analyze the number of patients for each thrombus age phase and the distribution trend, which is shown in

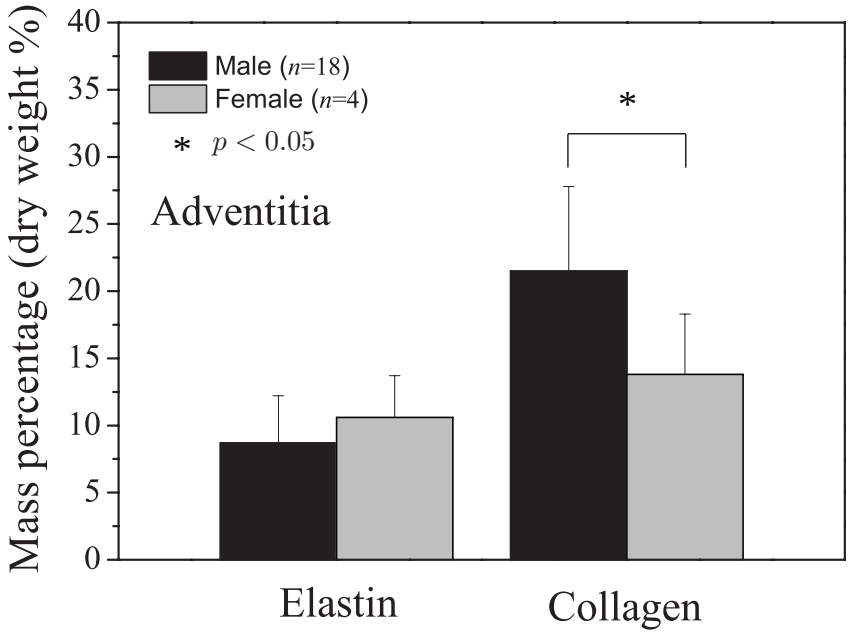

Figure 5.7: Mass fractions of elastin and collagen within the thrombus-covered adventitia for male and female patients. A significant difference is noted for the dry weight percentage of collagen between male and female.

Fig. 5.5. Due to the small size of the female group, it is not meaningful to compare patient numbers between male and female in each thrombus age phase but rather their percentages with respect to total male and female numbers. It appears that 82% of the females have relatively older thrombi (mainly in the age phases III and IV) when compared to that of males (43%). A consideration of the wall weakening effect of the ILT during aging [184] would probably suggest that female thrombi are more likely to lead to a lower underlying aneurysmal wall strength as compared to male thrombi. To further justify this assumption, a larger database of female patients and relevant mechanical data for individuals are needed.

Mass fraction analyses suggest that there is a pronounced lower elastin within the intima-media of the AAA wall for males when compared to females. However, the female AAA wall has a significantly lower dry weight percentage of collagen. In general, increased collagen contents is an indicator for increased collagen fiber cross-linking, which leads to a higher stiffness of the wall.

In the current study, 61 male and 9 female aneurysms (out of a total of 90) were asymptomatic. Regarding gender differences in the clinical data, female patients had (significantly) lower values of nicotine pack years, diabetes and renal function (serum creatinine) and AAA expansion rate, see Table 5.4. It is well known that nicotine abuse is the main

Table 5.4: Gender differences for the clinical data of 90 AAA patients; $^{*}p < 0.05$.

		Male ($n = 78$)	Female ($n = 12$)	p-value
Clinical presentation	asymptomatic	61	9	0.51
	symptomatic	12	3	
	ruptured	5	0	
Body mass index		26.3 ± 3.5	26.2 ± 4.5	0.91
Nicotine	(pack years)	46.7 ± 51.6	18.8 ± 18.9	0.03^{*}
Diabetes mellitus		11	3	0.28
Serum creatinine	(mg/dl)	1.26 ± 0.64	0.92 ± 0.22	0.002^{*}
Chronic obstructive pulmonary disease		11	2	0.68
Hypertension	normal	1	0	0.19
	controlled	51	11	
	poorly controlled	26	1	
AAA shape	fusiform	68	10	0.49
	saccular	10	2	
AAA expansion rate	(mm/year)	5.4 ± 2.4	3.3 ± 1.0	0.026^{*}

trigger to cause elastin loss of human aortas, which contributes to aneurysmal development. From this point of view, females show a lower risk of developing AAAs than males. According to clinical experience, rupture is more frequently associated with large and rapidly growing aneurysms and both parameters are significantly higher in males. However, these two clinically observed parameters cannot be applied to rupture risk prediction for females, since the female AAA walls show statistically significantly lower (longitudinal) tissue stiffness. Future effort is merited to the optimization of treatment strategies and to develop a more reliable rupture prediction system especially for female patients. Therefore, advanced data analyses of female patients are highly recommended.

5.5 Conclusion

In summary, the luminal layers of the female thrombi are, in general, less stiff when compared to males, while there is no significant difference in tissue stiffness for the medial and abluminal layers between males and females. The AAA wall strength in the longitudinal direction is significantly lower for females than for males. Gender differences are not shown in the dissection properties of the ILT and the adventitia within the thrombus-covered wall. However, a significantly lower fracture energy is quantified to dissect within the intima-media composite for females when compared to males. According to the relative thrombus age, 82% of female thrombi are in the age phases III and IV (relatively older ILT), which is much higher than those of male, i.e. 43%. Moreover, female AAA walls have significantly lower dry weight percentages of collagen, and a pronounced lower elastin content is identified for the intima-media composite of male AAA walls. In terms

of key clinical factors, males have significantly higher nicotine pack years, serum creatinine and AAA expansion rates than females, which relate to their higher risk of developing AAAs. These findings provide a more comprehensive understanding of gender differences in the AAA lesion and may explain higher risks of AAA development and rupture from a gender perspective.

Acknowledgement

The authors particularly thank R. Birner-Gruenberger, J. Kohlbacher and B. Obrist from the Medical University of Graz for their help during the mass fraction analysis.

6 RECENT ADVANCES IN THE BIOMECHANICS OF ABDOMINAL AORTIC ANEURYSMS

Abstract An abdominal aortic aneurysm (AAA) is a vascular pathology associated with permanent and irreversible localized dilatations. An untreated AAA may lead to an eventual rupture with a high mortality rate. In recent studies the biomechanics of AAA has been widely used to assess the rupture risk. In this review chapter, the biomechanical properties of aneurysm tissues including the intraluminal thrombus are first discussed. Benefits are reaped by a comprehensive understanding of the influence of these properties on the AAA growth and remodeling, from a biomechanical point of view. A subsequent section briefly summarizes and compares corresponding material models of AAA, as derived in recent studies, which plays a key role in providing a more reliable rupture prediction using computational techniques such as the finite element method. In the section on predicting the rupture risk, our effort is devoted to the review of a series of representative studies that were documented in the literature over the last decade. The discussion primarily focuses on a wide range of important findings and developments based on experimental and computational investigations. Regarding histology, particular attention is given to a possible way of thrombus age determination, a new topic in the biomechanical AAA research. The final section provides a brief summary of the current situation of AAA biomechanics and discusses some topics which may be relevant in future research.

6.1 Introduction

Abdominal aortic aneurysms (AAAs) are localized, balloon-like dilatations of abdominal aortas that exceed the normal diameter by more than 50%. This vascular pathology primarily occurs in the elderly male population [52, 142]. An untreated AAA may be at high risk of rupture, which has an overall mortality rate of between 75 and 90% [52]. The decision to electively repair AAA is frequently determined by the likelihood of rupture, which is mainly based on the unreliable ‘maximum diameter criterion’, i.e. 5-5.5 cm. Other factors such as aneurysm expansion rate [177], peak wall stress [105, 204], and geometrical factors [37] of the aneurysm are also considered to assess the AAA rupture potential. However, no reliable criterion can yet predict the risk of AAA rupture and help in the final clinical decision. A very recent study by Malkawi et al. [115] demonstrates that patient-specific biomechanical factors may be more reliable in predicting AAA rupture than currently available clinical and biochemical parameters.

From a biomechanical point of view, AAA rupture is a mechanical failure of the aneurysm wall, which occurs when the peak wall stress (PWS) exceeds the local strength of the aortic tissue. Therefore, the balance between PWS and wall strength is a critical point. The wall stress distribution has been investigated by many studies using, for example, computational approaches [48, 147], however, available data of wall strength are mainly obtained from in vitro experimental tests [120, 145], which do not represent the wall strength in the physiological environment *in vivo*.

Several recent studies have also focused on the intraluminal thrombus (ILT), which is a three-dimensional fibrin structure with blood proteins, blood cells, platelets and cellular debris [72]. Thrombus formation is a consequence of platelet activation and aggregation, and is much dependent on the aneurysm shape. As suggested by previous investigations [89, 133, 204], the presence of the ILT alters the wall stress distribution and reduces the PWS in AAAs. Owing to the fact that the ILT is usually found at the rupture site of AAAs [118], its wall weakening effect has also been explored and addressed by a series of studies [2, 93]. For example, Vorp et al. [199] propose that the ILT serves as a barrier to oxygen supply from the lumen, causing a hypoxia of the aortic wall. At least of similar importance, Schurink et al. [164] substantiated that a thrombus within the aneurysm does not reduce both the mean and the pulse pressure near the aneurysm wall, and thus would not reduce the risk of AAA rupture from the loading point of view. These observations suggest that the ILT may increase the risk of rupture for a given AAA morphology.

Over the last few years, the mechanics of AAA is a focus which has been widely studied, in particular within the biomechanical community. In this review chapter, we briefly describe and summarize recent developments in the biomechanics of AAA. In particular, we focus on (i) the biomechanical behaviors of the ILT and the aneurysm wall, (ii) the relevant material modeling, (iii) the morphological characteristics of both tissue types in terms of histology, and (iv) the thrombus age within AAA. A variety of aspects including both experimental and computational contributions from the last 10 years are also considered.

The content of this article is summarized as follows. In section 2, we provide an overview of the biomechanical behaviors of the ILT and the aneurysm wall. That section documents uniaxial and biaxial mechanical responses of the aneurysm tissue, failure properties, mechanical anisotropy, and microstructural characterization, which are helpful to better understand growth and remodeling of AAAs. In section 3, we mainly discuss material models to characterize the biomechanical behaviors of aneurysm tissues. The implementation of more appropriate constitutive relations into finite element codes would improve the reliability of stress prediction in patient-specific AAAs. Section 4 reviews some representative experimental and computational studies based on sophisticated patient-specific models to predict the wall stress distribution and the rupture risk. Morphological characteristics in terms of the histology is highlighted in section 5, with particular reference to the thrombus age in the AAA. The final section summarizes the current situation and points to challenges in future AAA research.

6.2 Biomechanical Properties of the ILT and the Aneurysm Wall

We present recent findings on the biomechanical properties of intraluminal thrombus and abdominal aortic aneurysm wall.

6.2.1 The intraluminal thrombus

It has been suggested that the mechanical failure in the ILT may propagate towards the weakened aneurysm wall underneath the ILT, and that it could initialize AAA failure. In order to investigate the influence of ILT on the biomechanics of AAAs, it is critically important to study and establish its biomechanical responses. Wang et al. [203] performed uniaxial tensile tests to evaluate the biomechanical ILT properties, and three individual layers (i.e., luminal, medial, abluminal) were identified, suggesting that ILT is a heterogeneous, nonlinear elastic and isotropic material. Using both uniaxial tensile and fatigue tests, Gasser et al. [56] reported that the ultimate tensile strength (i.e., the engineering stress) of ILT (156, 92 and 48 kPa for the luminal, media and abluminal layers, respectively) continuously decreases from the luminal to the abluminal side. In addition, it was suggested that the ILT is a vulnerable tissue against fatigue failure, which shows (significant) decreasing strength under cyclic loading. In recent studies, biaxial extension tests have been extensively used because uniaxial extension tests do not cover the physiological loading/stress domain appropriately. For example, by using planar biaxial tests of ILT luminal layers, van de Geest et al. [193] concluded that the luminal layers behave in an isotropic manner, which is consistent with the finding of previous uniaxial extension tests. More recently, our lab reported a set of biaxial data [184] with respect to the three individual ILT layers and fresh thrombi. When compared with previous results, we find that there is a clear indication of mechanical anisotropy for several investigated luminal layers. We concluded that the luminal layer of the ILT is, in general, not an isotropic material. The stiffness of the anisotropic luminal layers in the longitudinal direction is (much) larger with respect to that in the circumferential direction or to the luminal layers, which behaved isotropically, see, for example, Fig. 3.3. However, the circumferential stiffness in the stresscontrolled protocol (engineering stress $P_{\theta\theta} = P_{LL} = 20$ kPa) is not significantly different. Our experimental tests suggest that medial and abluminal layers are isotropic, see also Fig. 3.3. In addition, dark-red fresh thrombi have very unique characteristics, which are not layer-specific and homogeneous, and which is in contrast with old and organized thrombi. Indeed, a fresh thrombus is a very special material, which needs to be investigated in more detail. No reference could be found to clearly interpret the exact age of fresh thrombi within the AAA.

Based on biaxial extension tests, the average engineering stress values to cause the specimens to rupture for the luminal, medial and abluminal layers are determined as 61, 41 and 28 kPa [184] which are much lower rupture values as those documented previously in

the literature [56] pointing to the differences in, for example, the methods used for testing (uniaxial versus biaxial testing). To further interpret the mechanical properties of ILT tissues, a microstructural characterization is required. For example, we documented [184] that about 70% of the cracks in the luminal layers were found along the longitudinal direction. It is believed that this crack morphology is closely related to the microstructure of the ILT, i.e. the pore orientations, shapes, and protein bonds between two neighboring pores within the fibrin networks. The three-dimensional structural information of the ILT is not yet available; it may lead to a complex scenario of micro-scale stress distributions under macroscopic loading conditions. As a poroelastic material, the compressive biomechanical properties of the ILT are also investigated, and discussed in a recent study by Ashton et al. [7] These authors reported the water content of the native ILT and a thrombus mimic, providing a more comprehensive understanding of its permeability during the pressure transmission. These datasets may also serve as a key reference in manufacturing a thrombus mimic, particularly for experimental evaluations to AAA rupture. Moreover, as a key index, the thrombus volume is calculated and correlated to AAA growth rate using both idealized and patient-specific AAA models. In a very recent study Speelman et al. [176] concluded that a larger thrombus is associated with a higher AAA growth rate but with a lower wall stress (Fig. 6.1), emphasizing that the mechanical role of the ILT on AAA growth and remodeling should not be underestimated.

6.2.2 The abdominal aortic aneurysm wall

The AAA wall is a type of degenerated abdominal aortic wall which may also be associated with atherosclerosis. There is a notable regional variation on wall thickness to observe, as mentioned by Raghavan et al. [145], who also measure a failure stress range of aneurysm walls between 336 kPa and 2.35 MPa. Later, biaxial extension tests were performed on aneurysm tissues [191, 192], which allow for more realistic data (when compared with data from uniaxial extension tests, performed in one direction), and more appropriate material modeling; especially the understanding of the nature and extent of mechanical anisotropy is key.

As presented by Vande Geest et al. [191], the biaxial biomechanical response of the human abdominal aorta is affected by age. Typically, a higher extensibility is observed for younger tissue, which is less than 30 years. The old group (over 60 years), however, shows strong wall stiffening with much lower peak wall stretch values. A further study [192] details the effect of aneurysm degeneration on the normal abdominal aorta, showing that there is a pronounced increase of mechanical anisotropy associated with circumferential stiffening. These findings have a clinical significance to better interpret disease progression. Available experimental data show the biomechanical properties of aneurysm walls [145, 191, 192], however, from these studies, it is not clear if the wall is covered with thrombus or not. It is important to note here that due to aneurysm wall degeneration and wall weakening effects

of the ILT, the biomechanical properties and the histological structure of the thrombus-covered wall may be remarkably different from that of a thrombus-free wall, even in the same AAA. Hence, the biomechanical properties may vary in a significant manner for different types of AAA walls. Previously, Di Martino et al. [120] showed that the tensile strength of ruptured AAA tissues is significantly lower than that for an electively repaired AAA tissue, suggesting that AAA rupture is associated with aortic wall weakening. Our recent experimental results [184] demonstrate that the thrombus-covered walls exhibit exponential stiffening with loading and anisotropic responses, where the wall is stiffer in the circumferential than in the longitudinal direction, see, for example, the set of symbols in Fig. 3.4 as previously shown.

This finding is basically in agreement with an early study performed by Vande Geest et al. [192]. Compared with data from the normal aorta, the wall stiffening can be attributed to the destruction of elastin and the failure of the collagen cross-linkage [32]. In addition, we verified that there is an increase in wall anisotropy when the thrombus gets older. Thereby, a weakening of the wall occurs in the longitudinal direction. This conclusion is obtained by comparing the biaxial biomechanical responses between the aneurysm walls covered by younger thrombi and the relatively older thrombi. Note that the biomechanical properties of aneurysm walls strongly depend on the AAA location, and, therefore, it is not possible to characterize a general biomechanical behavior of wall tissues simply by using empirical experimental data and material parameters. Deriving patient-specific datasets, which are based on realistic geometries, is a prerequisite for reliable numerical stress predictions.

6.3 Material Modeling

Several material models regarding the ILT and the AAA wall have been proposed [10, 153, 191–193, 203]. In regard to the biaxial mechanical response of the ILT, Vande Geest et al. [193] proposed an isotropic strain-energy function Ψ of the form

$$\Psi = \sum_{i=0}^{\infty} \sum_{i=0}^{\infty} a_{ij} (I_1 - 3)^i (I_2 - 3)^i, \tag{6.1}$$

where a_{ij} are material constants and I_1 and I_2 are the first and second invariants of the left Cauchy-Green tensor, respectively. This model was designed to characterize the mechanical data of luminal tissues, however, it can also be used to model the medial and abluminal tissues. More importantly, the authors fitted the isotropic constitutive relation (6.1) to luminal tissue data obtained from uniaxial and biaxial tests, and they identified different material parameters, underscoring the importance of using adequate experimental methods when deriving constitutive relations to describe certain mechanical phenomena.

For the aneurysm wall, Vande Geest et al. [192] implemented a strain-energy function

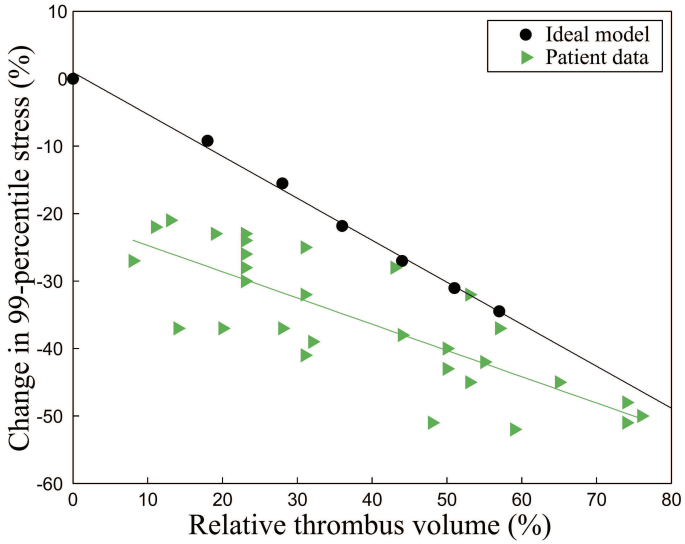

Figure 6.1: Change in (99-percentile) wall stress due to thrombus versus the relative thrombus volume for patient-specific abdominal aortic aneurysm models, and for idealized AAA models. Reproduced from Speelman et al. [176].

for the canine pericardium to fit their AAA biaxial data, and they suggested simultaneously that the four-parameter Fung elastic model is not able to fit the biaxial AAA data with physically realistic parameter values. Since AAA tissues exhibit an anisotropic material response, later, Rodríguez et al. [153] developed the first invariant-based model and stressed the need to utilize anisotropic modeling approaches in the AAA simulation. Another related study was conducted by Basciano and Kleinstreuer [10], who modified the model by Holzapfel et al. [79] to better capture the nonlinear and anisotropic mechanical responses of aneurysm walls. Our recent work [184] employed a strain-energy function Ψ, which was based on a model developed for arterial walls [79, 82], i.e.

$$\Psi = \mu(I_1 - 3) + \frac{k_1}{k_2}(\exp\{k_2[(1-\rho)(I_1-3)^2 + \rho(I_4-1)^2]\} - 1), \tag{6.2}$$

where $\mu > 0$ and $k_1 > 0$ are stress-like parameters with dimension (kPa), and $\rho \in [0,1]$ and $k_2 > 0$ are dimensionless parameters. In this material model μ is responsible for regulating the low loading domain, while k_1 and k_2 represent the load bearing capacity in the high loading domain. The value of ρ is a measure of mechanical anisotropy, and it may 'switch' between isotropy and anisotropy. Moreover, the invariants I_1 and I_4 can be expressed as:

$$I_1 = \lambda_r^2 + \lambda_\theta^2 + \lambda_z^2, \qquad I_4 = \lambda_\theta^2 \cos^2\varphi + \lambda_z^2 \sin^2\varphi, \tag{6.3}$$

where λ_r λ_θ and λ_z are the principal stretches in radial, circumferential and axial directions, respectively. In Eq. (6.3), φ is the angle between the fiber reinforcement and the circumferential direction of the AAA. Here, however, φ is treated as a phenomenological

variable since structural orientations were not investigated in the ILT and the thrombus-covered wall. The material model (6.2) is able to fit the three individual layers of the ILT very well, with a mean R^2 of 0.92 ± 0.05, 0.93 ± 0.04, 0.93 ± 0.04 and 0.94 ± 0.03 for the luminal, medial, abluminal and the fresh thrombus, respectively. The model (6.2) is also appropriate to characterize the biaxial biomechanical responses of the thrombus-covered walls with a 'goodness of fit' of 0.93 ± 0.04. Hence, this material model is able to capture the biaxial biomechanical behaviors of both the ILT and the aneurysm wall. The representative model results are shown in the Figs. 3.3 and 3.4 as solid curves, and averaged material parameters are then used to predict the mean stress-stretch responses of the ILT and the thrombus-covered wall, Figs. 3.6 and 3.7, respectively.

6.4 Prediction of Rupture Risk

Finite element analysis plays an important role in the evaluation of the rupture risk, and may help to reduce aneurysm mortality and unnecessary elective AAA repair in future. In the majority of recent computational studies [9, 48, 59, 151, 204, 210], multiple factors such as the 3D structure of ILT, the patient-specific geometry, the anisotropy of the wall and the fluid-structure interaction, to a great extent, improved the reliability of the finite element simulations in this field. However, much remains to be done, in particular, the incorporation of the mechanobiology is of pressing need.

It seems that Wang et al. [204] were the first who examined that the presence of ILT affects the AAA wall stress magnitude and distribution in actual 3D patient-specific models (Fig. 6.2). This study reminds that the ILT should be included in a patientspecific geometrical reconstruction. The latest study [59] in this regard show similar results as Wang et al. [204], namely that the presence of ILT reduces the PWS in all considered patients, who were divided into two groups according to aneurysm peak transverse diameter, i.e. intermediate group (5-7 cm) and large group (> 7 cm). A linear correlation between relative ILT volume and peak wall stress was determined for the intermediate group, whereas no such correlation was found in the large group. This is an important finding, which reveals that the effect of ILT on the reduction of PWS may vary with the AAA size. Based on a realistic patient-specific geometry, choosing the 'correct' material model is critically important for the accuracy of stress distributions.

For example, Rissland et al. [151] compared isotropic and anisotropic material models in patient-specific geometries, and showed that anisotropic material models have larger and broader ranges of stress values when compared to isotropic models (Fig. 6.3). That study indicates that isotropic material models may lead to stress predictions that underestimate the risk of rupture.

In a recent computational study both the ILT and the AAA wall are considered as porous materials [9]. Porohyperelastic finite element models of AAAs result in a 19.4, 40.1 and

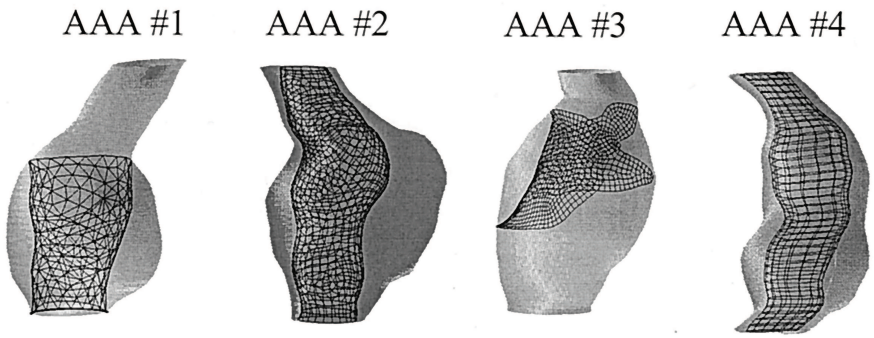

Figure 6.2: Four AAA models with different ILT configurations. The lumen through the ILT is indicated by a black mesh so that the remaining material between the mesh and the AAA wall is the ILT. Reproduced from Wang et al. [204].

81.0% increase of the maximum principal wall stress when compared to the corresponding hyperelastic simulations for maximum diameters of 35, 45 and 55 mm, respectively (Fig. 6.4).

Considering the porous microstructure of the ILT, which is only meaningful for certain ages of the thrombi, a porohyperelastic material model is more appropriate than nonlinear elastic models. However, it also requires more microstructural (mechanical) data of the material within a physiologically relevant environment, not as considered in the computational study [9].

In AAAs, calcifications frequently exist in atherosclerotic lesions within the intima or at the interface between the intima and the media. The influence of the calcification on the wall stresses has been discussed by recent studies [112, 175]. Representative CT images of three patients with contour lines of the lumen, the ILT and the calcification are shown in Fig. 6.5. Due to the calcification, the average stress within the wall is reduced by 9.7 to 59.2%, indicating a significant load-bearing effect of the calcification. If neglecting calcification in patient-specific simulations, results may lead to misinterpretation of the AAA rupture risk.

Compared to the wall stress distribution, the AAA wall strength distribution is not given the same amount of investigative attention. For the purpose of a clinical assessment of the AAA rupture potential, there is a need to develop a noninvasive method to predict/calculate the wall strength *in vivo*. It seems that the paper by Vande Geest et al. [195] was the first which documents a noninvasive method to determine the patientspecific wall strength, which is a promising technique in this aspect. Therein, a generalized statistical model was constructed by considering noninvasively measurable variables such as age, gender, smoking status, family history of AAA, AAA size and ILT thickness, etc... Using linear regression techniques, the statistical model is able to estimate the wall strength which matches the measured wall strength. However, one typical limitation for such a statistical model is the range of data from which the statistical model was constructed. For example, some

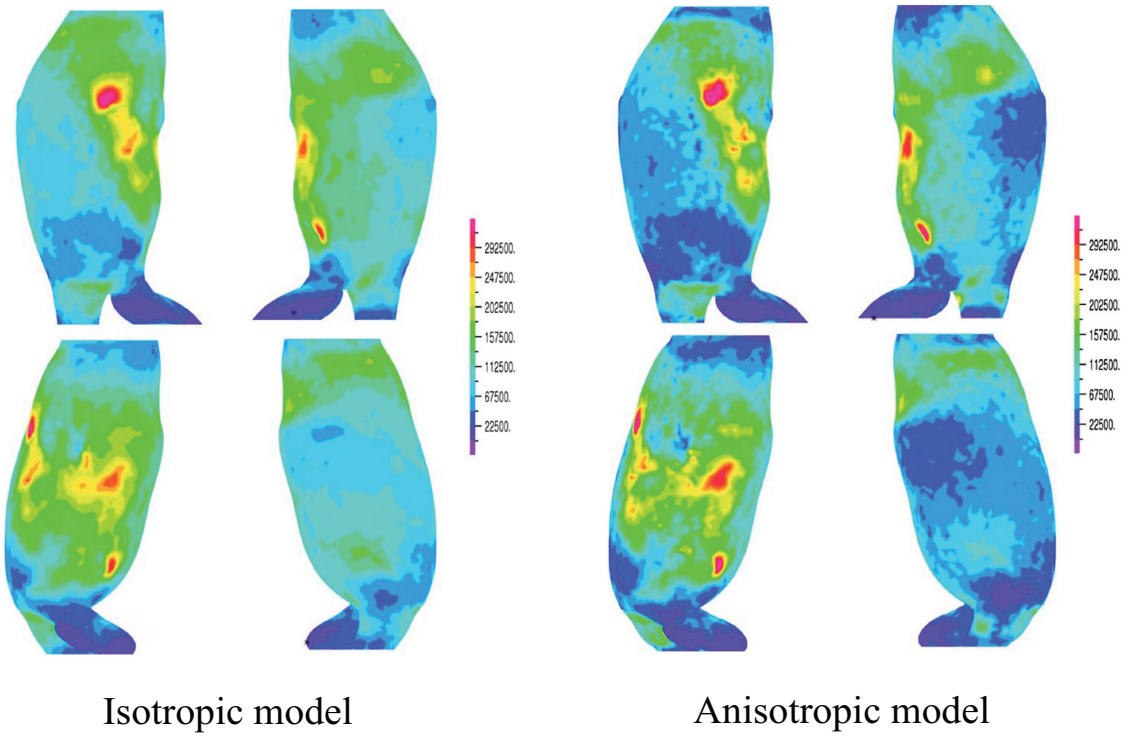

Figure 6.3: Patient-specific von Mises wall stresses at peak systolic pressure for isotropic and anisotropic models considering the ILT. Reproduced from Rissland et al. [151].

variables such as the age or the AAA size may be outside the range of data, which may lead to unreliable prediction of the wall strength. In order to avoid this limitation, a very large number of patients covering the whole range of possible predictor variables is required. Moreover, this statistical model does not consider individual failure mechanism of AAA samples. This may also lead to an incorrect estimation of the in vivo wall strength.

The recent study by our lab [184] proposed a new ingredient which may be very helpful to enrich computer models and to refine the accuracy of prediction; the new ingredient is thrombus age, which is currently determined by using micro-scale morphological characteristics. Relatively older thrombi, for example, contribute to wall weakening and to an increase of the mechanical anisotropy of their covered walls. The thrombus age provides new information to the examination of the strength of the thrombus-covered wall. Corresponding mathematical models, if developed, may be promising to link patient-specific ILT properties to the AAA wall strength.

Using refined experimental and computational techniques, some studies [38, 39] were also performed to better identify the rupture location of AAA, which has a great clinical significance. In contrary to traditional statistical studies [29, 64] on patients regarding rupture

sites and morphology, Doyle et al. [38, 39] manufactured an experimental AAA model with silicone rubber, which was then imaged using CT scans. The CT datasets were taken to generate the 3D geometry, which served within a numerical model utilized for validation. This experimental model approach is, to our knowledge, the first concerning both an arterial wall analogue and a numerical prediction. The results show that the experimental AAA models ruptured at inflection points in the proximal and distal regions of the aneurysm sac rather than at regions of maximum diameters (Fig. 6.6).

Of interest is also that the rupture locations are associated with regions of high wall stresses, which were computed numerically. Despite these findings, a cyclic pulsatile pressure to which the AAA is subjected *in vivo* is neglected. Instead, static air pressure is utilized to pressurize the inner surface of the experimental AAA model to cause the rupture, which is a limitation. Besides the biomechanical factors of AAA such as the wall stress and the strength, the rupture location is also closely correlated with the aneurysm shape (i.e. fusiform, saccular, spherical, hourglass, etc...) and the hemodynamic environment induced by the blood stream within the different AAA geometries. However, the implementation of aneurysm shape and the hemodynamic environment in the above mentioned experimental model is difficult. It should also be emphasized that the wall thickness is not necessary a critical factor to trigger rupture, although it may significantly influence the level of wall stress. Thus, an in vivo rupture does not necessarily occur at the thinnest wall region.

6.5 Histology

In this section, we mainly focus on a possible approach to determine the relative age of a thrombus within the AAA. Data of thrombus age are lacking in the literature, especially for the ILT within AAAs. It seems to be impossible to make an exact estimation of the thrombus age (for example, in days), since there is no vital tissue reaction for most specimens at all. However, the main components of the thrombotic materials differ in different specimens, which might be correlated with relative ages of thrombus tissues and their mechanical properties. Another challenge is that the individual layers of the thrombi do not consist of just one component. It is a mixture of diverse thrombotic components, however, it allows semi-quantitative measurements in terms of the component percentages.

In our recent study [184], we succeeded in the relative age determination of 32 ILT samples using histological images. In general, the thrombi within the AAAs mainly consist of four types of components including (i) erythrocytes, (ii) loose fibrin network with thin bundles, (iii) fibrin network with thick bundles and (iv) condensed small proteins. During all these stages neither reticulin, fibrotic fibers nor capillaries were detected, which is completely different from thrombi in small veins and arteries [49, 90]. Moreover, neither collagenous nor elastic fibers were existent in the ILT.

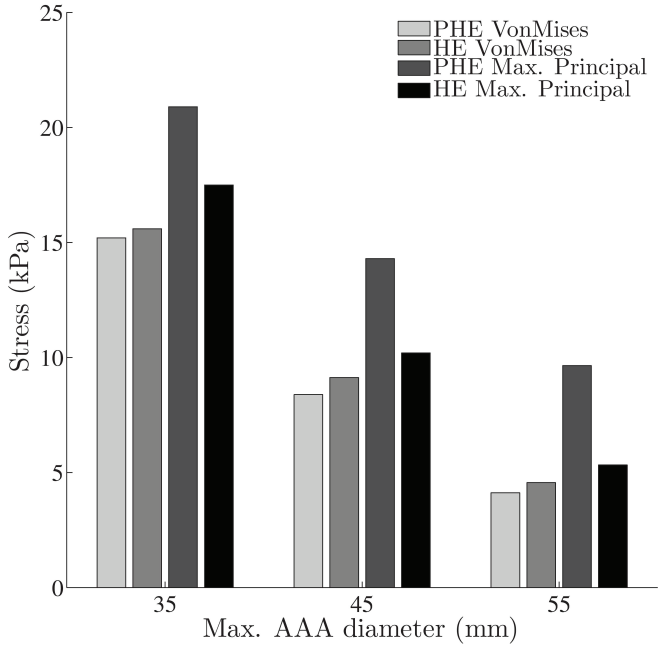

Figure 6.4: Variation of stresses with maximum AAA diameter for the porohyperelastic (PHE) and the hyperelastic (HE) models. Reproduced from Ayyalasomayajula et al. [9].

Based on the above-mentioned preliminary investigations, a four-phase thrombus evolution within AAA seems to be meaningful. In phase I (very fresh), the thrombus forms with (almost) only the erythrocytes from the blood stream. It might contain some other components such as loose fibrin network, leucocytes, or thrombocytes, but they are all in low percentages. In phase II (young), the fibrin network starts to grow in a very loose manner and it catches erythrocytes in between. During this phase, the thrombi have a large percentage of loose fibrin network (thin bundles) which are combined with relatively lower percentages of both erythrocytes and fibrin networks with thick bundles. In phase III (intermediate), the erythrocytes disrupt and proteins are washed out from the fibrin network. During this process the fibrin network remains and becomes more condensed with thick bundles. In the subsequent phase IV (old), fibrin networks disrupt and residue small proteins are more condensed as compared to the previous phase. It is notable that neither erythrocytes nor loose fibrin network with thin bundles are inspected in this phase. Representative histological images and statistical quantification of the relative percentage of cellular contents in each phase are shown in Figs. 3.8(a)-(d), and 3.9. EvG-stained sections of the thrombus-covered wall show a complete loss of elastic fibers and of myocytes, whereas relatively more collagen fibers are discerned in the media, as shown in Figs. 3.8(e) and (f) shows the morphological characteristics of thick and thin bundles of fibrin network.

By comparing the maximum tangential modulus (MTM) values of all specimens at the same stress level of 20 kPa, it is found that the stiffness of the thrombotic material con-

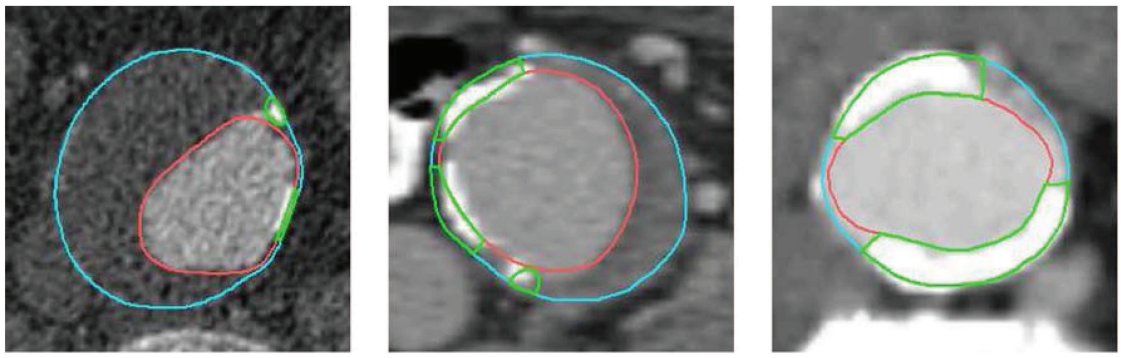

(a) patient 1, moderate calcification

(b) patient 2, severe calcification

(c) patient 3, extreme calcification

Figure 6.5: Representative CT images of three patients displaying different severities of calcification and contour lines obtained from 3D image analysis. Reproduced from Maier et al. [112].

tinuously increases with thrombus age for each individual ILT layer. Simultaneously, the luminal layer may become anisotropic during this aging process (Fig. 3.10). A strong positive correlation between the ILT thickness and the thrombus age is also observed.

To further interpret the change in the ILT mechanical properties, we classified all tested specimens within different age phases. All fresh thrombi belong to phase I and almost all isotropic luminal layers are of phase II, however, anisotropic luminal layers are either of phases III or IV. Medial layers cover phases II–IV, while abluminal layers belong mainly to phases III and IV. For each individual ILT sample, the luminal and medial layers usually have the same age phase. Initially, the thrombotic materials are very compliant and isotropic (phase I). Starting from phase II, they become stiffer due to the formation of the loose fibrin network. In this situation, the thrombi are sponge-like materials with fluid inside, and they are mechanically isotropic. During phase III, the thrombi become much stiffer as the fibrin networks are composed of much thicker bundles. The thrombotic material can be either isotropic or anisotropic for different individual ILT layers. As a consequence of the fibrin network disruption and the more condensed residue proteins, the thrombi are much stiffer in phase IV, comprising the anisotropic luminal and the isotropic medial and abluminal layers.

One possible explanation for the mechanical isotropy of the luminal and medial layers in the phases II and III is that the fibrin network plays a dominant role in the biaxial stretching, as compared to erythrocytes or other degraded proteins during the younger phases. Importantly, fibrin polymers have a large extensibility and elasticity when compared with other protein polymers, as described in previous studies [18, 108].

Factors to trigger the mechanical anisotropy of several luminal layers in the phases III and IV can be summarized as follows: (i) differences between the thick and thin bundles

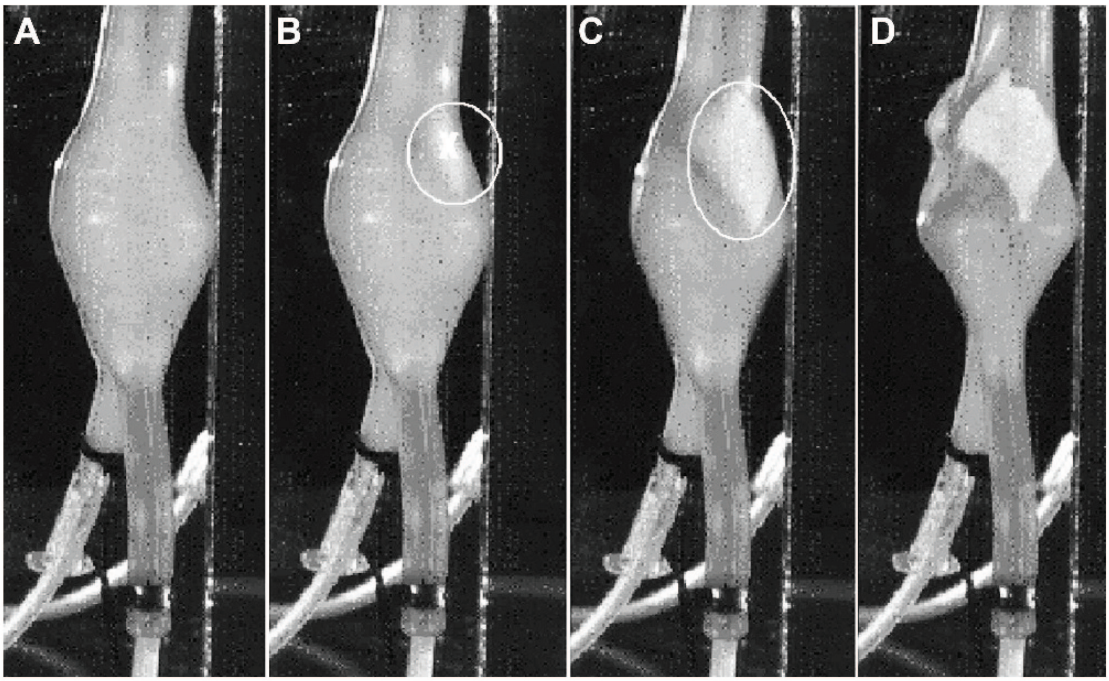

Figure 6.6: Sequence of the process of an experimental model rupture including (A) the inflated model, (B) the initial point of rupture, (C) propagation of the failure zone, and (D) complete failure of a silicone rubber model. Reproduced from Doyle et al. [39].

within the fibrin network, evident from histology, may lead to different mechanical properties during biaxial stretching. The microstructure might be a factor for the mechanical anisotropy of the thrombotic material, which needs to be further investigated. ii As a scaffold, pore densities, shapes and orientations of the fibrin network in the younger phase may considerably influence the distributions and depositions of residue small proteins in the later phases. Thus, the older thrombotic material may exhibit mechanical anisotropy probably due to unequal distributions of residue proteins. (iii) Shear stresses due to the blood stream should also be, to some extent, taken into account in such a complex and potentially dynamic environment, finally leading to thrombi with preferred directions.

One limitation of the histological analysis in the work by Tong et al. [184] is that the proposed age determination of thrombus does not provide the actual number of days but rather the relative age phases. The main reason is that there is no cellular reaction (inflammatory response) for the ILT to organize the thrombotic material, which differs from thrombi in small arteries and veins [49, 90]. To the best of our knowledge, there is no current technique in terms of histology to accomplish that. The proposed approach of age determination may further be improved by considering more biochemical factors and, besides that, a full transversal section of the thrombus from the lumen to the ablumen may be helpful

to explore more morphological characteristics in the histology and to further analyze the microstructure of the ILT with thrombus aging.

Regarding the histology of the aneurysm wall, elastin and collagen are two major fibrous proteins, which are mainly responsible for the mechanical properties. It has been long suggested that elastin degradation is important in developing aneurysm dilatation, while changes in the collagen structure may lead to aneurysm rupture [33]. Findings from Carmo et al. [23] show a decrease of elastin cross-links, collagen and total protein content in aneurysm walls. Simultaneously, these authors confirm an increase of old collagen cross-links, accompanied by a stoppage of new collagen biosynthesis. This interesting finding is a good supplement to an early study by Dobrin et al. [32] regarding structural changes of collagen within AAA walls. By focusing on which effect the thrombi has on the wall histology, Kazi et al. [93] reported that the aneurysm wall covered with thrombus is thinner and contains less elastin, and is often fragmented. Remarkably, this type of wall also contains fewer smooth muscle cells, more frequent signs of inflammation, and more apoptotic nuclei than the wall which is not covered by a thrombus. Hence, the thrombus formation and accumulation of inflammatory cells may lead to a structural instability of the vessel wall and an increase of the rupture risk thereafter.

6.6 Conclusion

In current AAA research, care is particularly taken to predict more reliable wall stress distributions in a biomechanical rupture risk assessment. Thus, investigators are striving to consider a variety of biomechanical factors related to AAA progression in vivo. These efforts, associated with advanced imaging and numerical techniques, have led to an improved estimation of peak wall stresses. In the literature there is an attempt documented that makes clear the importance of the wall strength, however, no study can yet provide a reliable strength evaluation, even when evaluations are based on patient-specific models. In the authors' opinion, the (mechano)biology, on the first place, and then the wall strength and the individual failure mechanism of AAA are currently more significant than wall stress distributions. Therefore, future work is needed to better understand the underlying biology, the failure mechanisms of different aneurysm wall types, the formulation of more proper constitutive mechanochemical relations including experimental data and the development of more sophisticated numerical tools. Once the wall strength can be determined more reliably, which turns out to be a key point of future investigations, then a rupture risk prediction will be more meaningful. The proposed determination of the relative thrombus age is a new approach in AAA research. Translating this approach into clinical practice is an important goal that we have to pursue in the near future. However, more clinical data of different patients and a noninvasive methodology to evaluate the relative thrombus age are required. Once these targets are reached, clinical diagnosis of the individual AAA wall condition such as strength as well as the prediction of rupture risk, will be more reliable.

REFERENCES

[1] H. Abboud, E. Houdart, E. Meseguer, and P. Amarenco. Stent assisted endovascular thrombolysis of internal carotid artery dissection. *J. Neurol. Neurosurg. Psychiatry*, 76:292–293, 2005.

[2] R. Adolph, D. A. Vorp, D. L. Steed, M. W. Webster, M. V. Kameneva, and S. C. Watkins. Cellular content and permeability of intraluminal thrombus in abdominal aortic aneurysm. *J. Vasc. Surg.*, 25:916–926, 1997.

[3] G. Ailawadi, J. L. Eliason, K. J. Roelofs, I. Sinha, K. K. Hannawa, E. P. Kaldjian, G. Lu, P. K. Henke, J. C. Stanley, S. J. Weiss, R. W. Thompson, and G. R. Upchurch Jr. Gender differences in experimental aortic aneurysm formation. *Arterioscler. Thromb. Vasc. Biol.*, 24:2116–2122, 2004.

[4] J. J. Alexander. The pathobiology of aortic aneurysms. *J. Surg. Res.*, 117:163–175, 2004.

[5] S. Amirbekian, R. C. Long Jr, M. A. Consolini, J. Suo, N. J. Willett, S. W. Fielden, D. P. Giddens, W. R. Taylor, and J. N. Oshinski. *In vivo* assessment of blood flow patterns in abdominal aorta of mice with MRI: implications for AAA localization. *Am. J. Physiol. Heart Circ. Physiol.*, 297:1290–1295, 2009.

[6] T. Arita, N. Matsunaga, K. Takano, S. Nagaoka, H. Nakamura, S. Katayama, N. Zempo, and K. Esato. Abdominal aortic aneurysm: rupture associated with the high-attenuating crescent sign. *Radiology*, 204:765–768, 1997.

[7] J. H. Ashton, J. P. Vande Geest, B. R. Simon, and D. G. Haskett. Compressive mechanical properties of the intraluminal thrombus in abdominal aortic aneurysms and fibrin-based thrombus mimics. *J. Biomech.*, 42:197–201, 2009.

[8] S. W. Atlas. Magnetic resonance imaging of intracranial aneurysms. *Neuroimaging Clin. N. Am.*, 7:709–720, 1997.

[9] A. Ayyalasomayajula, J. P. Vande Geest, and B. R. Simon. Porohyperelastic finite element modeling of abdominal aortic aneurysms. *J. Biomech. Eng.*, 132:104502, 2010.

[10] C. A. Basciano and C. Kleinstreuer. Invariant-based anisotropic constitutive models of the healthy and aneurysmal abdominal aortic wall. *J. Biomech. Eng.*, 131:021009, 2009.

[11] B. T. Baxter, V. A. Davis, D. J. Minion, Y. P. Wang, T. G. Lynch, and B. M. McManus. Abdominal aortic aneurysms are associated with altered matrix proteins of the nonaneurysmal aortic segments. *J. Vasc. Surg.*, 19:797–802, 1994.

[12] E. N. Beckman. Plasma cell infiltrates in atherosclerotic abdominal aortic aneurysms. *Am. J. Clin. Pathol.*, 85:21–24, 1986.

[13] J. Biasetti, F. Hussain, and T. C. Gasser. Blood flow and coherent vortices in the normal and aneurysmatic aortas: a fluid dynamical approach to intra-luminal thrombus formation. *J. R. Soc. Interface*, 8:1449–1461, 2011.

[14] D. Bluestein, L. Niu, R. T. Schoephroerster, and M. K. Dewanjee. Steady flow in an aneurysm model: Correlation between fluid dynamics and blood platelet deposition. *J. Biomech. Eng.*, 118:280–294, 1996.

[15] M. L. Bots, A. Hofman, and D. E. Grobbee. Increased common carotid intima-media thickness: adaptive response or a reflection of atherosclerosis? Findings from the Rotterdam Study. *Stroke*, 28:2442–2447, 1997.

[16] A. R. Brady, S. G. Thompson, G. R. Fowkes, R. M. Greenhalgh, and J. T. Powell. Abdominal aortic aneurysm expansion: risk factors and time intervals for surveillance. *Circulation*, 110:16–21, 2004.

[17] C. M. Brophy, J. M. Reilly, G. J. Smith, and M. D. Tilson. The role of inflammation in nonspecific abdominal aortic aneurysm disease. *Ann. Vasc. Surg.*, 5:229–233, 1991.

[18] E. A. Brown, R. I. Litvinov, D. E. Disher, P. K. Purohit, and J. W. Weisel. Multiscale mechanics of fibrin polymer: gel stretching with protein unfolding and loss of water. *Science*, 325:741–744, 2009.

[19] L. C. Brown and J. T. Powell. Risk factors for aneurysm rupture in patients kept under ultrasound surveillance. UK small aneurysm trial participants. *Ann. Surg.*, 230:289–296, 1999.

[20] P. M. Brown, D. T. Zelt, B. Sobolev, and K. A. Harris. The risk of rupture in untreated aneurysms: the impact of size, gender, and expansion rate. *J. Vasc. Surg.*, 37:280–284, 2003.

[21] R. W. Busuttil, H. Rinderbriecht, A. Flesher, and C. Carmack. Elastase activity: The role of elastase in aortic aneurysm formation. *J. Surg. Res.*, 32:214–217, 1982.

[22] J. S. Campa, R. M. Greenhalgh, and J. T. Powell. Elastin degradation in abdominal aortic aneurysms. *Atherosclerosis*, 65:13–21, 1987.

[23] M. Carmo, L. Colombo, A. Bruno, F. R. Corsi, L. Roncoroni, M. S. Cuttin, F. Radice, E. Mussini, and P. G. Settembrini. Alteration of elastin, collagen and their cross-links in abdominal aortic aneurysms. *Eur. J. Vasc. Endovasc. Surg.*, 23:543–549, 2002.

[24] H. S. Choi and R. P. Vito. Two-dimensional stress-strain relationship for canine pericardium. *J. Biomech. Eng.*, 112:153–159, 1990.

[25] E. Choke, G. Cockerill, W. R. W. Wilson, S. Sayed, J. Dawson, I. Loftus, and M. M. Thompson. A review of biological factors implicated in abdominal aortic aneurysm rupture. *Eur. J. Vasc. Endovasc. Surg.*, 30:227–244, 2005.

[26] S. A. Choksy, A. B. Wilmink, and C. R. Quick. Ruptured abdominal aortic aneurysm in the Huntingdon district: a 10-year experience. *Ann. R. Coll. Surg. Engl.*, 81:27–31, 1999.

[27] M. A. Coady, J. A. Rizzo, L. J. Goldstein, and J. A. Elefteriades. Natural history, pathogenesis, and etiology of thoracic aortic aneurysms and dissections. *Cardiol. Clin.*, 17:615–635, 1999.

[28] J. E. Cohen, T. Ben-Hur, G. Rajz, F. Umansky, and J. M. Gomori. Endovascular stent-assisted angioplasty in the management of traumatic internal carotid artery dissections. *Stroke*, 36:e45–47, 2005.

[29] R. C. Darling. Ruptured arteriosclerotic abdominal aortic aneurysms. A pathologic and clinical study. *Am. J. Surg.*, 119:397–401, 1970.

[30] R. C. Darling, C. R. Messina, D. C. Brewster, and L. W. Ottinger. Autopsy study of unoperated abdominal aortic aneurysms. *Circulation*, 56 (II suppl):161–164, 1977.

[31] J. M. Davis and R. A. Zimmerman. Injury of the carotid and vertebral arteries. *Neuroradiology*, 25:55–69, 1983.

[32] P. B. Dobrin. Pathophysiology and pathogenesis of aortic aneurysms. Current concepts. *Surg. Clin. North Am.*, 69:687–703, 1989.

[33] P. B. Dobrin, W. H. Baker, and W. C. Gley. Elastolytic and collagenolytic studies of arteries. implications for the mechanical properties of aneurysms. *Arch. Surg.*, 119:405–409, 1984.

[34] P. B. Dobrin and T. R. Canfield. Elastase, collagenase, and the biaxial elastic properties of dog carotid artery. *Am. J. Physiol.*, 247:H124–H131, 1984.

[35] R. Doll, R. Peto, J. Boreham, and I. Sutherland. Mortality in relation to smoking:50 years' observations on male British doctors. *Br. Med. J.*, 328:1519, 2004.

[36] R. F. Doolittle. Fibrinogen and fibrin. *Annu. Rev. Biochem.*, 53:195–229, 1984.

[37] B. J. Doyle, A. Callanan, P. E. Burke, P. A. Grace, M. T. Walsh, D. A. Vorp, and T. M. McGloughlin. Vessel asymmetry as an additional diagnostic tool in the assessment of abdominal aortic aneurysms. *J. Vasc. Surg.*, 49:443–454, 2009.

[38] B. J. Doyle, A. J. Cloonan, M. T. Walsh, D. A. Vorp, and T. M. McGloughlin. Identification of rupture locations in patient-specific abdominal aortic aneurysms using experimental and computational techniques. *J. Biomech.*, 43:1408–1416, 2010.

[39] B. J. Doyle, T. J. Corbett, A. Callanan, M. T. Walsh, D. A. Vorp, and T. M. McGloughlin. An experimental and numerical comparison of the rupture locations of an abdominal aortic aneurysm. *J. Endovas. Ther.*, 16:322–335, 2009.

[40] M. Dryjski, J. L. Driscoll, R. C. Blair, M. A. McGurrin, F. J. Dagher, M. J. Ceraoloand, O'Donnell, and W. M. Blackshear Jr. The small abdominal aortic aneurysm: the eternal dilemma. *J. Cell Sci.*, 35:95–100, 1994.

[41] C. A. Edwards and W. D. O'Brien Jr. Modified assay for determination of hydroxyproline in a tissue hydrolyzate. *Clin. Chim. Acta*, 104:161–167, 1980.

[42] D. F. Elger, R. S. Blackketter, R. S. Budwig, and K. H. Johansen. The influence of shape on the stresses in model abdominal aortic aneurysms. *J. Biomed. Eng.*, 118:326–332, 1996.

[43] M. S. Enevoldsen, K. A. Henneberg, J. A. Jensen, L. Lönn, and J. D. Humphrey. New interpretation of arterial stiffening due to cigarette smoking using a structurally motivated constitutive model. *J. Biomech.*, 44:1209–1211, 2011.

[44] T. C. Fabian, J. H. Patton Jr., M. A. Croce, G. Minard, K. A. Kudsk, and F. E. Pritchard. Blunt carotid injury. Importance of early diagnosis and anticoagulant therapy. *Ann. Surg.*, 223:513–525, 1996.

[45] J. Ferruzzi, D. A. Vorp, and J. D. Humphrey. On constitutive descriptors of the biaxial mechanical behaviour of human abdominal aorta and aneurysms. *J. R. Soc. Interface*, 8:435–450, 2011.

[46] M. F. Fillinger, S. P. Marra, M. L. Raghavan, and F. E. Kennedy. Prediction of rupture risk in abdominal aortic aneurysm during observation: wall stress versus diameter. *J. Vasc. Surg.*, 37:724–732, 2003.

[47] M. F. Fillinger, J. Racusin, R. K. Baker, J. L. Cronenwett, A. Teutelink, M. L. Schermerhorn, R. M. Zwolak, R. J. Powell, D. B. Walsh, and E. M. Rzucidlo. Anatomic characteristics of ruptured abdominal aortic aneurysm on conventional CT scans: Implications for rupture risk. *J. Vasc. Surg.*, 39:1243–1252, 2004.

[48] M. F. Fillinger, M. L. Raghavan, S. P. Marra, J. L. Cronenwett, and F. E. Kennedy. In vivo analysis of mechanical wall stress and abdominal aortic aneurysm rupture risk. *J. Vasc. Surg.*, 36:589–597, 2002.

[49] V. Fineschi, E. Turillazzi, M. Neri, C. Pomara, and I. Riezzo. Histological age determination of venous thrombosis:a neglected forensic task in fatal pulmonary thrombo-embolism. *Forensic Sci. Int.*, 186:22–28, 2009.

[50] E. A. Finol and C. H. Amon. Blood flow in abdominal aortic aneurysms: Pulsatile flow hemodynamics. *J. Biomech. Eng.*, 123:474–484, 2001.

[51] E. A. Finol, K. Keyhani, and C. H. Amon. The effect of asymmetry in abdominal aortic aneurysms under physiologically realistic pulsatile flow conditions. *J. Biomech. Eng.*, 125:207–217, 2003.

[52] C. Fleming, E. P. Whitlock, T. L. Beil, and F. A. Lederle. Screening for abdominal aortic aneurysm: a best-evidence systematic review for the U.S. Preventive Services Task Force. *Ann. Intern. Med.*, 142:203–211, 2005.

[53] V. Fontaine, M. P. Jacob, X. Houard, P. Rossignol, D. Plissonnier, E. Angles-Cano, and J. B. Michel. Involvement of the mural thrombus as a site of protease release and activation in human aortic aneurysms. *Am. J. Pathol.*, 161:1701–1710, 2002.

[54] T. L. Forbes, D. K. Lawlor, G. DeRose, and K. A. Harris. Gender differences in relative dilatation of abdominal aortic aneurysms. *Ann. Vasc. Surg.*, 20:564–568, 2006.

[55] T. C. Gasser, M. Auer, F. Labruto, J. Swedenborg, and J. Roy. Biomechanical rupture risk assessment of abdominal aortic aneurysms: model complexity versus predictability of finite element simulations. *Eur. J. Vasc. Endovasc. Surg.*, 40:176–185, 2010.

[56] T. C. Gasser, G. Görgülü, M. Folkesson, and J. Swedenborg. Failure properties of intraluminal thrombus in abdominal aortic aneurysm under static and pulsating mechanical loads. *J. Vasc. Surg.*, 48:179–188, 2008.

[57] T. C. Gasser and G. A. Holzapfel. Modeling the propagation of arterial dissection. *Eur. J. Mech. A/Solids*, 25:617–633, 2006.

[58] E. Georgakarakos, C. V. Ioannou, Y. Papaharilaou, T. Kostas, and A. N. Katsamouris. Computational evaluation of aortic aneurysm rupture risk: what have we learned so far? *J. Endovas. Ther.*, 18:214–225, 2011.

[59] E. Georgakarakos, C. V. Ioannou, S. Volanis, Y. Papaharilaou, J. Ekaterinaris, and A. N. Katsamouris. The influence of intraluminal thrombus on abdominal aortic aneurysm wall stress. *Int. Angiol.*, 28:325–333, 2009.

[60] S. Glagov, H. S. Bassiouny, D. P. Giddens, and C. K. Zarins. Intimal thickening: morphogenesis, functional significance and detection. *J. Vasc. Invest.*, 1:2–14, 1995.

[61] S. Glagov, C. Zarins, D. P. Giddens, and D. N. Ku. Hemodynamics and atherosclerosis. Insights and perspectives gained from studies of human arteries. *Arch. Pathol. Lab. Med.*, 112:1018–1031, 1988.

[62] S. Glagov, C. K. Zarins, N. Masawa, C. P. Xu, H. Bassiouny, and D. P. Giddens. Mechanical functional role of non-atherosclerotic intimal thickening. *Front. Med. Biol. Engr.*, 5:37–43, 1993.

[63] C. J. Goergen, B. L. Johnson, J. M. Greve, C. A. Taylor, and C. K. Zarins. Increased anterior abdominal aortic wall motion: possible role in aneurysm pathogenesis and design of endovascular devices. *J. Endovas. Ther.*, 14:574–584, 2007.

[64] J. Golledge, J. Abrokwah, K. N. Shenoy, and R. H. Armour. Morphology of ruptured abdominal aortic aneurysms. *Eur. J. Vasc. Endovasc. Surg.*, 18:96–104, 1999.

[65] H. Gray. *Gray's Anatomy: The Anatomical Basis of Medicine and Surgery*. Churchill Livingstone, Oxford, 39 edition, 2004.

[66] N. Grootenboer, J. L. Bosch, J. M. Hendriks, and M. R. H. M. van Sambeek. Epidemiology, aetiology, risk of rupture and treatment of abdominal aortic aneurysms: does sex matter? *Eur. J. Vasc. Endovasc. Surg.*, 38:278–284, 2009.

[67] B. Guillon, C. Tzourio, V. Biousse, V. Adrai, M. G. Bousser, and P. J. Touboul. Arterial wall properties in carotid artery dissection: an ultrasound study. *Neurology*, 55:663–666, 2000.

[68] B. G. Halloran and B. T. Baxter. Pathogenesis of aneurysms. *Semin. Vasc. Surg.*, 8:85–92, 1995.

[69] M. T. Haneline and G. Lewkovich. Identification of internal carotid artery dissection in chiropractic practice. *J. Can. Chiropr. Assoc.*, 48:206–210, 2004.

[70] K. K. Hannawa, J. L. Eliason, and G. R. Upchurch Jr. Gender differences in abdominal aortic aneurysms. *Vascular*, 17:S30–S39, 2009.

[71] S. S. Hans, O. Jareunpoon, M. Balasubramaniam, and G. B. Zelenock. Size and location of thrombus in intact and ruptured abdominal aortic aneurysms. *J. Vasc. Surg.*, 41:584–588, 2005.

[72] L. P. Harter, B. H. Gross, R. A. W. Callen, and R. A. Barth. Ultrasonic evalution of abdominal aortic thrombus. *J. Ultrasound. Med.*, 1:315–318, 1982.

[73] C. M. He and M. R. Roach. The composition and mechanical properties of abdominal aortic aneurysms. *J. Vasc. Surg.*, 20:6–13, 1994.

[74] M. Heikkinen, J. P. Salenius, and O. Auvinen. Ruptured abdominal aortic aneurysm in a well-defined geographic area. *J. Vasc. Surg.*, 36:291–296, 2002.

[75] E. L. Henderson, Y. J. Geng, G. K. Sukhova, A. D. Whittemore, J. Knox, and P. Libby. Death of smooth muscle cells and expression of mediators of apoptosis by T lymphocytes in human abdominal aortic aneurysms. *Circulation*, 99:96–104, 1999.

[76] G. A. Holzapfel. *Nonlinear Solid Mechanics. A Continuum Approach for Engineering*. John Wiley & Sons, Chichester, 2000.

[77] G. A. Holzapfel. Determination of material models for arterial walls from uniaxial extension tests and histological structure. *J. Theor. Biol.*, 238:290–302, 2006.

[78] G. A. Holzapfel. Collagen in arterial walls: Biomechanical aspects. In P. Fratzl, editor, *Collagen. Structure and Mechanics*, pages 285–324, Heidelberg, 2008. Springer-Verlag.

[79] G. A. Holzapfel, T. C. Gasser, and R. W. Ogden. A new constitutive framework for arterial wall mechanics and a comparative study of material models. *J. Elasticity*, 61:1–48, 2000.

[80] G. A. Holzapfel and R. W. Ogden. On planar biaxial tests for anisotropic nonlinearly elastic solids. a continuum mechanical framework. *Math. Mech. Solids*, 14:474–489, 2009.

[81] G. A. Holzapfel, G. Sommer, M. Auer, P. Regitnig, and R. W. Ogden. Layer-specific 3D residual deformations of human aortas with non-atherosclerotic intimal thickening. *Ann. Biomed. Eng.*, 35:530–545, 2007.

[82] G. A. Holzapfel, G. Sommer, C. T. Gasser, and P. Regitnig. Determination of the layer-specific mechanical properties of human coronary arteries with non-atherosclerotic intimal thickening, and related constitutive modelling. *Am. J. Physiol. Heart Circ. Physiol.*, 289:H2048–2058, 2005.

[83] G. A. Holzapfel, G. Sommer, and P. Regitnig. Anisotropic mechanical properties of tissue components in human atherosclerotic plaques. *J. Biomech. Eng.*, 126:657–665, 2004.

[84] G. A. Holzapfel, J. Tong, T. Cohnert, and P. Regitnig. Recent advances in the biomechanics of abdominal aortic aneurysms. In N. Chakfé, B. Durand, and W. Meichelboeck, editors, *ESVB 2011-New Endovascular Technologies-From Bench Test to Clinical Practice*, pages 23–40, Strasbourg, France, 2011. Europrot.

[85] J. D. Humphrey. Mechanics of the arterial wall: Review and directions. *Crit. Rev. Biomed. Eng.*, 23:1–162, 1995.

[86] J. D. Humphrey. *Cardiovascular Solid Mechanics. Cells, Tissues, and Organs*. Springer-Verlag, New York, 2002.

[87] J. D. Humphrey and G. A. Holzapfel. Mechanics, mechanobiology, and modeling of human abdominal aorta and aneurysms. *J. Biomech.*, 45:805–814, 2012.

[88] J. D. Humphrey and C. A. Taylor. Intracranial and abdominal aortic aneurysms: similarities, differences, and need for a new class of computational models. *Annu. Rev. Biomed. Eng.*, 10:221–246, 2008.

[89] F. Inzoli, F. Boschetti, M. Zappa, T. Longo, and R. Fumero. Biomechanical factors in abdominal aortic aneurysm rupture. *Eur. J. Vasc. Surg.*, 7:667–674, 1993.

[90] W. Irniger. Histologische Altersbestimmung von Thrombosen und Embolien. *Virchows Arch. path. Anat.*, 336:220–237, 1963.

[91] L. M. Kachanov. *Introduction to Continuum Damage Mechanics*. Martinus Nijhoff Publishers, Dordrecht, The Netherlands, 1986.

[92] I. Karšaj and J. D. Humphrey. A mathematical model of evolving mechanical properties of intraluminal thrombus. *Biorheology*, 46:509–527, 2009.

[93] M. Kazi, J. Thyberg, P. Religa, J. Roy, P. Eriksson, U. Hedin, and J. Swedenborg. Influence of intraluminal thrombus on structural and cellular composition of abdominal aortic aneurysm wall. *J. Vasc. Surg.*, 38:1283–1292, 2003.

[94] M. Kazi, C. Zhu, J. Roy, G. Paulsson-Berne, A. Hamsten, J. Swedenborg, U. Hedin, and P. Eriksson. Difference in matrix-degrading protease expression and activity between thrombus-free and thrombus-covered wall of abdominal aortic aneurysm. *Arterioscler. Thromb. Vasc. Biol.*, 25:1341–1346, 2005.

[95] J. H. Kim, S. Avril, A. Duprey, and J. P. Favre. Experimental characterization of rupture in human aortic aneurysms using a full-field measurement technique. *Biomech. Model. Mechanobiol.*, 11:841–853, 2012.

[96] A. E. Koch, G. K. Haines, R. J. Rizzo, J. A. Radosevich, R. M. Pope, P. G. Robinson, and W. H. Pearce. Immunophenotypic analysis suggesting an immune-mediated response. *Am. J. Pathol.*, 137:1199–1213, 1990.

[97] R. R. Kraus, J. M. Bergstein, and J. R. DeBord. Diagnosis, treatment, and outcome of blunt carotid arterial injuries. *Am. J. Surg.*, 178:190–193, 1999.

[98] A. Krettek, G. K. Sukhova, and P. Libby. Elastogenesis in human arterial disease: A role for macrophages in disordered elastin synthesis. *Arterioscler. Thromb. Vasc. Biol.*, 23:582–587, 2003.

[99] E. G. Lakatta, M. Wang, and S. S. Najjar. Arterial aging and subclinical arterial disease are fundamentally intertwined at macroscopic and molecular levels. *Med. Clin. North. Am.*, 93:583–604, 2009.

[100] T. Lanne, T. Sandgren, and B. Sonesson. A dynamic view on the diameter of abdominal aortic aneurysms. *Eur. J. Vasc. Endovasc. Surg.*, 15:308–312, 1998.

[101] E. Larsson, F. Labruto, T. C. Gasser, J. Swedenborg, and R. Hultgren. Analysis of aortic wall stress and rupture risk in patients with abdominal aortic aneurysm with a gender perspective. *J. Vasc. Surg.*, 54:295–299, 2011.

[102] F. A. Lederle, G. R. Johnson, S. E. Wilson, I. L. Gordon, E. P. Chute, F. N. Littooy, W. C. Krupski, D. Bandyk, G. W. Barone, L. M. Graham, R. J. Hye, and D. B. Reinke. Relationship of age, gender, race, and body size to infrarenal aortic diameter. the aneurysm detection and management (adam) veterans affairs cooperative study investigators. *J. Vasc. Surg.*, 26:595–601, 1997.

[103] F. A. Lederle, S. E. Wilson, G. R. Johnson, D. B. Reinke, F. N. Littooy, C. W. Acher, D. J. Ballard, L. M. Messina, I. L. Gordon, E. P. Chute, W. C. Krupski, S. J. Busuttil, G. W. Barone, S. Sparks, L. M. Graham, J. H. Rapp, M. S. Makaroun, G. L. Moneta, R. A. Cambria, R. G. Makhoul, D. Eton, H. J. Ansel, J. A. Freischlag, D. Bandyk, and Aneurysm Detection and Management Veterans Affairs Cooperative Study Group. Immediate repair compared with surveillance of small abdominal aortic aneurysms. *N. Engl. J. Med.*, 346:1437–1444, 2002.

[104] V. H. Lee, R. D. Brown Jr., J. N. Mandrekar, and B. Mokri. Incidence and outcome of cervical dissection: a population-based study. *Neurology*, 67:1809–1812, 2006.

[105] Z. Li and C. Kleinstreuer. A new wall stress equation for aneurysm-rupture prediction. *Ann. Biomed. Eng.*, 33:209–213, 2003.

[106] Z. Li and C. Kleinstreuer. A new wall stress equation for aneurysm-rupture prediction. *Ann. Biomed. Eng.*, 33:209–213, 2005.

[107] Z. Y. Li, J. U-King-Im, T. Y. Tang, E. Soh, T. C. See, and J. H. Gillard. Impact of calcification and intraluminal thrombus on the computed wall stresses of abdominal aortic aneurysm. *J. Vasc. Surg.*, 47:928–935, 2008.

[108] W. Liu, L. M. Jawerth, E. A. Sparks, M. R. Falvo, R. R. Hantgan, R. Superfine, S. T. Lord, and M. Guthold. Fibrin fibers have extraordinary extensibility and elasticity. *Science*, 313:634, 2006.

[109] C. Lucas, T. Moulin, D. Deplanque, L. Tatu, and D. Chavot. Stroke patterns of internal carotid artery dissection in 40 patients. *Stroke*, 29:2646–2648, 1998.

[110] N. F. MacLean, N. L. Dudek, and M. R. Roach. The role of radial elastic properties in the development of aortic dissections. *J. Vasc. Surg.*, 29:703–710, 1999.

[111] S. T. R. MacSweeney, G. Young, R. M. Greenhalgh, and J. T. Powell. Mechanical properties of the aneurysmal aorta. *Br. J. Surg.*, 79:1281–1284, 1992.

[112] A. Maier, M. W. Gee, C. Reeps, H. H. Eckstein, and W. A. Wall. Impact of calcifications on patient-specific wall stress analysis of abdominal aortic aneurysms. *Biomech. Model. Mechanobiol.*, 9:511–521, 2010.

[113] A. Maier, M. W. Gee, C. Reeps, J. Pongratz, H. H. Eckstein, and W. A. Wall. A comparison of diameter, wall stress, and rupture potential index for abdominal aortic aneurysm rupture risk prediction. *Ann. Biomed. Eng.*, 38:3124–3134, 2010.

[114] S. Makita, A. Ohira, Y. Naganuma, Y. Moriai, H. Niinuma, A. Abiko, and K. Hiramori. Increased carotid artery stiffness without atherosclerotic change in patients with aortic dissection. *Angiology*, 57:478–486, 2006.

[115] A. H. Malkawi, R. J. Hinchliffe, Y. Xu, P. J. Holt, I. M. Loftus, and M. M. Thompson. Patient-specific biomechanical profiling in abdominal aortic aneurysm development and rupture. *J. Vasc. Surg.*, 52:480–488, 2010.

[116] S. P. Marra, C. P. Daghlian, M. F. Fillinger, and F. E. Kennedy. Elemental composition, morphology and mechanical properties of calcified deposits obtained from abdominal aortic aneurysms. *Acta Biomater.*, 2:515–520, 2006.

[117] P. Matusik, P. Mazur, E. Stepień, R. Pfitzner, J. Sadowski, and A. Undas. Architecture of intraluminal thrombus removed from abdominal aortic aneurysm. *J. Thromb. Thrombolysis.*, 30:7–9, 2010.

[118] E. S. da Silva, A. J. Rodrigues, E. Magalhaes Castro de Tolosa, C. J. Rodrigus, G. Villas Boas do Prado, and J. C. Nakamoto. Morphology and diameter of infrarenal aortic aneurysms: a prospective autopsy study. *Cardiovasc. Surg.*, 8:526–532, 2000.

[119] J. M. de Bray and R. W. Baumgartner. History of spontaneous dissection of the cervical carotid artery. *Arch. Neurol.*, 62:1168–1170, 2005.

[120] E. S. Di Martino, A. Bohra, J. P. Vande Geest, N. Y. Gupta, M. S. Makaroun, and D. A. Vorp. Biomechanical properties of ruptured versus electively repaired abdominal aortic aneurysm wall tissue. *J. Vasc. Surg.*, 43:570–576, 2006.

[121] E. S. Di Martino, S. Mantero, F. Inzoli, G. Melissano, D. Astore, R. Chiesa, and R. Fumero. Biomechanics of abdominal aortic aneurysm in the presence of endoluminal thrombus: Experimental characterisation and structural static computational analysis. *Eur. J. Vasc. Endovasc. Surg.*, 15:290–299, 1998.

[122] E. S. Di Martino and D. A. Vorp. Effect of variation in intraluminal thrombus constitutive properties on abdominal aortic aneurysm wall stress. *Ann. Biomed. Eng.*, 31:804–809, 2003.

[123] F. J. Miller Jr. Aortic aneurysms: it's all about the stress. *Arterioscler. Thromb. Vasc. Biol.*, 22:1948–1949, 2002.

[124] J. E. Moore Jr., S. E. Maier, D. N. Ku, and P. Boesiger. Hemodynamics in the abdominal aorta: a comparison of *in vitro* and *in vivo* measurements. *J. Appl. Physiol.*, 76:1520–1527, 1994.

[125] W. B. Mehard, J. P. Heiken, and G. A. Sicard. High-attenuating crescent in abdominal aortic aneurysm wall at ct: a sign of acute or impending rupture. *Radiology*, 192:359–362, 1994.

[126] S. Menashi, J. S. Campa, R. M. Greenhalgh, and J. T. Powell. Collagen in abdominal aortic aneurysm: typing, content, and degradation. *J. Vasc. Surg.*, 6:578–582, 1987.

[127] J. S. Milner, J. A. Moore, B. K. Rutt, and D. A. Steinman. Hemodynamics of human carotid artery bifurcations: computational studies with models reconstructed from magnetic resonance imaging of normal subjects. *J. Vasc. Surg.*, 28:143–156, 1998.

[128] R. Mofidi, V. J. Goldie, J. Kelman, A. R. Dawson, J. A. Murie, and R. T. Chalmers. Influence of sex on expansion rate of abdominal aortic aneurysms. *Br. J. Surg.*, 94:310–314, 2007.

[129] B. Mokri. Traumatic and spontaneous extracranial internal carotid artery dissections. *J. Neurol.*, 237:356–361, 1990.

[130] B. Mokri, T. M. Sundt Jr., O. W. Houser, and D. G. Piepgras. Spontaneous dissection of the cervical internal carotid artery. *Ann. Neurol.*, 19:126–138, 1986.

[131] B. Mokri, D. G. Piepgras, and O. W. Houser. Traumatic dissections of the extracranial internal carotid artery. *J. Neurosurg.*, 68:189–197, 1988.

[132] W. R. Mower, L. J. Baraff, and J. Sneyd. Stress distributions in vascular aneurysms: factors affecting risk of aneurysm rupture. *J. Surg. Res.*, 55:155–161, 1993.

[133] W. R. Mower, W. J. Quinones, and S. S. Gambhir. Effect of intraluminal thrombus on abdominal aortic aneurysm wall stress. *J. Vasc. Surg.*, 26:602–608, 1997.

[134] K. M. Newman, J. Jean-Claude, H. Li, J. V. Scholes, Y. Ogata, H. Nagase, and M. D. Tilson. Cellular localization of matrix metalloproteinases in the abdominal aortic aneurysm wall. *J. Vasc. Surg.*, 20:814–820, 1994.

[135] S. C. Nicholls, J. B. Gardner, M. H. Meissner, and K. H. Johansen. Rupture in small abdominal aortic aneurysms. *J. Vasc. Surg.*, 28:884–888, 1998.

[136] M. F. O'Rourke and J. Hashimoto. Mechanical factors in arterial aging: A clinical perspective. *J. Am. Coll. Cardiol.*, 50:1–13, 2007.

[137] A. Parr, M. McCann, B. Bradshaw, A. Shahzad, P. Buttner, and J. Golledge. Thrombus volume is associated with cardiovascular events and aneurysm growth in patients who have abdominal aortic aneurysms. *J. Vasc. Surg.*, 53:828–835, 2011.

[138] S. Pasta, J. A. Phillippi, T. G. Gleason, and D. A. Vorp. Effect of aneurysm on the mechanical dissection properties of the human ascending thoracic aorta. *J. Thorac. Cardiovasc. Surg.*, 143:460–467, 2011.

[139] W. H. Pearce, M. S. Slaughter, S. LeMaire, A. N. Salyapongse, J. Feinglass, W. J. McCarthy, and J. S. Yao. Aortic diameter as a function of age, gender, and body surface area. *Surgery*, 114:691–697, 1993.

[140] S. Polzer, T. C. Gasser, J. Swedenborg, and J. Bursa. The impact of intraluminal thrombus failure on the mechanical stress in the wall of abdominal aortic aneurysms. *Eur. J. Vasc. Endovasc. Surg.*, 41:467–473, 2011.

[141] J. T. Powell and A. R. Brady. Detection, management, and prospects for the medical treatment of small abdominal aortic aneurysms. *Arterioscler. Thromb. Vasc. Biol.*, 24:241–245, 2004.

[142] J. T. Powell and L. C. Brown. The natural history of abdominal aortic aneurysms and their risk of rupture. *Acta Chir. Belg.*, 101:11–16, 2001.

[143] M. L. Raghavan, M. F. Fillinger, S. P. Marra, B. P. Naegelein, and F. E. Kennedy. Automated methodology for determination of stress distribution in human abdominal aortic aneurysm. *J. Biomech. Eng.*, 127:868–871, 2005.

[144] M. L. Raghavan, M. M. Hanaoka, J. A. Kratzberg, M. de Lourdes Higuchi, and E. S. da Silva. Biomechanical failure properties and microstructural content of ruptured and unruptured abdominal aortic aneurysms. *J. Biomech.*, 44:2501–2507, 2011.

[145] M. L. Raghavan, J. Kratzberg, E. M. Castro de Tolosa, M. M. Hanaoka, P. Walker, and E. S. da Silva. Regional distribution of wall thickness and failure properties of human abdominal aortic aneurysm. *J. Biomech.*, 39:3010–3016, 2006.

[146] M. L. Raghavan and D. A. Vorp. Toward a biomechanical tool to evaluate rupture potential of abdominal aortic aneurysm: identification of a finite strain constitutive model and evaluation of its applicability. *J. Biomech.*, 33:475–482, 2000.

[147] M. L. Raghavan, D. A. Vorp, M. P. Federle, M. S. Makaroun, and M. W. Webster. Wall stress distribution on three-dimensionally reconstructed models of human abdominal aortic aneurysm. *J. Vasc. Surg.*, 31:760–769, 2000.

[148] M. L. Raghavan, M. W. Webster, and D. A. Vorp. Ex vivo biomechanical behavior of abdominal aortic aneurysm: assesment using a new mathematical model. *Ann. Biomed. Eng.*, 24:573–582, 1996.

[149] G. K. Reddy and C. S. Enwemeka. A simplified method for the analysis of hydroxyproline in biological tissues. *Clin. Biochem.*, 29:225–229, 1996.

[150] J. A. G. Rhodin. Architecture of the vessel wall. In D. F. Bohr, A. D. Somlyo, and H. V. Sparks, editors, *Handbook of Physiology, The Cardiovascular System*, volume 2, pages 1–31. American Physiologial Society, Bethesda, Maryland, 1980.

[151] P. Rissland, Y. Alemu, S. Einav, J. Ricotta, and D. Bluestein. Abdominal aortic aneurysm risk of rupture: patient-specific FSI simulations using anisotropic model. *J. Biomech. Eng.*, 131:031001, 2009.

[152] J. F. Rodríguez, G. Martufi, M. Doblaré, and E. A. Finol. The effect of material model formulation in the stress analysis of abdominal aortic aneurysms. *Ann. Biomed. Eng.*, 37:2218–2221, 2009.

[153] J. F. Rodríguez, C. Ruiz, M. Doblaré, and G. A. Holzapfel. Mechanical stresses in abdominal aortic aneurysms: influence of diameter, asymmetry and material anisotropy. *J. Biomech. Eng.*, 130:021023–1–10, 2008.

[154] A. G. Rose and D. M. Dent. Inflammatory variant of abdominal atherosclerotic aneurysm. *Arch. Pathol. Lab. Med.*, 105:409–413, 1981.

[155] J. Roy, F. Labruto, M. O. Beckman, J. Danielson, G. Johansson, and J. Swedenborg. Bleeding into the intraluminal thrombus in abdominal aortic aneurysms is associated with rupture. *J. Vasc. Surg.*, 48:1108–1113, 2008.

[156] M. S. Sacks. A method for planar biaxial mechanical testing that includes in-plane shear. *J. Biomech. Eng.*, 121:551–Ű555, 1999.

[157] M. S. Sacks. Biaxial mechanical evaluation of planar biological materials. *J. Elasticity*, 61:199–246, 2000.

[158] M. S. Sacks, D. A. Vorp, M. L. Raghavan, M. P. Federle, and M. W. Webster. *In vivo* three-dimensional surface geometry of abdominal aortic aneurysms. *Ann. Biomed. Eng.*, 27:469–479, 1999.

[159] N. Sakalihasan, R. Limet, and O. D. Defawe. Abdominal aortic aneurysm. *Lancet*, 365:1577–1589, 2005.

[160] J. Satta, E. Läärä, and T. Juvonen. Intraluminal thrombus predicts rupture of an abdominal aortic aneurysm. *J. Vasc. Surg.*, 23:737–739, 1996.

[161] W. I. Schievink. Spontaneous dissection of the carotid and vertebral arteries. *N. Engl. J. Med.*, 344:898–906, 2001.

[162] A. J. Schriefl, M. J. Collins, D. M. Pierce, G. A. Holzapfel, L. E. Niklason, and J. D. Humphrey. Remodeling of intramural thrombus and collagen in an Ang-II infusion ApoE-/- model of dissecting aortic aneurysms. *Thromb. Res.*, 130:e139–e146, 2012.

[163] A. J. Schriefl, G. Zeindlinger, D. M. Pierce, P. Regitnig, and G. A. Holzapfel. Determination of the layer-specific distributed collagen fiber orientations in human thoracic and abdominal aortas and common iliac arteries. *J. R. Soc. Interface*, 9:1275–1286, 2012.

[164] G. W. H. Schurink, J. M. van Baalen, M. J. T. Visser, and J. H. van Bockel. Thrombus within an aortic aneurysm does not reduce pressure on the aneurysmal wall. *J. Vasc. Surg.*, 31:501–506, 2000.

[165] C. M. Scotti, J. Jimenez, S. C. Muluk, and E. A. Finol. Wall stress and flow dynamics in abdominal aortic aneurysms: finite element analysis vs. fluid-structure interaction. *Comput. Meth. Biomech. Biomed. Eng.*, 11:301–322, 2008.

[166] C. L. Seidel. Cellular heterogeneity of the vascular tunica media: implications for vessel wall repair. *Arterioscler. Thromb. Vasc. Biol.*, 17:1868–1871, 1997.

[167] J. B. Semmens, P. E. Norman, M. M. Lawrence-Brown, and C. D. Holman. Influence of gender on outcome from ruptured abdominal aortic aneurysm. *Br. J. Surg.*, 87:191–194, 2000.

[168] P. K. Shah. Inflammation, metalloproteinases, and increased proteolysis: an emerging pathophysiologic paradigm in aortic aneurysm. *Circulation*, 96:2228–2232, 1997.

[169] P. K. Shah. Mechanisms of plaque vulnerability and rupture. *J. Am. Coll. Cardiol.*, 41(4 Suppl S):15S–22S, 2003.

[170] K. Shimizu, R. N. Mitchell, and P. Libby. Inflammation and cellular immune responses in abdominal aortic aneurysms. *Arterioscler. Thromb. Vasc. Biol.*, 26:987–994, 2006.

[171] K. Singh, K. H. Bonaa, B. K. Jacobsen, L. Bjork, and S. Solberg. Prevalence of and risk factors for abdominal aortic aneurysms in a population-based study: The tromso study. *Am. J. Epidemiol.*, 154:236–244, 2001.

[172] S. Solberg, K. Singh, T. Wilsgaard, and B. K. Jacobsen. Increased growth rate of abdominal aortic aneurysms in women. the tromso study. *Eur. J. Vasc. Endovasc. Surg.*, 29:145–149, 2005.

[173] G. Sommer, T. C. Gasser, P. Regitnig, M. Auer, and G. A. Holzapfel. Dissection of the human aortic media: an experimental study. *J. Biomech. Eng.*, 130:021007–1–12, 2008.

[174] B. Sonesson, T. Lanne, F. Hansen, and T. Sandgren. Infrarenal aortic diameter in the healthy person. *Eur. J. Vasc. Endovasc. Surg.*, 8:89–95, 1994.

[175] L. Speelman, A. Bohra, E. M. H. Bosboom, G. W. H. Schurink, F. N. van de Vosse, M. S. Makaorun, and P. A. Vorp. Effects of wall calcifications in patient-specific wall stress analyses of abdominal aortic aneurysms. *Eur. J. Vasc. Endovasc. Surg.*, 129:105–109, 2007.

[176] L. Speelman, G. W. Schurink, E. M. Bosboom, J. Buth, M. Breeuwer, F. N. van de Vosse, and M. H. Jacobs. The mechanical role of thrombus on the growth rate of an abdominal aortic aneurysm. *J. Vasc. Surg.*, 51:19–26, 2010.

[177] J. Stenbaek, B. Kalin, and J. Swedenborg. Growth of thrombus may be a better predictor of rupture than diameter in patients with abdominal aortic aneurysms. *Eur. J. Vasc. Endovasc. Surg.*, 20:466–499, 2000.

[178] M. M. Stringfellow, P. F. Lawrence, and R. G. Stringfellow. The influence of aorta-aneurysm geometry upon stress in the aneurysm wall. *J. Surg. Res.*, 42:425–433, 1987.

[179] D. S. Sumner, D. E. Hokanson, and D. E. Strandness. Stress-strain characteristics and collagen-elastin content of abdominal aortic aneurysms. *Surg. Gyn. Obst.*, 130:459–466, 1970.

[180] J. Swedenborg and P. Eriksson. The intraluminal thrombus as a source of proteolytic activity. *Ann. N.Y. Acad. Sci.*, 1085:133–138, 2006.

[181] J. Swedenborg, M. Kazi, P. Eriksson, and U. Hedin. Influence of the intraluminal thrombus in abdominal aortic aneurysms. *Acta Chir. Belg.*, 104:606–608, 2004.

[182] T. W. Taylor and T. Yamaguchi. Three-dimensional simulation of blood flow in an abdominal aortic aneurysm: Steady and unsteady flow cases. *J. Biomech. Eng.*, 116:89–97, 1994.

[183] R. W. Thompson. Aneurysm treatments expand. *Nat. Med.*, 11:1279–1281, 2005.

[184] J. Tong, T. Cohnert, P. Regitnig, and G. A. Holzapfel. Effects of age on the elastic properties of the intraluminal thrombus and the thrombus-covered wall in abdominal aortic aneurysms: biaxial extension behavior and material modeling. *Eur. J. Vasc. Endovasc. Surg.*, 42:207–219, 2011.

[185] J. Tong, T. Cohnert, P. Regitnig, J. Kohlbacher, R. Birner-Gruenberger, A.J. Schriefl, G. Sommer, and G. A. Holzapfel. Variations of dissection properties and mass fractions with thrombus age in human abdominal aortic aneurysms. *J. Vasc. Surg.*, submitted, 2013.

[186] J. Tong, A. J. Schriefl, T. Cohnert, and G. A. Holzapfel. Gender differences in biomechanical properties, thrombus age, mass fraction and clinical factors of abdominal aortic aneurysms. *Eur. J. Vasc. Endovasc. Surg.*, 45:364–372, 2013.

[187] J. Tong, G. Sommer, P. Regitnig, and G. A. Holzapfel. Dissection properties and mechanical strength of tissue components in human carotid bifurcations. *Ann. Biomed. Eng.*, 39:1703–1719, 2011.

[188] P. Tong and Y. C. Fung. The stress-strain relationship for the skin. *J. Biomech.*, 9:649–657, 1976.

[189] S. R. Vallabhaneni, G. L. Gilling-Smith, T. V. How, S. D. Carter, J. A. Brennan, and P. L. Harris. Heterogeneity of tensile strength and matrix metalloproteinase activity in the wall of abdominal aortic aneurysms. *J. Endovas. Ther.*, 11:494–502, 2004.

[190] J. P. Vande Geest, E. D. Dillavou, E. S. Di Martino, M. Oberdier, A. Bohra, M. S. Makaroun, and D. A. Vorp. Gender-related differences in the tensile strength of abdominal aortic aneurysm. *Ann. N.Y. Acad. Sci.*, 1085:400–402, 2006.

[191] J. P. Vande Geest, M. S. Sacks, and D. A. Vorp. Age dependency of the biaxial biomechanical behavior of human abdominal aorta. *J. Biomech. Eng.*, 126:815–822, 2004.

[192] J. P. Vande Geest, M. S. Sacks, and D. A. Vorp. The effects of aneurysm on the biaxial mechanical behavior of human abdominal aorta. *J. Biomech.*, 39:1324–1334, 2006.

[193] J. P. Vande Geest, M. S. Sacks, and D. A. Vorp. A planar biaxial constitutive relation for the luminal layer of intra-luminal thrombus in abdominal aortic aneurysms. *J. Biomech.*, 39:2347–2354, 2006.

[194] J. P. Vande Geest, D. E. Schmidt, M. S. Sacks, and D. A. Vorp. The effect of anisotropy on the stress analyses of patient-specific abdominal aortic aneurysms. *Ann. Biomed. Eng.*, 36:921–932, 2008.

[195] J. P. Vande Geest, D. H. J. Wang, S. R. Wisniewski, M. S. Makaroun, and D. A. Vorp. Towards a noninvasive method for determination of patient-specific wall strength distribution in abdominal aortic aneurysms. *Ann. Biomed. Eng.*, 34:1098–1106, 2006.

[196] K. A. Vardulaki, T. C. Prevost, N. M. Walker, N. E. Day, A. B. Wilmink, C. R. Quick, H. A. Ashton, and R. A. Scott. Growth rates and risk of rupture of abdominal aortic aneurysms. *Br. J. Surg.*, 85:1674–1680, 1998.

[197] D. A. Vorp. Biomechanics of abdominal aortic aneurysm. *J. Biomech.*, 40:1887–1902, 2007.

[198] D. A. Vorp, J. Gorcsan, W. A. Mandarino, and M. W. Webster. The potential influence of intraluminal thrombus on abdominal aortic aneurysm as assessed by a noninvasive method. *Cardiovasc. Surg.*, 4:732–739, 1996.

[199] D. A. Vorp, P. C. Lee, D. H. Wang, M. S. Makaroun, E. M. Nemoto, S. Ogawa, and M. W. Webster. Association of intraluminal thrombus in abdominal aortic aneurysm with local hypoxia and wall weakening. *J. Vasc. Surg.*, 34:291–299, 2001.

[200] D. A. Vorp and J. P. Vande Geest. Biomechanical determinants of abdominal aortic aneurysm rupture. *Arterioscler. Thromb. Vasc. Biol.*, 25:1558–1566, 2005.

[201] D. A. Vorp, M. L. Raghavan, S. C. Muluk, M. S. Makaroun, D. L. Steed, R. Shapiro, and M. W. Webster. Wall strength and stiffness of aneurysmal and nonaneurysmal abdominal aorta. *Ann. N.Y. Acad. Sci.*, 800:274–276, 1996.

[202] D. A. Vorp, D. H. Wang, M. W. Webster, and W. J. Federspiel. Effect of intraluminal thrombus thickness and bulge diameter on the oxygen flow in abdominal aortic aneurysm. *J. Biomech. Eng.*, 120:579–583, 1998.

[203] D. H. J. Wang, M. S. Makaroun, M. W. Webster, and D. A. Vorp. Mechanical properties and microstructure of intraluminal thrombus from abdominal aortic aneurysm. *J. Biomech. Eng.*, 123:536–539, 2001.

[204] D. H. J. Wang, M. S. Makaroun, M. W. Webster, and D. A. Vorp. Effect of intraluminal thrombus on wall stress in patient-specific models of abdominal aortic aneurysm. *J. Vasc. Surg.*, 36:598–604, 2002.

[205] P. N. Watton, N. A. Hill, and M. Heil. A mathematical model for the growth of the abdominal aortic aneurysm. *Biomech. Model. Mechanobiol.*, 3:98–113, 2004.

[206] M. W. Webster, C. E. McAuley, D. L. Steed, D. D. Miller, and C. H. Evans. Collagen stability and collagenolytic activity in the normal and aneurysmal human abdominal aorta. *Am. J. Surg.*, 161:635–638, 1991.

[207] J. V. White, K. Haas, S. Phillips, and A. J. Comerota. Adventitial elastolysis is a primary event in aneurysm formation. *J. Vasc. Surg.*, 17:371–380, 1993.

[208] W. Witkewicz, J. Gnus, W. Hauser, and L. Czernilewski. Biomechanical characterization of the wall of abdominal aortic aneurysm exposed to infection. *Angiol. Sosud. Khir.*, 11:25–29, 2005.

[209] Y. G. Wolf, W. S. Thomas, F. J. Brennan, W. G. Goff, M. J. Sise, and E. F. Bernstein. Computed tomography scanning findings associated with rapid expansion of abdominal aortic aneurysms. *J. Vasc. Surg.*, 20:529–535, 1994.

[210] M. Xenos, S. H. Rambhia, Y. Alemu, S. Einav, N. Labropoulos, A. Tassiopoulos, J. J. Ricotta, and D. Bluestein. Patient-based abdominal aortic aneurysm rupture risk prediction with fluid structure interaction modeling. *Ann. Biomed. Eng.*, 38:3323–3337, 2010.

[211] Z. Xu, N. Chen, M. M. Kamocka, E. D. Rosen, and M. Alber. A multiscale model of thrombus development. *J. R. Soc. Interface*, 5:705–722, 2008.

[212] S. C. Yu, W. K. Chan, B. T. Ng, and L. P. Chua. A numerical investigation on the steady and pulsatile flow characteristics in axisymmetric abdominal aortic aneurysm models with some experimental conditions. *J. Med. Eng. Technol.*, 23:228–239, 1999.

[213] C. K. Zarins, D. P. Giddens, B. K. Bharadvaj, V. S. Sottiurai, R. F. Mabon, and S. Glagov. Carotid bifurcation atherosclerosis. quantitative correlation of plaque localization with flow velocity profiles and wall shear stress. *Circ. Res.*, 53:502–514, 1983.

[214] C. K. Zarins, A. Runyon-Hass, M. A. Zatina, C.-T. Lu, and S. Glagov. Increased collagenase activity in early aneurysmal dilatation. *J. Vasc. Surg.*, 3:238–248, 1986.

Monographic Series TU Graz

Computation in Engineering and Science

Vol. 1 Steffen Alvermann

Effective Viscoelastic Behaviour of Cellular Auxetic Materials
2008
ISBN 978-3-902465-92-4

Vol. 2 Sendy Fransiscus Tantono

The Mechanical Behaviour of a Soilbag under Vertical Compression
2008
ISBN 978-3-902465-97-9

Vol. 3 Thomas Rüberg

Non-conforming FEM/BEM Coupling in Time Domain
2008
ISBN 978-3-902465-98-6

Vol. 4 Dimitrios E. Kiousis

Biomechanical and Computational Modeling of Atherosclerotic Arteries
2008
ISBN 978-3-85125-023-7

Vol. 5 Lars Kielhorn

A Time-Domain Symmetric Galerkin BEM for Viscoelastodynamics
2009
ISBN 978-3-85125-042-8

Vol. 6 Gerhard Unger

Analysis of Boundary Element Methods for Laplacian Eigenvalue Problems
2009
ISBN 978-3-85125-081-7

Monographic Series TU Graz

Computation in Engineering and Science

Vol. 7 Gerhard Sommer

Mechanical Properties of Healthy and Diseased Human Arteries
2010
ISBN 978-3-85125-111-1

Vol. 8 Mathias Nenning

Infinite Elements for Elasto- and Poroelastodynamics
2010
ISBN 978-3-85125-130-2

Vol. 9 Thanh Xuan Phan

Boundary Element Methods for Boundary Control Problems
2011
ISBN 978-3-85125-149-4

Vol. 10 Loris Nagler

Simulation of Sound Transmission through Poroelastic Plate-like Structures
2011
ISBN 978-3-85125-153-1

Vol. 11 Markus Windisch

Boundary Element Tearing and Interconnecting Methods for Acoustic and Electromagnetic Scattering
2011
ISBN: 978-3-85125-152-4

Monographic Series TU Graz

Computation in Engineering and Science

Vol. 12 Christian Walchshofer

Analysis of the Dynamics at the Base of a Lifted Strongly Buoyant Jet Flame Using Direct Numerical Simulation
2011
ISBN 978-3-85125-185-2

Vol. 13 Matthias Messner

Fast Boundary Element Methods in Acoustics
2012
ISBN 978-3-85125-202-6

Vol. 14 Peter Urthaler

Analysis of Boundary Element Methods for Wave Propagation in Porous Media
2012
ISBN 978-3-85125-216-3

Vol. 15 Peng Li

Boundary Element Method for Wave Propagation in Partially Saturated Poroelastic Continua
2012
ISBN 978-3-85125-236-1

Vol. 16 Jörg Schriefl

Quantification of Collagen Fiber Morphologies in Human Arterial Walls
2012
ISBN 978-3-85125-238-5

Vol. 17 Thomas S. E. Eriksson

Cardiovascular Mechanics
2013
ISBN 978-3-85125-277-4

Monographic Series TU Graz

Computation in Engineering and Science

Vol. 18 Jianhua Tong

Biomechanics of Abdominal Aortic Aneurysms
2013
ISBN 978-3-85125-279-8